REPORT DOCUMENTATION PAGE

Form Approved OMB NO. 0704-0188

1. REPORT DATE (DD-MM-YYYY)	2. REPORT TYPE	3. DATES COVERED (From - To)
23-09-2008	Final Report	1-Jul-2005 - 30-Jun-2008

4. TITLE AND SUBTITLE
Globally convergent numerical methods for coefficient inverse problems

5a. CONTRACT NUMBER
W911NF-05-1-0378

5b. GRANT NUMBER

5c. PROGRAM ELEMENT NUMBER
611102

6. AUTHORS
Michael V. Klibanov

5d. PROJECT NUMBER

5e. TASK NUMBER

5f. WORK UNIT NUMBER

7. PERFORMING ORGANIZATION NAMES AND ADDRESSES
University of North Carolina - Charlotte
Office of Sponsored Programs
9201 University City Blvd.
Charlotte, NC 28223 -0001

8. PERFORMING ORGANIZATION REPORT NUMBER

9. SPONSORING/MONITORING AGENCY NAME(S) AND ADDRESS(ES)
U.S. Army Research Office
P.O. Box 12211
Research Triangle Park, NC 27709-2211

10. SPONSOR/MONITOR'S ACRONYM(S)
ARO

11. SPONSOR/MONITOR'S REPORT NUMBER(S)
45750-MA.28

12. DISTRIBUTION AVAILABILITY STATEMENT
Approved for public release; federal purpose rights

13. SUPPLEMENTARY NOTES
The views, opinions and/or findings contained in this report are those of the author(s) and should not contrued as an official Department of the Army position, policy or decision, unless so designated by other documentation.

14. ABSTRACT

Coefficient Inverse Problems (CIPs) for Partial Differential Equations (PDEs) represent a very important tool for such needs of the Army as imaging of unknown targets hidden in cluttered heterogeneous backgrounds. The goal of this project is the development of globally convergent numerical methods for a wide class of CIPs. These methods are tested on mathematical models of the interest to the Army such as imaging of antipersonnel land mines and targets on battlefields covered by smogs and flames. In our definition ``global convergence'' entails: (1) a rigorous convergence analysis that does not depend on the

15. SUBJECT TERMS
global convergence, coefficient inverse problems, convexification, Carleman Weight Functions, numerical studies, comparative analysis, imaging of land mines, stable layer stripping procedures

16. SECURITY CLASSIFICATION OF: a. REPORT	b. ABSTRACT	c. THIS PAGE	17. LIMITATION OF ABSTRACT	15. NUMBER OF PAGES	19a. NAME OF RESPONSIBLE PERSON
U	U	U	SAR		Michael Klibanov
					19b. TELEPHONE NUMBER
					704-687-2645

Standard Form 298 (Rev 8/98)
Prescribed by ANSI Std. Z39.18

Report Title

Globally convergent numerical methods for coefficient inverse problems

ABSTRACT

Coefficient Inverse Problems (CIPs) for Partial Differential Equations (PDEs) represent a very important tool for such needs of the Army as imaging of unknown targets hidden in cluttered heterogeneous backgrounds. The goal of this project is the development of globally convergent numerical methods for a wide class of CIPs. These methods are tested on mathematical models of the interest to the Army such as imaging of antipersonnel land mines and targets on battlefields covered by smogs and flames. In our definition ``global convergence'' entails: (1) a rigorous convergence analysis that does not depend on the quality of the initial guess, and (2) numerical simulations that confirm the advertised convergence property.
A conventional way to solve a CIP is via the minimization of a least squares objective functional. This functional characterizes misfit between the data and the solution of that PDE with a ``guess'' for the unknown coefficient. However, it is well known to researchers working on computations of inverse problems that the phenomenon of multiple local minima of these functionals represents the major obstacle for the development of reliable numerical methods for multidimensional CIPs. This phenomenon in turn is caused by the above mentioned non-linearity and ill-posedness. Because of local minima, one should somehow guess in advance about a good approximation for the solution. Without the availability of a first good guess, however, there is no guarantee that the calculated coefficient is indeed close to the correct one. In our terminology these are locally convergent numerical methods. In other words, their convergence to the correct solution can be guaranteed only if the starting point is located in a small neighborhood of this solution. Because of local minima, conventional numerical methods for multidimensional CIPs are locally convergent ones. However, in many important applications the first good guess is unavailable. In particular, locally convergent algorithms are \QTR{bf}{fundamentally unsatisfactory} for the needs of the Army, because an accurate a priori knowledge of the properties of a medium is rarely available in military applications. This is because military environments are cluttered and, therefore, heterogeneous.
The main focus of this project was the so-called convexification method. This is the globally convergent algorithm of the first generation. This method was fully investigated. The first breakthrough result on the convexification was reported in the Annual report of 2006 and was published in 2007. This publication got quite a warm reception of the scientific community. Because the convexification is a new method, it is natural that a number of its different aspects was studied, which was done in this project. Three versions of the numerical realization of the convexification were implemented and tested. Applications to imaging of both antipersonnel land mines and targets on battlefields covered by smogs and flames were addressed. In late 2007 the second breakthrough result was obtained. This is a globally convergent numerical method of the second generation. This technique deserves to be investigated further, because it is very promising. This method is radically different from the convexification.

The PI believes that globally convergent algorithms for CIPs, which are developed in this project, have a serious potential to radically improve} the performance of many imaging modalities of the interest to the Army. Along with numerical results, a number of analytical results were also obtained in this project. Nineteen (19) papers in refereed journals with the acknowledgment of this grant support were published/accepted/submitted. Results of this effort were presented at eighteen (18) international professional meetings. One Ph.D. thesis was defended based on some results of this project.

List of papers submitted or published that acknowledge ARO support during this reporting period. List the papers, including journal references, in the following categories:

(a) Papers published in peer-reviewed journals (N/A for none)

1. M.V. Klibanov and A. Timonov, Numerical studies on the globally convergent convexification algorithm in 2D, Inverse Problems, 23, 123-138, 2007.

2. M.V. Klibanov and A. Timonov, A globally convergent convexification algorithm for multidimensional coefficient inverse problems, Journal of Inverse and Ill-Posed Problems, 15, 13-17, 2007.

3. J. Xin and M.V. Klibanov, Imaging of land mines by the globally convergent convexification method using a simplified mathematical model, Inverse Problems in Science and Engineering, 16, 631-653, 2008.

4. J. Xin and M.V. Klibanov, Comparative studies of the globally convergent convexification algorithm with application to imaging of antipersonnel land mines, Applicable Analysis, 86, 1147-1176, 2007.

5. H. Shan, M.V. Klibanov, H. Li, N. Pantong, and J. Su, Numerical implementation of the convexification algorithm for an optical diffusion tomograph, Inverse Problems, 24, 025006 (18 pages), 2008.

6. J. Su, H. Shan, H. Liu and M.V. Klibanov, A reconstruction method with data from a multiple-site continuous-wave source for 3-Dimensional optical tomography, J. of Optical Society of America, A, 23, 2388-2395, 2006.

7. C. Clason and M.V. Klibanov, The quasi-reversibility method for the thermoacoustic tomography in heterogeneous medium, SIAM J. Sci. Computing, }30, 1-23, 2007.

8. M.V. Klibanov, A.V. Kuzhuget, S.I. Kabanikhin and D.V. Nechaev, The quasi-reversibility method for the thermoacoustic tomography and a coefficient inverse problem, Applicable Analysis, iFirst, 1-28, 2008.

9. M.V. Klibanov, S.I. Kabanikhin and D.V. Nechaev, Numerical solution of the problem of computational time reversal in the quadrant, Waves in Random and Complex Media, 16, 473-494, 2006.

10. B. Kaltenbacher and M.V. Klibanov, An inverse problem for a nonlinear parabolic equation with applications in population dynamics and magnetics, SIAM J. Math. Analysis, 39, 1863-1889, 2008.

11. M.V. Klibanov and S.E. Pamyatnykh, Lipschitz stability of a non-standard problem for the non-stationary transport equation via a Carleman estimate, Inverse Problems, 22, 881-890, 2006.

12. M.V. Klibanov and S.E. Pamyatnykh, Global uniqueness for a coefficient inverse problem for the non-stationary transport equation via a Carleman estimate, J. Math. Analysis and Applications, 343, 352-365, 2008.

13. M.V. Klibanov and M. Yamamoto, Exact controllability for the time dependent transport equation, SIAM J. Control and Optimization, }46, 2071-2195, 2007.

14. M.V. Klibanov, Estimates of initial conditions of parabolic equations and inequalities via lateral Cauchy data, Inverse Problems, 22, 495-514, 2006.

15. M.V. Klibanov and A.V. Tikhonravov, Estimates of initial conditions of parabolic equations and inequalities in infinite domains via lateral Cauchy data, J. Differential Equations, 237, 198-224, 2007.

16. M.V. Klibanov, On the recovery of a 2-D function from the modulus of its Fourier transform, J. Math. Analysis and Applications, 323, 818-843, 2006.

Number of Papers published in peer-reviewed journals: 16.00

(b) Papers published in non-peer-reviewed journals or in conference proceedings (N/A for none)

none

Number of Papers published in non peer-reviewed journals: 0.00

(c) Presentations

none

Number of Presentations: 0.00

Non Peer-Reviewed Conference Proceeding publications (other than abstracts):

none

Number of Non Peer-Reviewed Conference Proceeding publications (other than abstracts): 0

Peer-Reviewed Conference Proceeding publications (other than abstracts):

none

Number of Peer-Reviewed Conference Proceeding publications (other than abstracts): 0

(d) Manuscripts

1. J. Xin and M.V. Klibanov, Numerical solution of an inverse problem of imaging of antipersonnel land mines by the globally convergent convexification algorithm,accepted for publication in SIAM J. Sci. Computing, 2008.

2. J. Xin and M.V. Klibanov, Towards real time imaging of antipersonnel land mines by the convexification algorithm, accepted for publication in J. Inverse and Ill-Posed Problems, 2008.

3. H. Shan, M.V. Klibanov, H. Li, N. Pantong, and J. Su, A globally accelerated numerical method for optical tomography with continuous wave source, submitted for publication to J. Inverse and Ill-Posed Problems, 2008.

4. L. Beilina and M.V. Klibanov, A globally convergent numerical method for a coefficient inverse problem, accepted for publication in SIAM J. Sci. Computing, 2008.

Number of Manuscripts: 4.00

Number of Inventions:

Graduate Students

NAME	PERCENT_SUPPORTED
Andrey Kuzhuget	0.36
FTE Equivalent:	**0.36**
Total Number:	**1**

Names of Post Doctorates

NAME	PERCENT_SUPPORTED
Jianguo Xin	1.00
FTE Equivalent:	**1.00**
Total Number:	**1**

Names of Faculty Supported

NAME	PERCENT_SUPPORTED	National Academy Member
Michael V. Klibanov, The PI	0.22	No
FTE Equivalent:	**0.22**	
Total Number:	**1**	

Names of Under Graduate students supported

NAME	PERCENT_SUPPORTED
none	
FTE Equivalent:	
Total Number:	**1**

Student Metrics

This section only applies to graduating undergraduates supported by this agreement in this reporting period

The number of undergraduates funded by this agreement who graduated during this period:	0.00
The number of undergraduates funded by this agreement who graduated during this period with a degree in science, mathematics, engineering, or technology fields:......	0.00
The number of undergraduates funded by your agreement who graduated during this period and will continue to pursue a graduate or Ph.D. degree in science, mathematics, engineering, or technology fields:......	0.00
Number of graduating undergraduates who achieved a 3.5 GPA to 4.0 (4.0 max scale):......	0.00
Number of graduating undergraduates funded by a DoD funded Center of Excellence grant for Education, Research and Engineering:......	0.00
The number of undergraduates funded by your agreement who graduated during this period and intend to work for the Department of Defense	0.00
The number of undergraduates funded by your agreement who graduated during this period and will receive scholarships or fellowships for further studies in science, mathematics, engineering or technology fields:	0.00

Names of Personnel receiving masters degrees

NAME	
none	
Total Number:	**1**

Names of personnel receiving PHDs

NAME	
Sergey Pamyatnykh	
Total Number:	**1**

Names of other research staff

NAME	PERCENT_SUPPORTED	
none		No
FTE Equivalent:		
Total Number:	**1**	

Sub Contractors (DD882)

1 a. University of South Carolina Research Foundat

1 b. Office of Sponsored Programs & Researc
James F. Byrnes International Center
Columbia SC 29208

Sub Contractor Numbers (c): 2975-03-0469-USCRF
Patent Clause Number (d-1): 37 CFR Part 401
Patent Date (d-2):
Work Description (e): Details of the work on the subcontract can be found in section 7 of the final report (see the pdf file ir
Sub Contract Award Date (f-1): 1/1/2007 12:00:00AM
Sub Contract Est Completion Date(f-2): 12/31/2007 12:00:00AM

---

1 a. University of South Carolina Research Foundat

1 b. 712 Main St.
Columbia SC 29208

Sub Contractor Numbers (c): 2975-03-0469-USCRF
Patent Clause Number (d-1): 37 CFR Part 401
Patent Date (d-2):
Work Description (e): Details of the work on the subcontract can be found in section 7 of the final report (see the pdf file ir
Sub Contract Award Date (f-1): 1/1/2007 12:00:00AM
Sub Contract Est Completion Date(f-2): 12/31/2007 12:00:00AM

Inventions (DD882)

REPORTAGE PERIOD: July 1, 2005-June 30, 2008

PROJECT TITLE: Globally Convergent Numerical Methods for Coefficient Inverse Problems

ARO GRANT NUMBER: W911NF-05-1-0378

PRINCIPAL INVESTIGATOR: Michael V. Klibanov, Ph.D., Professor of The Department of Mathematics and Statistics, The University of North Carolina at Charlotte

ABSTRACT

Coefficient Inverse Problems (CIPs) for Partial Differential Equations (PDEs) represent a very important tool for such needs of the Army as imaging of unknown targets hidden in cluttered heterogeneous backgrounds. The goal of this project is the development of globally convergent numerical methods for a wide class of CIPs. These methods are tested on mathematical models of the interest to the Army such as imaging of antipersonnel land mines and targets on battlefields covered by smogs and flames. In our definition "global convergence" entails: (1) a rigorous convergence analysis that does not depend on the quality of the initial guess, and (2) numerical simulations that confirm the advertised convergence property.

A conventional way to solve a CIP is via the minimization of a least squares objective functional. This functional characterizes misfit between the data and the solution of that PDE with a "guess" for the unknown coefficient. However, it is well known to researchers working on computations of inverse problems that the phenomenon of multiple local minima of these functionals represents the major obstacle for the development of reliable numerical methods for multidimensional CIPs. This phenomenon in turn is caused by the above mentioned nonlinearity and ill-posedness. Because of local minima, one should somehow guess in advance about a good approximation for the solution. Without the availability of a first good guess, however, there is no guarantee that the calculated coefficient is indeed close to the correct one. In our terminology these are *locally convergent* numerical methods. In other words, their convergence to the correct solution can be guaranteed only if the starting point is located in a small neighborhood of this solution. Because of local minima, conventional numerical methods for multidimensional CIPs are locally convergent ones. However, in many important applications the first good guess is unavailable. In particular, locally convergent algorithms are **fundamentally unsatisfactory** for the needs of the Army, because an accurate a priori knowledge of the properties of a medium is rarely available in military applications. This is because military environments are cluttered and, therefore, heterogeneous.

The main focus of this project was the so-called *convexification* method. This is the globally convergent algorithm of the first generation. This method was fully investigated. The **first breakthrough** result on the convexification was reported in the Annual report of 2006 and was published in 2007. This publication got quite a warm reception of the scientific community (section 1). Because the convexification is a new method, it is natural that a number of its different aspects was studied, which was done in this project. Three versions of the numerical realization of the convexification were implemented and tested. Applications to imaging of both antipersonnel land mines and targets on battlefields covered by smogs

and flames were addressed. In late 2007 the **second breakthrough** result was obtained. This is a globally convergent numerical method of the second generation. This technique deserves to be investigated further, because it is very promising. This method is radically different from the convexification.

The PI believes that globally convergent algorithms for CIPs, which are developed in this project, have a serious potential to **radically improve** the performance of many imaging modalities of the interest to the Army. Along with numerical results, a number of analytical results were also obtained in this project. Nineteen (19) papers in refereed journals with the acknowledgment of this grant support were published/accepted/submitted. Results of this effort were presented at eighteen (18) international professional meetings. One Ph.D. thesis was defended based on some results of this project.

CONTENT

1 Introduction

In this final report only most interesting results of the project are presented. Other results can be found in 2006 and 2007 annual reports as well as in publications of the PI, which are cited in section named "Publications".

1.1 State of the art of numerical methods for CIPs and crucial role of globally convergent numerical methods

CIPs play a rapidly growing role in military applications. Indeed, one of the needs of the Army is to detect and image unknown targets. Examples of those targets include land mines, underground bunkers, tanks on battlefields covered by smogs and flames, etc.. In all these scenarios targets are incorporated in cluttered, heterogenous and, therefore, unknown backgrounds. Probing radiations are usually thought as electric and acoustic waves for the first two applications and light originated by lasers in the third. Output radiations are measured by sensors. Interestingly, the diffuse (because of smogs and flames) light propagation in the third application is even helpful. This is because even if the direct light would miss the target, diffuse photons would not, and, therefore, detectors would still sense the presence of that target. Propagations of those signals are covered by Partial Differential Equations (PDEs), which are derived from the fundamental laws of physics. Electric, acoustic or light scattering properties of both unknown targets and the backgrounds are described by coefficients of those PDEs. Since such properties of targets usually differ sharply from the properties of the surroundings, the presence of targets of interest is revealed by the differences in the output signals measured by sensors.

Therefore, the goal of a CIP is to calculate a good approximation to the unknown coefficient(s) of that PDE from the measured data. However, the latter is an **enormously challenging** mathematical problem. Two main factors causing a substantial difficulty of construction of stable globally convergent algorithms for CIPs are their non-linearity and ill-posedness. The nonlinearity is because solutions of PDEs depend nonlinearly on their coefficients. The ill-posedness is a well known feature of inverse problems. This means that small fluctuations in the input data can cause large fluctuations of solutions. This feature led to the development of regularization algorithms, see, e.g., [50].

A conventional way to solve a CIP is via the minimization of a least squares objective functional. This functional characterizes misfit between the data and the solution of that PDE with a "guess" for the unknown coefficient. However, it is well known to researchers working on computations of inverse problems that the phenomenon of multiple local minima of these functionals represents the major obstacle for the development of reliable numerical methods for multidimensional CIPs. This phenomenon in turn is caused by the above mentioned nonlinearity and ill-posedness. Because of local minima, one should somehow guess in advance about a good approximation for the solution. Without the availability of a first good guess, however, there is no guarantee that the calculated coefficient is indeed close to the correct one. In our terminology these are *locally convergent* numerical methods. In other words, their

convergence to the correct solution can be guaranteed only if the starting point is located in a small neighborhood of this solution. Because of local minima, conventional numerical methods for multidimensional CIPs are locally convergent ones. However, in many important applications the first good guess is unavailable. In particular, locally convergent algorithms are **fundamentally unsatisfactory** for the needs of the Army, because an accurate a priori knowledge of the properties of a medium is rarely available in military applications. This is because military environments are cluttered and, therefore, heterogeneous.

In our definition "global convergence" entails: (1) a rigorous convergence analysis that does not depend on the quality of the initial guess, and (2) numerical simulations that confirm the advertised convergence property. Two new globally convergent algorithms for a broad class of CIPs were developed in this project: the convexification [1-7] and an algorithm which is based on a layer stripping procedure with respect to the so-called pseudo frequency [12], which is the positive parameter s of the Laplace transform of either hyperbolic or parabolic PDE. We call s pseudo frequency. These algorithms represent respectively the first and the second generation of globally convergent numerical methods. While the convexification was fully investigated in this project, the second one is only in an infant age and requires a detailed further investigation.

Since the convexification is a new method, it is natural to investigate its main features from a number of different perspectives, which was the main goal of this project and was reflected in publications [1-7]. However, during the work on this project a new main goal occurred in 2007 [12]. This one was the development of a new globally convergent algorithm for CIPs, which is based on the layer stripping procedure with respect to the pseudo frequency rather than the layer stripping with respect to a spatial variable (convexification). Since the differential operator with respect to the pseudo frequency is not a part of a corresponding PDE, it is anticipated that this new method will have a good stability property. Thus, the recent work [12] has started the second generation of globally convergent numerical methods for CIPs. In addition to computational results, a number of analytical results concerning with the important issues of uniqueness and stability of inverse problems were obtained during the work on this grant [14-19].

1.2 Warm reception by the scientific community

Two publications with the acknowledgment of the support of this grant were publicly warmly accepted by the scientific community. First, this was the result of [1], where the first numerical result of the convexification in the 2-d case was published. As a clear manifestation of a warm reception of the publication [1], the PI was requested for an interview by The Institute of Physics Publishing, www.iop.org, The Publisher, which publishes the journal named "Inverse Problems", which is the most popular journal in the field. PI's interview can be found at http://www.iop.org/ej/authors_edition/. It is stated at that site that "*60 Seconds With showcases interviews with IOP authors who have published papers that were key to the advancement of physics research in their particular subject area.*" In addition, a theoretical result of the PI [18], which is reported in subsection 11.2, was highlighted by the

Editorial Board of Inverse Problems among best publications of 2006.

2 An Outline of the Convexification

The convexification works with a single location of the source (equivalently, a single direction of the incident plane wave) and with the data collected at a piece of the boundary rather than on the whole boundary. This means the minimal requirement on the data collection scheme. The so-called "transformation procedure" of the convexification has deep roots in the method of Carleman estimates for CIPs, which was originally introduced in 1981 in the work of Bukhgeim and Klibanov [29] (also, see, e.g., [38], [39], [41] for some follow up works) and became since then one of very few classic tools in the field of Inverse Problems. Initially Carleman estimates were introduced in the field of Inverse Problems only for the proofs of uniqueness and stability results. Hence, prior to the convexification, Carleman estimates were not applied to numerical developments. The sequence of Carleman Weight Functions (CWFs) $\exp\left[-\lambda\left(z-z_{i-1}\right)\right],\ i=1,\cdots,n$ for the operator d^2/dz^2 is involved in the numerical scheme of the convexification. It was explained in [1] that this sequence of weights ensures the strict convexity of the sequence of residual least squares functionals, as well as the stabilization of the resulting layer stripping procedure, also see subsection 2.6. Here n is the number of layers $\{z : z \in (z_{i-1}, z_i]\}$.

First, the original CIP is approximated with the Cauchy problem for a coupled system of ordinary nonlinear integral-differential equations for the vector-valued function $p(z,s)$. An important feature of this system is that the unknown coefficient is not present in it. From the computational standpoint the major complicating factor of this system is the presence of nonlinearities with Volterra-like integrals with respect to the pseudo frequency s, whereas derivatives are taken with respect to the spatial variable z. To solve this Cauchy problem, a stable layer stripping procedure is applied. On each thin z-layer one approximates the vector-valued function $p(z,s)$ as a quadratic polynomial with the unknown quadratic term and two other terms being known from the data at the interface. Next, one constructs a residual least squares functional $J_{\lambda,i}$ with the CWF in it. The CWF for any differential operator ensures that in the weighted L_2 norm of this operator the principal part dominates the rest. Hence, due to the presence of the CWF in the functional $J_{\lambda,i}$, the principal linear part p'' of the differential operator for the vector-valued function p in $J_{\lambda,i}$ dominates all other terms, including nonlinear ones. Because of this domination, the functional $J_{\lambda,i}$ is strictly convex on a certain a priori given bounded set (this is not a small set!). Furthermore, the unique minimizer of $J_{\lambda,i}$ belongs to the interior of this set. In addition, this minimizer is close to the one which corresponds to the exact solution of the CIP (Theorem 2.1).

2.1 Forward problems

Below in section 2 $x = (x_1, x_2, z)$. First, consider the Cauchy problem for a hyperbolic equation

$$c\left(x\right)u_{tt}=\Delta u-a(x)u \text{ in } \mathbb{R}^3\times\left(0,\infty\right), \tag{2.1}$$

$$u(x,0)=0,\ u_t(x,0)=\delta(x-x_0). \tag{2.2}$$

In addition we consider the Cauchy problem for a parabolic equation

$$c(x)\widetilde{u}_t=\Delta\widetilde{u}-a(x)\widetilde{u} \text{ in } \mathbb{R}^3\times(0,\infty), \tag{2.3}$$

$$\widetilde{u}(x,0)=\delta(x-x_0). \tag{2.4}$$

Consider the Laplace transform of both functions u and $\widetilde{u}$,

$$w(x,s)=\int\limits_0^\infty u(x,t)e^{-st}dt=\int\limits_0^\infty \widetilde{u}(x,t)e^{-s^2t}dt \tag{2.5}$$

for positive $s>s_0>0$. Since both integrals of (2.5) lead to the same elliptic equation (2.9a) for the function w, it is more convenient to us to consider the theory for the function w.

We use the Laplace transform with the positive parameter s only because we need to make sure that the function $w(x,s)>0$ by the maximum principle, see (2.10). As to the coefficients of equations (2.1) and (2.3), we assume that

$$c(x)\in[d_1,2d_2],\ \text{where } d_1,d_2=const.>0. \tag{2.6}$$

$$c(x)\in C^2\left(\mathbb{R}^3\right), c(x)=2d_1 \text{ for } x\in\mathbb{R}^3\diagdown\Omega, \tag{2.7}$$

$$a(x)\in C^2\left(\mathbb{R}^3\right),\ a(x)\geq 0 \text{ and } a(x)=0 \text{ for } x\in\mathbb{R}^3\diagdown\Omega, \tag{2.8}$$

where $\Omega\subset\mathbb{R}^3$ is a convex bounded domain. Note that in the field of CIPs a certain over-smoothness of coefficients is usually assumed.

The equation for the function w is

$$\Delta w-\left[s^2c^{-2}(x)+a(x)\right]w=-\delta(x-x_0),\ \forall s>s_0=const.>0. \tag{2.9a}$$

with the condition at the infinity

$$\lim_{|\vec{x}|\to\infty}w(x,s)=0,\ \forall s>s_0=const.>0. \tag{2.9b}$$

The maximum principle and conditions (2.6)-(2.8) imply that for all $s>s_0$ there exists unique solution $w(,s)\in C^3\left(\mathbb{R}^3\diagdown\{|x-x_0|<\varepsilon\}\right),\ \forall\varepsilon>0$ of the problem (2.9a,b). Furthermore,

$$w(x,s)>0,\ \forall s>s_0. \tag{2.10}$$

Under certain conditions imposed on coefficients $c(x)$ and $a(x)$ the following asymptotic behavior holds [41], [44]

$$D_x^\alpha D_s^\beta w(x,s)=D_x^\alpha D_s^\beta\left\{\frac{\exp\left[-sl(x,x_0)\right]}{4\pi l(x,x_0)}\left[1+O\left(\frac{1}{s}\right)\right]\right\},\ s\to\infty,\ |\alpha|\leq 2,\ \beta=0,1. \tag{2.11}$$

This asymptotic behavior was derived in [41], [44] on the basis of Theorem 4.1 in [47].

2.2 The inverse problem

We formulate the inverse problem for the elliptic equation (2.9a) with the condition (2.9b), because formulations of this problem for above hyperbolic and parabolic equations are similar due to (2.5). In the case when the data either for the inverse parabolic or for the inverse hyperbolic problem are given on a large but finite time interval $t \in (0, T)$ one should assume that in (2.5)

$$\int\limits_0^\infty \widetilde{u}(x,t)e^{-s^2t}dt \approx \int\limits_0^T \widetilde{u}(x,t)e^{-s^2t}dt, \int\limits_0^\infty u(x,t)e^{-st}dt \approx \int\limits_0^T u(x,t)e^{-st}dt, s > s_0 = const. > 0.$$

Inverse Problem. Let Ω be a rectangular prism,

$$\Omega = \{-A < x_1, x_2 < A,\ z \in (0, L)\},$$

where A and L are positive numbers. Suppose that one of coefficients of the equation (2.9a) is unknown in Ω and known in $\mathbb{R}^3 \diagdown \Omega$ and all other coefficients are known everywhere. Determine that unknown coefficient for $\in \Omega$, assuming that the following two functions $\varphi(x_1, x_2, s)$ and $\psi(x_1, x_2, s)$ are known for a single source position $\vec{x}_0 \notin \overline{\Omega}$

$$w(x_1, x_2, 0, s) = \varphi(x_1, x_2, s),\ w_z(x_1, x_2, 0, s) = \psi(x_1, x_2, s), \tag{2.12}$$
$$\text{for } (x_1, x_2, s) \in (-A, A)^2 \times [s_0, \overline{s}],$$

where s_0 and $\overline{s}$ are certain positive numbers.

In the case when only one of functions φ or ψ is given for all $(x_1, x_2, s) \in \mathbb{R}^2 \times (s_0, \infty)$, another one can be determined uniquely via solution of the corresponding boundary value problem for the equation (2.9a) in the lower half space $\{z < 0\}$.

2.3 Transformation

Since we present numerical examples for the case $a(x) = 0$, we consider this case only below for brevity. The numerical scheme for the case of the unknown function $a(x)$ was considered in [41] and [44]. We first transform our problem to the Cauchy problem for a nonlinear elliptic integral-differential equation, in which the unknown coefficient is not present. Because of (2.10) we can consider the function $v = \ln w$. Then (2.9a) and (2.12) lead to

$$\Delta v + |\nabla v|^2 = s^2 c(x) \text{ in } \Omega, \tag{2.13}$$

$$v(x_1, x_2, 0, s) = \varphi_1(x_1, x_2, s),\ v_z(x_1, x_2, 0, s) = \psi_1(x_1, x_2, s), \tag{2.14}$$
$$\text{for } (x_1, x_2, s) \in (-A, A)^2 \times (s_0, \infty),$$

where

$$\varphi_1 = \ln \varphi,\ \psi_1 = \frac{\psi}{\varphi}.$$

Divide both sides of (2.13) by s^2 and denote

$$\widetilde{v}(x,s) = \frac{v}{s^2}.$$

Then

$$\Delta\widetilde{v} + s^2 \left|\nabla\widetilde{v}\right|^2 = c\left(x\right). \tag{2.15}$$

It follows from (2.11) that

$$D_x^\alpha \widetilde{v}(x,s) = O\left(\frac{1}{s}\right), D_x^\alpha \partial_s \widetilde{v}(x,s) = O\left(\frac{1}{s^2}\right), \text{ for } s \to \infty. \tag{2.16}$$

We now want to eliminate the unknown coefficient $c(x)$ from equation (2.15). To do so, differentiate its both sides with respect to the parameter s and observe that $\partial_s c(x) \equiv 0$. Denote

$$q\left(x,s\right) = \partial_s \widetilde{v}\left(x,s\right), \ \varphi_2\left(x,s\right) = \partial_s\left[s^{-2}\varphi_1\left(x,s\right)\right], \ \psi_2(x,s) = \partial_s\left[s^{-2}\psi_1\left(x,s\right)\right]. \tag{2.17}$$

Then by (2.11) and (2.16)

$$\widetilde{v}\left(x,s\right) = -\int\limits_s^\infty q\left(x,\tau\right) d\tau.$$

We truncate this integral as

$$\widetilde{v}\left(x,s\right) \approx -\int\limits_s^{\bar{s}} q\left(x,\tau\right) d\tau + V(x), \tag{2.18}$$

where $\bar{s} > s_0$ is a large number which should be chosen in numerical experiments. This truncation is similar to the truncation of high frequencies, which is routinely done in science and engineering. Here $V(x)$ is the so-called "tail function" which complements the integral. This function is unknown and $V(x) \approx \widetilde{v}\left(x,\bar{s}\right)$. Thus, we obtain the following (approximate) nonlinear integral differential equation

$$\Delta q - 2s^2 \nabla q \int\limits_s^{\bar{s}} \nabla q\left(x,\tau\right) d\tau + 2s\left[\int\limits_s^{\bar{s}} \nabla q\left(x,\tau\right) d\tau\right]^2 \tag{2.20a}$$

$$+2s^2 \nabla q \nabla V - 4s \nabla V \int\limits_s^{\bar{s}} \nabla q\left(x,\tau\right) d\tau + 2s\left(\nabla V\right)^2 = 0$$

In addition, the following Cauchy data are given

$$q\left(x_1,x_2,0,s\right) = \varphi_2\left(x_1,x_2,s\right), \ q_z\left(x_1,x_2,0,s\right) = \psi_2\left(x_1,x_2,s\right), \tag{2.20b}$$

$$\text{for } (x_1, x_2, s) \in (-A, A)^2 \times (s_0, \bar{s}).$$

Equation (2.20a) has two unknown functions in it q and V. A good point of this equation, however is that it does not contain the unknown coefficient. Thus, these two unknown functions are approximated differently in our algorithms. One of the key points which helps us to approximate the tail function is that it is small for large values of $\bar{s}$, as it follows from (2.16). If the tail function is given, then the problem (2.20a,b) is the Cauchy problem for a nonlinear integral differential equation with Volterra-like integrals depending on the parameter s, which is not involved in the differential operator. If the second and third terms in (2.20a) would be absent, then this would be a well-known Cauchy problem for the Laplace equation, which is discussed in many publications (we are not in a position to list those). Compared with the latter, two major difficulties of the problem (2.20a,b) are the nonlinearity and the presence of integrals.

2.4 Approximation

Now the main question is: *How to solve numerically the problem (2.20a,b)?* This question is addressed in follow up subsections of this section. Let $\left\{\phi_j(x_1, x_2)\right\}_{j=1}^{N} \subset C^2\left([-A, A]^2\right)$ be a set of linearly independent functions approximating the function $q(\vec{x}, s)$ up to its second derivatives

$$D_x^{\alpha} q(x_1, x_2, z, s) \approx D_x^{\alpha} \sum_{j=1}^{N} p_j(z, s) \phi_j(x_1, x_2), \ (x, s) \in \overline{\Omega} \times [s_0, \bar{s}], \ |\alpha| \leq 2, \tag{2.21}$$

We assume that functions $\phi_j(x_1, x_2)$ are given via analytical formulas, so that their derivatives can be calculated analytically. For example, one can take functions ϕ_j in the form $\phi_j(x_1, x_2) = Q_{j_1}(x_1) Q_{j_2}(x_2)$, where Q_{j_1} and Q_{j_2} are either parts of an orthogonal basis in L_2 or cubic B-splines. Denote for brevity $\vec{y} := (x_1, x_2)$, $\Theta = (-A, A) \times (-A, A)$. Substitute (2.21) in (2.20a). Denote $p_j'(z, s) := \partial_z p_j(z, s)$. Next, multiply both sides of the resulting equation by the function $\phi_r(\vec{y})$, $r = 1, \cdots, N$, and integrate over the rectangle Θ. We obtain the following coupled system of nonlinear ordinary integral-differential equations

$$\Pi(p, z, s) := Bp'' - F\left(p, p', \int_s^{\bar{s}} p(z, \tau)\, d\tau, \int_s^{\bar{s}} p'(z, \tau)\, d\tau, s\right) = 0, \tag{2.22}$$

$$(z, s) \in [0, L] \times [s_0, \bar{s}],$$

where B is invertible matrix and the N-dimensional vector-valued function $F \in C^2\left(\mathbb{R}^{5N+1}\right)$. In addition (2.20b) and (2.21) imply that the following Cauchy data $p^0(s)$ and $p^1(s)$

$$p(0, s) = p^0(s), \ p'(0, s) = p^1(s), \ s \in [s_0, \bar{s}]. \tag{2.23}$$

The main question now is: *How to solve the problem (2.22), (2.23) in a stable way?* A stable layer stripping procedure is described in the next two subsections.

2.5 Numerical Method for the Problem (2.22), (2.23)

Consider a uniform partition of the interval $[0, L]$ with the grid step size h,

$$0 = z_0 < z_1 < \cdots < z_n = L,\ h = z_i - z_{i-1}.$$

In each layer $(z_{i-1}, z_i]$ we approximate the vector-valued function $p(z, s)$ with quadratic polynomials

$$p(z,s) :\approx \widetilde{p}_i(z,s) = \frac{(z - z_{i-1})^2}{2} a_i(s) + (z - z_{i-1})\, b_i(s) + c_i(s), \tag{2.24}$$

$$z \in (z_{i-1}, z_i]\,,\ s \in [s_0, \bar{s}]\,.$$

Hence, $c_i(s) = \widetilde{p}_i(z_{i-1}, s)$ and $b_i(s) = \widetilde{p}_i'(z_{i-1}, s)$. By (2.23) functions $b_0(s) = \widetilde{p}_1'(z_0, s) = p^1(s)$ and $c_0(s) = \widetilde{p}_1(z_0, s) = p^0(s)$ are known from the available data for the inverse problem. Functions $b_i(s)$ and $c_i(s)$ are assumed to be known from the previous step of the layer stripping procedure. Hence, the only unknown function in (2.24) is the quadratic term $a_i(s)$. As soon as this term is approximately found, one sets

$$\widetilde{p}_i(z_i, s) := c_{i+1}(s) = \frac{h^2}{2} a_i(s) + h b_i(s) + c_i(s),$$

$$\widetilde{p}_i'(z_i, s) := b_{i+1}(s) = h a_i(s) + b_i(s).$$

We now focus on the procedure of finding an approximation for the quadratic term $a_i(s)$. Consider the weight function $\mathcal{C}_{\lambda,i}(z)$,

$$\mathcal{C}_{\lambda,i}(z) = \exp\left[-\lambda\,(z - z_{i-1})\right],$$

where $\lambda > 1$ is a parameter which will be chosen later. It was proven in [41] that $\mathcal{C}_{\lambda,i}(z)$ is the weight function involved in the Carleman estimate for the operator d^2/dz^2 on the interval (z_{i-1}, z_i). In other words, this is a CWF. Construct the weighted least squares objective function $J_{\lambda,i}$,

$$J_{\lambda,i}(a_i(s)) = \int\limits_{s_0}^{\bar{s}} ds \int\limits_{z_{i-1}}^{z_i} \Pi^2\left[\widetilde{p}_i(z,s), s\right] \mathcal{C}_{\lambda,i}(z)\, dz. \tag{2.25}$$

Let M be a positive number. Consider the bounded set $G(M) \subset C[s_0, \bar{s}]$,

$$G(M) = \left\{ a(s) \in C[s_0, \bar{s}] : \|a(s)\|_{C[s_0,\bar{s}]} \leq M \right\}. \tag{2.26}$$

We search for a minimizer $\bar{a}_i(s) \in G(M)$ of the functional $J_{\lambda,i}$. Hence, (2.24) and (2.26) imply that $\left|\widetilde{p}_i^{(k)}(z,s)\right| \leq M',\ k = 0, 1, 2,$ where $M' = M'(M)$ is a positive constant depending on M. Hence, by the Archela theorem the condition (2.26) implies that the function $\widetilde{p}_i(z,s)$ belongs to a subset of *a priori* chosen compact set (depending on M) in $C^1[z_{i-1}, z_i] \times$

$C[s_0, \bar{s}]$, which correspond well with the above mentioned Tikhonov theorem. Note that our theory does not impose a "smallness" condition on the constant M. In accordance with the Tikhonov concept the constant M should be chosen for a specific set of applied problems under consideration. It was proven in [41]-[44] that the functional $J_{\lambda,i}$ is strictly convex on the set $G(M)$ for an appropriate choice of a sufficiently large parameter $\lambda \geq \lambda_0(M)$. Furthermore, its unique minimizer can be found as the unique solution of an equation with a contractual mapping operator. In addition, the convergence theorem of [41]-[44] implies that this minimizer is close to the value $a_i^*(s) = (p^*)''(z_i, s)$, where the function $p^*(z,s)$ corresponds to the exact solution. We combine these statements in Theorem 2.1 below.

We now formulate convergence theorem for our method assuming that tail functions are small. Suppose that there exists the exact solution $q^*(x,s) \in C^3\left(\bar{\Omega} \times [s_0, \bar{s}]\right)$ of the equation (2.20a) with the Cauchy data (2.20b). We assume first that these Cauchy data are "ideal" ones, i.e., they are given without an error. If such a solution exists, then it is unique, see Theorem 6.5.1 in [41]. Let $p^*(z,s)$ be the vector-valued function $p(z,s)$ which is obtained from $q^*(x,s)$ via the approximation (2.22). Since (2.22) is only an approximation, we assume that the function $p^*(z,s) \in C^3([0,L] \times [s_0, \bar{s}])$ satisfies the following analog of equation (2.24) (recall that we set tails to zero in our convergence theorem)

$$B(p^*)''(z,s) - F\left((p^*)'(z,s), p^*(z,s), \int_s^{\bar{s}} (p^*)'(z,\tau)\,d\tau, \int_s^{\bar{s}} p^*(z,\tau)\,d\tau, 0, 0, s\right) \tag{2.27}$$

$$= \varepsilon(z,s), \quad z \in (0,L), \ s \in [s_0, \bar{s}].$$

And by (2.23) Cauchy data for $p^*(z,s)$ are

$$p^*(0,s) = p^{0*}(s), \ (p^*)'(0,s) = p^{1*}(s). \tag{2.28}$$

We assume that the function $\varepsilon(z,s)$ is sufficiently small (actually, this function is unknown),

$$\|\varepsilon(z,s)\|_{C([0,L]\times[s_0,\bar{s}])} \leq \varepsilon, \tag{2.29}$$

where ε is a small positive number. Because in the reality the Cauchy data (2.23) are always given with an error, we assume that

$$\left\|p^0(s) - p^{0*}(s)\right\|_{C[s_0,\bar{s}]} + \left\|p^1(s) - p^{1*}(s)\right\|_{C[s_0,\bar{s}]} \leq \varepsilon. \tag{2.30}$$

Denote

$$I_0(\lambda, h) = \frac{1 - e^{-\lambda h}}{\lambda} = \int_0^h e^{-\lambda z} dz. \tag{2.31}$$

Let $\widetilde{G}(M)$ be the set of functions $a(s) \in G(M)$ with the $L_2(s_0, \bar{s})-$norm in it. Hence, by (2.26)

$$a \in C[s_0, \bar{s}], \ \|a\|_{C[s_0,\bar{s}]} \leq M, \ \|a\|_{L_2(s_0,\bar{s})} \leq M\sqrt{\bar{s} - s_0}, \ \forall a \in \widetilde{G}(M).$$

We formulate Theorem 2.1 for the case of a general coupled system of ordinary integral differential equations.

Theorem 2.1 [41]-[44]. *Let* $p(z,s) \in C^2\ [0,L] \times C[s_0,\bar{s}]$ *be an* N*-dimensional vector-valued function and* $F \in C^2\left(\mathbb{R}^{5N+1}\right)$ *also be an* N*-dimensional vector-valued function. Let the vector-valued function* $p^*(z,s) \in C^3([0,L] \times C[s_0,\bar{s}])$ *satisfies conditions (2.27)- (2.30) and* $\|p^*(z,s)\|_{C^3[0,L]\times C[s_0,\bar{s}]} \le M/2$. *Then there exists a positive constant* $C = C(M,F,s_0,\bar{s},L,N)$ *and small positive numbers* $\varepsilon_0 = \varepsilon_0(M,F,s_0,\bar{s},L,N)$, $h_0 = h_0(M,F,s_0,\bar{s},L,N)$ *depending only on numbers* $s_0,\bar{s},L,M$ *and the vector-valued function* F *such that if* $\varepsilon \in (0,\varepsilon_0)$, $h \in (0,h_0)$,

$$\lambda \ge \lambda_0 := \frac{C}{\varepsilon},$$

and that the tail function is such that $\|\nabla V\|_{C(\overline{\Omega})} \le \varepsilon$, *then functions*

$$\widetilde{p}_i(z_{i-1},s),\ \widetilde{p}_i'(z_{i-1},s) \in \widetilde{G}(M),\ i = 1,\cdots,n,$$

and all functionals $J_{\lambda,i}$ *are strictly convex on the set* $\widetilde{G}(M)$ *with the property*

$$\frac{1}{I_0(\lambda,h)}\left[J_{\lambda,i}(a+b) - J_{\lambda,i}(a) - J_{\lambda,i}'(a)(b)\right] \ge \rho\|b\|_{L_2(s_0,\bar{s})}^2,\ \forall a, a+b \in \widetilde{G}(M), \tag{2.32}$$

where $J_{\lambda,i}'(a)$ *is the Fréchet derivative of the functional* $J_{\lambda,i}$ *at the point* a, *and the convexity constant* $\rho \in (1/2,1)$. *The unique minimizer* $\widetilde{a}_{\lambda,i} \in \widetilde{G}(M)$ *of the functional* $J_{\lambda,i}$ *is an interior point of the set* $\widetilde{G}(M)$ *and can be found as the solution of the equation*

$$a = \Phi_{\lambda,i}(a),\ i = 1,\cdots,n \tag{2.33}$$

with the contraction mapping operator $\Phi_{\lambda,i} : \widetilde{G}(M) \to \widetilde{G}(M)$ *and*

$$\|\widetilde{a}_{\lambda_1,i} - \widetilde{a}_{\lambda_2,i}\| \le \frac{C}{\lambda_0},\ \forall \lambda_1,\lambda_2 \ge \lambda_0,\ i = 1,\cdots,n. \tag{2.34}$$

Furthermore, the following stability and convergence estimate holds

$$\max_{1\le i\le n}\ \sup_{z\in(z_{i-1},z_i)} \|D_z^r[\widetilde{p}_i(z,s) - p^*(z,s)]\|_{C([s_0,\bar{s}])} \le C(\varepsilon + h),\ r = 0,1,2. \tag{2.35}$$

Remark. We assume that the tail function is sufficiently small because it is indeed small for sufficiently large truncation pseudo frequency $\bar{s}$, see (2.16). The function $I_0(\lambda,h)$ (see (2.31)) plays the role of a calibration factor here. The estimate (2.34) means that the minimizers are “almost” independent on the parameter λ, as long as this parameter is sufficiently large. The estimate (2.35) implies that the difference between the exact solution and the one obtained by the above method is small as soon as parameters ε and h are sufficiently small. It is important that estimates (2.34), (2.35) are actually confirmed in our numerical experiments, see section 5.

A peculiar question of Theorem 2.1 is that the strict convexity of functionals $J_{\lambda,i}$ is guaranteed only on the bounded set $\widetilde{G}(M)$ rather than on the whole space $L_2(s_0,\bar{s})$. Hence, it seems to be, at least at the first glance, that in a practical use of a gradient-like method one should make sure that points resulting from iterations of such a method belong to the interior of $\widetilde{G}(M)$, which would complicate things. However, Theorems 1.2 and 1.3 of [40] ensure that one should not be concerned with the latter. These theorems basically state that if the exact solution belongs to the set $\widetilde{G}(M/2)$ and the starting point is also chosen on this set, then the distance between the sequential points obtained by the gradient method and the true minimizer of a strictly convex functional is decreasing, up to a certain level, as the number of iterations of the gradient method is increasing. This level, in turn is determined by the level ε of the error in the data. Thus, assuming that our exact solution p^* is such that (Theorem 2.1) $\|p^*(z,s)\|_{C^3([0,L]\times[s_0,\bar{s}])} \leq M/2$ and starting iterations of a gradient-like method from a point $\widehat{a}_i(s) \in \widetilde{G}(M/2)$, one is guaranteed that consecutive iterations will not lead outside of $\widetilde{G}(M)$.

2.6 A crucial role of Carleman Weight Functions

It is important for the understanding of the convexification to explain the role of the Carleman Weight Functions. Let the vector function $p(z,s) \in C^3[0,L] \times C[s_0,\overline{s}]$ be the solution of the Cauchy problem (2.22), (2.23). By the Taylor formula

$$p(z,s) = p''(z_{i-1},s)\frac{(z-z_{i-1})^2}{2} + p'(z_{i-1},s)(z-z_{i-1}) + p(z_{i-1},s)$$

$$+\frac{1}{2}\int\limits_{z_{i-1}}^{z} p'''(\xi,s)(z-\xi)^2\,d\xi, \quad (z,s) \in (z_{i-1},z_i] \times [s_0,\overline{s}].$$

Hence, the quadratic approximation (2.24) provides $O(z-z_{i-1})$ error for the equation (2.22) for $(z,s) \in (z_{i-1},z_i] \times [s_0,\overline{s}]$ as $(z-z_{i-1}) \to 0^+$. Recall that $z_i - z_{i-1} = h$. Hence, if the CWFs would not be present, then after considering $n = L/h$ layers, one would have the total error of at least $O(nh) = O(L)$, which is large. Denote $E_i(z,s)$ the error function due to the approximation (2.24) on the layer $(z_{i-1},z_i]$. Hence,

$$E_i(z,s) = (z-z_{i-1})\,\widetilde{E}_i(z,s), \text{ where } \left|\widetilde{E}_i(z,s)\right| \leq M \text{ for } (z,s) \in [z_{i-1},z_i] \times [s_0,\overline{s}]. \quad (2.36)$$

Denote

$$F_i(s) = Q\left(b_i(s), c_i(s), \int\limits_s^{\overline{s}} b_i(\tau)\,d\tau, \int\limits_s^{\overline{s}} c_i(\tau)\,d\tau, z_{i-1}, s\right) :=$$

$$Q\left(\widetilde{p}'(z_{i-1},s), \widetilde{p}(z_{i-1},s), \int\limits_s^{\overline{s}} \widetilde{p}'(z_{i-1},\tau)\,d\tau, \int\limits_s^{\overline{s}} \widetilde{p}(z_{i-1},\tau)\,d\tau, z_{i-1}, s\right).$$

Substituting (2.24) in (2.22) and using Taylor formula, one can represent the equation (2.22) in the form

$$a_i(s) - F_i(s) - (z - z_{i-1}) H_i \left(z, s, a_i(s), \int_s^{\bar{s}} a_i(\tau)\, d\tau \right) - (z - z_{i-1}) \widetilde{E}_i(z,s) = 0, \quad (2.37)$$

where H_i is a C^1-function of its variables. One can easily prove that

$$\int_0^h z\,|f(z)|\, e^{-\lambda z} dz \leq \frac{1}{\lambda} \left[h e^{-\lambda h} + I_0(\lambda, h) \right] \|f\|_{C[0,h]}, \forall f \in C[0,h], \quad (2.38)$$

where $I_0(\lambda, h)$ was introduced in (2.31).

Suppose that we choose such values of the parameter λ that $\lambda h > 1$. Since $h/\lambda = (\lambda h)/\lambda^2$, then

$$\frac{1}{I_0(\lambda,h)} \int_0^h z\,|f(z)|\, e^{-\lambda z} dz \leq \frac{2}{\lambda} \|f\|_{C[0,h]}, \forall f \in C[0,h], \quad (2.39)$$

Hence, by (2.36)

$$\frac{1}{I_0(\lambda,h)} \int_{z_{i-1}}^{z_i} (z - z_{i-1}) \left| \widetilde{E}_i(z,s) \right| \mathcal{C}_{\lambda,i}(z)\, dz \leq \frac{2M}{\lambda}. \quad (2.40)$$

Also,

$$\frac{1}{I_0(\lambda,h)} \int_{z_{i-1}}^{z_i} (z - z_{i-1})^2 \left| \widetilde{E}_i(z,s) \right|^2 \mathcal{C}_{\lambda,i}(z)\, dz \leq \frac{2M^2 h}{\lambda}. \quad (2.41)$$

Thus, it follows from (2.39)-(2.41) that after $n = L/h$ layers the error due to the quadratic approximation will be of the order of

$$O\left(\frac{1}{\lambda h}\right).$$

Choosing $\lambda = \lambda(h, \varepsilon)$ such that

$$\lambda > \frac{1}{h^2},$$

we obtain that, regardless on the approximation error $E_i(z,s)$ in (2.37), the estimate (2.35) of the convergence rate still holds.

Summary

It is shown both in this subsection and in Theorem 2.1 that the role of Carleman Weight Functions is threefold. They ensure: (1) the stability of the layer stripping procedure, (2) the convergence of the convexification method and (3) the strict convexity of the residual functionals $J_{\lambda,i}$.

2.7 Inversion

Suppose that functions

$$\partial_z^r \widetilde{p}(z,s) := \partial_z^r \widetilde{p}_i(z,s),\ (z,s) \in (z_{i-1}, z_i] \times (s_0, \bar{s}),\ i = 1, \cdots, n,\ r = 0, 1, 2 \tag{2.36}$$

are found by the above layer stripping procedure and tails are also approximated. To approximate the target coefficient $c(x)$, we use the backwards calculation. First, we calculate the function $\widetilde{v}(x_1, x_2, z, s)$ and its corresponding derivatives by (2.21) and (2.18). Finally, we approximate the coefficient $c(x)$ via calculating the left hand side of (2.36) at $s := s_0$. In principle, one can use any value of s in (2.36). However, our computational experience shows that the best value is the lowest one $s := s_0$. An explanation of this is that at $s := s_0$ the truncation at $s = \bar{s}$ of the integral (2.18) causes the least error.

2.8 The first numerical result in 2-D

We now present the first 2-D numerical result, which was obtained by the convexification, and which has impressed the scientific community (subsection 1.2), when it was published in [1] (also, see [2]). This result was obtained by Dr. A. Timonov. Although it seems at the first glance that this result is restricted only to a medical application, but actually since we work with the back-reflected data here, Army applications are quite feasible. The 2-D inverse problem of the determination of the unknown electric conductivity coefficient $\sigma(x,y)$ in the equation

$$u_{xx} + u_{zz} - i\omega\mu\sigma(x,z)\,u = 0,$$

was solved. Here ω is the modulated frequency and $\mu = 4\pi \cdot 10^7 H/m$ is the magnetic permeability of the vacuum. The problem of microwave imaging of the human abdomen was considered. The realistic case of the frequency sweep $\omega \in 2\pi \cdot [0.5, 10]\ GHz$ was used. Since the maximum sensitivity depth of the back-reflected microwave signal is 6 centimeters (see reference [16] in the annual report [21]), the X-ray Computed Tomography image of the abdomen was re-scaled to 6 cm thickness. In data simulations for the forward problem a realistic range of the parameter $\sigma(x,z) \in [0.4, 4.8]$ *Siemens/meter* was used. Namely, different values of this parameter were assigned to different parts of the CT image: highest values were assigned to the white areas and lowest to the white ones. Next, those values were linearly interpolated for the rest. Instead of the point source the initializing plane wave $e^{i\omega z}$ was used.

This plane wave has propagated downwards (positive direction of the z-axis) and then was scattered when entering the heterogeneous medium. Measurements of the back-reflected wave were modeled on the top side of the image. Additive random noise of 1%, 5% and 10% was added to the data. The inverse problem was solved for 15 realizations of the noisy data and then averaged the resulting functions $\sigma(x,z)$. Trigonometric series were used in (2.21) with $\phi_j(x) = \sin(k\alpha j)$ and also $\phi_j(x) = \cos(k\alpha j)$, where the parameter α depends on the size of the medium in the horizontal direction (to make sure that these functions are orthogonal in L_2). We have used $k \in [0, N]$ with $N \in [10, 20]$. Significant differences in

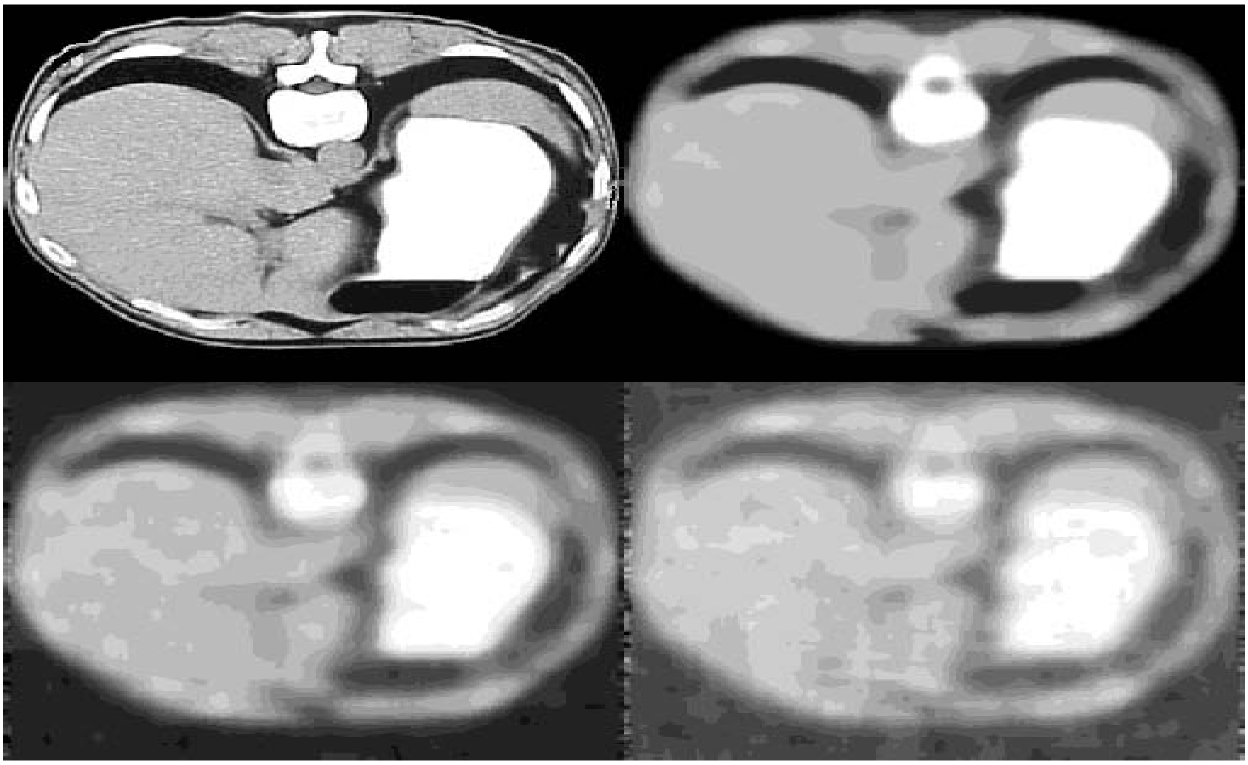

Figure 1: The original (top left) and reconstructed images of the function $\sigma(x, z)$ **via the convexification**. The plane wave falls from the above and measurements of the backreflected signal were also simulated at the top side of the square. The top right image represents the reconstruction result at the 1% noise in the data, the bottom left and bottom right images correspond to 5% and 10% noise respectively.

images with the change of N were not observed. As to the tail function $V(z, z)$, we have taken the one, which corresponds to the uniform background, i.e., the background outside of the heterogeneous medium. This background was assumed to be known, according to the above statement of the inverse problem. Figures 1 and 2 display the computational results.

3 The Second Numerical Implementation of the Convexification

Results of this and next sections represent the joint effort of the Postdoctoral Research Associate Dr. J. Xin and the PI [3-6]. Dr. Xin has been working on a new numerical implementation of the convexification. Dr. Xin has been fully supported by this grant from 8/15/05 to 6/30/07. His effort has been focused on the development of new numerical ideas of the convexification and their numerical implementation. In these publications a

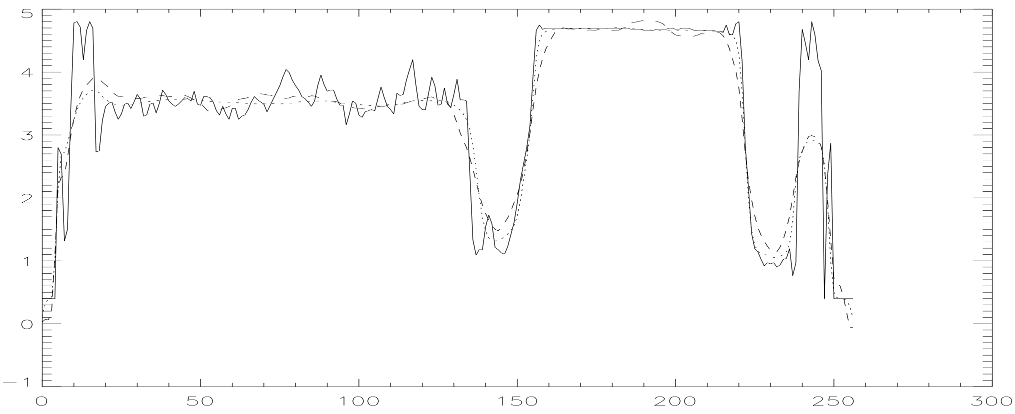

Figure 2: The cross-section of images of Figure 1 by horizontal line through the middle. Solid line corresponds to the original image. Dotted and dashed lines correspond to images at 1% and 5% noise respectively.

simplified mathematical model of imaging of the spatially distributed dielectric constant in antipersonnel land mines was treated by the convexification.

Compared with previous works [1,2] on the convexification algorithm, four new ingredients of the second numerical implementation are: (I) we minimize strictly convex functionals directly for each generic layer rather than via the solution of the equivalent equation (2.33) with the contraction mapping operator, (II) a local basis consisting of cubic B-splines is employed in the spatial approximation instead of the global trigonometric basis [1], [2], hence, enabling sharper resolution of the reconstructed material property at the interface between the inclusion and the background, (III) tails in truncated integrals (2.18) are fitted in to compensate the missing information, and (IV) we approximate the functions which depend on the pseudo-frequency s by Legendre polynomials, thus calculating the integrals involving pseudo-frequency explicitly rather than numerically. An advantage of the direct minimization of the convex functionals over solving the operator equation (2.33) is that the time-consuming pre-programming and pre-computational effort to derive the operator equation is avoided.

In addition to the new ingredients of the numerical implementation, a systematic, comparative analysis of various aspects on the convexification algorithm was performed [4]. No such study has been performed before, and the parameters in the algorithm were taken in an *ad hoc* manner. Certainly the comparative study is useful for the further development of the convexification algorithm. Throughout this section we use notation δz for h, the thickness of each layer in the layer stripping procedure of the convexification.

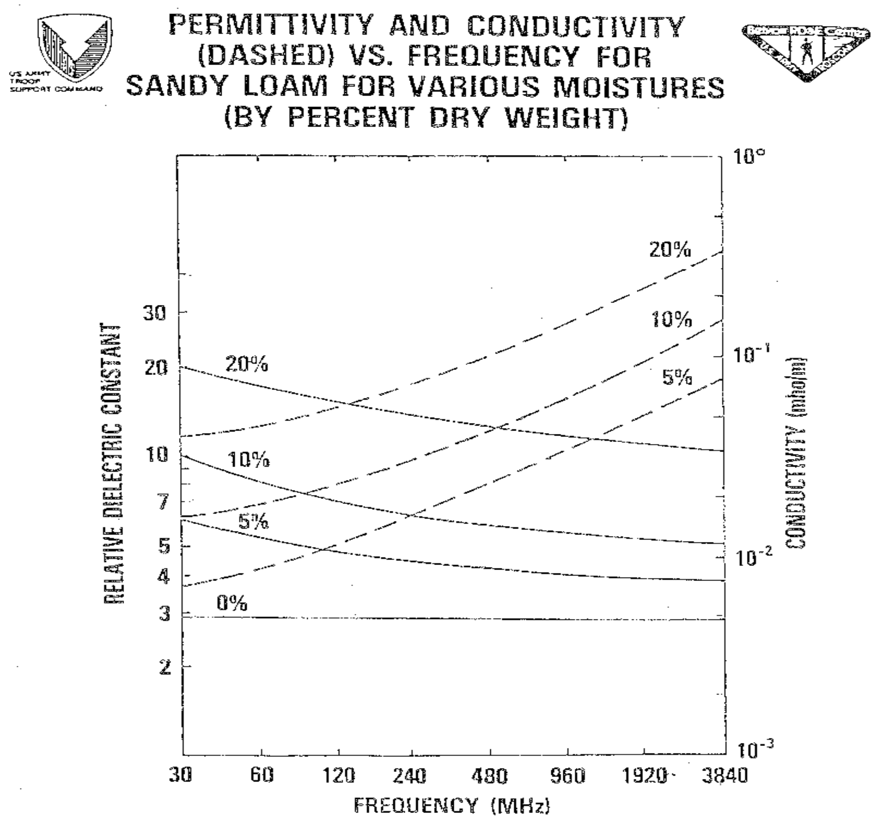

Figure 3: Dielectric permittivity and electric conductivity constants in soil.

3.1 A simplified mathematical model of imaging of antipersonnel land mines

We present a mathematical model for our Coefficient Inverse Problem - identification of antipersonnel land mines. We work with a simplified 2D model and consider realistic ranges of parameters. We neglect the irregularities of ground surface. In order to avoid difficulties of solutions of forward and inverse problems at the air-ground interface, we assume that the dielectric permittivity ε of the media is continuous everywhere. Further, we take no account of the electric conductivity of the media. This can be justified in the case of dry soil, whose electric conductivity is small, see Figure 3.

Suppose a pulse generating a polarized electric field occurs at the point $x_0(0, -\xi)$ when the initial time is $t = 0$, where $\xi = const. > 0$. The following hyperbolic equation can be derived from the Maxwell equations

$$-\mu\varepsilon(x)u_{tt} + \Delta u = 0, \ (x,t) \in \mathbb{R}^2 \times \mathbb{R}^+, \tag{3.1}$$

$$u\left(x,0\right)=0,\ u_t\left(x,0\right)=\delta\left(x-x_0\right). \tag{3.2}$$

In (3.1), (3.2) the function $u(x,t)$ is one component of the electric field and the parameter $\mu = 4\pi \times 10^{-7}\left(\frac{Henry}{m}\right)$ is the magnetic permeability in free space and

$$\varepsilon = \varepsilon_0 \varepsilon_r(x) \tag{3.3}$$

is the dielectric permittivity, where $\varepsilon_0 \approx 8.854 \times 10^{-12}\left(\frac{Farad}{m}\right)$ is the dielectric permittivity of free space and $\varepsilon_r(x)$ is the dimensionless relative dielectric permittivity of the medium.

In both dry soil and trinitrotoluene (TNT) we have $\varepsilon_r \approx 2.9$, see Figure 3. We are interested in the identification of antipersonnel plastic mines, which is more difficult in a practical scenario since the metal component in them is very small. Thus, we need to find one parameter inside the mine which can give us sufficient contrast with the surrounding dry soil. It is well known that a noticeable part of the volume of any mine is filled with air and $\varepsilon_r = 1$ for the air. Since the mine does not wholly consist of air, it is reasonable to assume that $\varepsilon_r = 1.5$ inside the mine, which is about the average value of the coefficient ε_r within the mine. Therefore, for all our computation we assume

$$\varepsilon_r(x) = \begin{cases} 2.9 \text{ outside mines} \\ 1.5 \text{ inside mines} \end{cases} \tag{3.4}$$

The sizes of antipersonnel mines vary between 5 cm and 10 cm, and usually they lay at a small depth underneath the ground, not exceeding 10 cm. Hence, we model mines as disks of radius 5 cm which are located in the range $z \in [0, 9]$ cm.

If we could identify the coefficient $\varepsilon_r(x)$, then points whose values are close to 1.5 will be those inside or close to the mine. Thus, finding an approximation for this coefficient via solution of the inverse problem formulated below could provide one with a useful information about the location and relative dielectric permittivity of the mine. This value, in turn, might in the future serve as one parameter in a 'classifier' procedure, which would distinguish mines from the clutter.

Consider the Laplace transform of the function $u(\mathbf{x}, t)$

$$w(x,s) = \int\limits_0^\infty u(x,t)e^{-st}dt.$$

Since the parameters μ and ε_0 are rather small, by combining the parameter s we re-scale these two parameters and introduce a new variable $\kappa := s\sqrt{\mu\varepsilon_0}$, which we call "pseudo-frequency". Equation (3.1) with the initial condition (3.2) is transformed into

$$-\Delta w + \kappa^2 \varepsilon_r(x) w = \delta\left(x - x_0\right),\ x \in \mathbb{R}^2, \tag{3.4}$$

$$\lim_{|\mathbf{x}| \to \infty} w(x,\kappa) = 0. \tag{3.5}$$

We formulate our inverse problem, termed **IP**.

Inverse Problem (IP). Consider a rectangle $\Omega \subset \mathbb{R}^2$

$$\Omega := \{-A < x < A,\ z \in (0, L)\},\ A, L > 0.$$

Suppose the coefficient $\varepsilon_r(x)$ of the equation (3.4) is unknown in Ω and is a known positive constant in $\mathbb{R}^2 \diagdown \Omega$. Determine the relative dielectric permittivity $\varepsilon_r(x)$ for $x \in \Omega$, assuming the following two functions $\varphi(x, \kappa)$ and $\psi(x, \kappa)$ are known for a single source position x_0

$$w(x, 0, \kappa) = \varphi(x, \kappa),\ w_z(x, 0, \kappa) = \psi(x, \kappa),\ \forall (x, \kappa) \in (-A, A) \times [\kappa_0, \bar{\kappa}]. \tag{3.6}$$

We need to decide the lower limit κ_0 and upper limit $\bar{\kappa}$ of pseudo-frequency κ for our inverse problem. To find an appropriate constant $\bar{\kappa}$, we compute solutions of the forward problem (3.4), (3.5) for different values of the parameter $\kappa > 0$ and determine such a value $\kappa := \bar{\kappa}$, beyond which the asymptotic behavior, i.e., exponential decay, of the function $w(x, \kappa)$ holds, see (2.11). Thus, we identify such large values of κ for which

$$\ln w(x, \kappa) = v(x, \kappa) \approx l_1(x)\kappa + l_0(x) \tag{3.7}$$

for many points $\mathbf{x} \in \overline{\Omega}$. The function $v(x, \kappa)$ looks like a straight line with respect to κ for $\kappa > \bar{\kappa}$. We solve the forward problem on a large domain $\Xi := \{-6 \le x, z \le 6\}$ using the finite element package - COMSOL $Multiphysics^{TM}$ version 3.2. Zero Dirichlet boundary is imposed on the boundary $\partial\Xi$. We use triangular elements with Lagrange cubic basis. We obtain $\bar{\kappa} = 10$ after rounding to integers. One is free to choose the lower bound κ_0. We may take a smaller value that is close to $\bar{\kappa}$, e.g., $\kappa_0 = \{8, 9\}$. The influence of the lower limit κ_0 on the resolution of the reconstructed unknown coefficient ε_r was also studied in [4].

3.2 Tails

Recall that by (2.18)

$$\widetilde{v}(x, \kappa) = -\int_{\kappa}^{\overline{\kappa}} q(x, \tau)\, d\tau + V(x), \tag{3.9}$$

where $V(x) = \widetilde{v}(x, \overline{\kappa})$ is the so-called "tail function". This function is unknown and we now describe the procedure of approximating it. While in [1,2] the tail function was taken from the uniform background (subsection 2.8), we use here a different procedure to approximate this function. First, we represent this function similarly with (2.21),

$$D_x^\alpha V(x_1, x_2, z) \approx D_x^\alpha \sum_{j=1}^{N} V_j(z)\, \phi_j(x_1, x_2),\ x \in \overline{\Omega},\ |\alpha| \le 2. \tag{3.10}$$

Below in this section we describe a procedure of approximating functions $V_j(z), V_j'(z), V_j''(z)$.

3.2.1 Piecewise constant approximation

From (2.11) and (2.15) the asymptotic behavior of the function $\widetilde{v}(x,\kappa) = \ln w(x,\kappa)/\kappa^2$ at $\kappa \to \infty$ is

$$\widetilde{v}(x,\kappa) = \frac{f_1(x)}{\kappa} + \frac{g_1(x)}{\kappa^2} + O\left(\frac{1}{\kappa^3}\right), \ \kappa \to \infty, \tag{3.11}$$

where functions $f_1(x)$ and $g_1(x)$ are unknown because the coefficient $\varepsilon_r(x)$ is unknown. Therefore, they should be found approximately. These two functions are connected with each other by the relation $g_1(x) = -\ln(-4\pi f_1(x))$. However, we do not use this connection explicitly in this study. It follows from (3.11) and (2.21) that

$$D_x^\alpha D_\kappa^\beta \widetilde{v}(x,\kappa) = D_x^\alpha D_\kappa^\beta \left(\frac{f_1(x)}{\kappa} + \frac{g_1(x)}{\kappa^2}\right) + O\left(\frac{1}{\kappa^3}\right), \ \kappa \to \infty, \ |\alpha| \le 2, \ \beta = 0,1.$$

We approximate functions $f_1(x)$, $g_1(x)$ sequentially layer-by-layer ignoring the higher order term $O(1/\kappa^3)$. We approximate functions $f_1(x)$, $g_1(x)$ as constants with respect to z in each thin layer $z \in [z_{i-1}, z_i)$, i.e.,

$$f_1(x) := f_1(x,y,z_{i-1}), \ g_1(x) := g_1(x,y,z_{i-1}), \ z \in [z_{i-1}, z_i). \tag{3.12}$$

We also set

$$\partial_z^\beta f_1(x) := \partial_z^\beta f_1(x,y,z_{i-1}), \ \partial_z^\beta g_1(x) := \partial_z^\beta g_1(x,y,z_{i-1}), \ z \in [z_{i-1}, z_i), \ \beta = 1,2. \tag{3.13}$$

By (3.9), (3.10) and (2.21)

$$\widetilde{v}(x,s) = -\sum_{j=1}^{N} \phi_j(x,y) \int_{\kappa}^{\overline{\kappa}} p_j(z,\tau)d\tau + \sum_{j=1}^{N} V_j(z)\phi_j(x,y) = \sum_{j=1}^{N} \widetilde{v}_j(z,s)\,\phi_j(x,y),$$

where

$$\widetilde{v}_j(z,s) = -\int_{\kappa}^{\overline{\kappa}} p_j(z,\tau)d\tau + V_j(z). \tag{3.14}$$

Furthermore, from (3.11)-(3.13) we assume that for a sufficiently large number $\widehat{\kappa} \in (\kappa_0, \overline{\kappa})$

$$\widetilde{v}_j(z,\kappa) = \frac{k_j(z_{i-1})}{\kappa} + \frac{t_j(z_{i-1})}{\kappa^2}, \ z \in [z_{i-1}, z_i), \ \kappa \in (\widehat{\kappa}, \overline{\kappa}), \tag{3.15}$$

$$\partial_z^\gamma \widetilde{v}_j(z,\kappa) = \frac{k_j^{(\gamma)}(z_{i-1})}{\kappa} + \frac{t_j^{(\gamma)}(z_{i-1})}{\kappa^2}, \ z \in [z_{i-1}, z_i), \ \kappa \in (\widehat{\kappa}, \overline{\kappa}), \ \gamma = 1,2. \tag{3.16}$$

Once numbers $k_j^{(\gamma)}(z_{i-1})$ are found, we set

$$V_j^{(\gamma)}(z_{i-1}) := \frac{k_j^{(\gamma)}(z_{i-1})}{\overline{\kappa}}, \gamma = 0,1,2.$$

Suppose we found all numbers

$$k_j\left(z_{i-1}\right),\ t_j\left(z_{i-1}\right),\ k_j^{(\gamma)}\left(z_{i-1}\right),\ t_j^{(\gamma)}\left(z_{i-1}\right). \tag{3.17}$$

Thus, by (3.11)-(3.16) we set

$$D_{(x,y)}^{\alpha}\widetilde{v}\left(x,\kappa\right):=\sum_{j=1}^{N}\left[-\int_{\kappa}^{\overline{\kappa}}p_j(z,\tau)d\tau+\frac{k_j\left(z_{i-1}\right)}{\overline{\kappa}}+\frac{t_j\left(z_{i-1}\right)}{\overline{\kappa}^2}\right]D_{(x,y)}^{\alpha}\phi_j\left(x,y\right) \tag{3.18}$$

$$:=\sum_{j=1}^{N}\widetilde{v}_j(z,\kappa)D_{(x,y)}^{\alpha}\phi_j\left(x,y\right),\ z\in\left[z_{i-1},z_i\right),\ \kappa\in\left[\kappa_0,\overline{\kappa}\right],\ |\alpha|\leq 2,$$

$$\partial_z^{\gamma}\widetilde{v}\left(x,\kappa\right):=\sum_{j=1}^{N}\left[-\int_{\kappa}^{\overline{\kappa}}\partial_z^{\gamma}p_j(z,\tau)d\tau+\frac{k_j^{(\gamma)}\left(z_{i-1}\right)}{\overline{\kappa}}+\frac{t_j^{(\gamma)}\left(z_{i-1}\right)}{\overline{\kappa}^2}\right]\phi_j\left(x,y\right) \tag{3.19}$$

$$:=\sum_{j=1}^{N}\partial_z^{\gamma}\widetilde{v}_j(z,\kappa)\phi_j\left(x,y\right),\ z\in\left[z_{i-1},z_i\right),\ \kappa\in\left[\kappa_0,\overline{\kappa}\right],\ \gamma=1,2.$$

We end up with finding the approximate values in (3.17).

3.2.2 Approximation of numbers in (3.17)

We consider a step-by-step procedure to find these numbers.

Step 1. Consider the first layer $z\in\left[0,z_1\right]$, with $z_0=0,z_1=\delta z$.

We compute functions $\widetilde{v}_j\left(0,\kappa\right),\ \partial_z^{\gamma}\widetilde{v}_j\left(0,\kappa\right)$ from the expansions

$$\widetilde{v}\left(x,y,0,\kappa\right)=\sum_{j=1}^{N}\widetilde{v}_j\left(0,\kappa\right)\phi_j(x,y),$$

$$\partial_z^{\gamma}\widetilde{v}\left(x,y,0,\kappa\right)=\sum_{j=1}^{N}\partial_z^{\gamma}\widetilde{v}_j\left(0,\kappa\right)\phi_j(x,y),\ \gamma=1,2.$$

Since the functions $\widetilde{v}\left(x,y,0,\kappa\right),\widetilde{v}_z\left(x,y,0,\kappa\right)$ are known, functions $\widetilde{v}_j\left(0,\kappa\right),\ \partial_z\widetilde{v}_j\left(0,\kappa\right)$ can be obtained by solving a system of linear equations. For the second derivatives $\partial_z^2\widetilde{v}_j\left(0,\kappa\right)$, we assume the coefficient $c(x)$ is known at the surface of measurements $z=0$, which is often the case in practice. So the second derivatives $\partial_z^2\widetilde{v}_j\left(0,\kappa\right)$ can be computed from equation (2.22).

To approximate numbers in (3.17), we combine (3.15), (3.16) and apply the least squares minimization in L^2, i.e.,

$$\min_{k_j^{(\gamma)}(z_0),t_j^{(\gamma)}(z_0)}\int_{\widehat{\kappa}}^{\overline{\kappa}}\left[\partial_z^{\gamma}\widetilde{v}_j\left(0,\kappa\right)-\frac{k_j^{(\gamma)}\left(z_0\right)}{\kappa}-\frac{t_j^{(\gamma)}\left(z_0\right)}{\kappa^2}\right]^2d\kappa,\ \gamma=0,1,2, \tag{3.20}$$

where $k_j^{(0)}(z_0) := k_j(z_0), t_j^{(0)}(z_0) := t_j(z_0)$. By imposing the critical condition, the vector $\left(k_j^{(\gamma)}(z_0), t_j^{(\gamma)}(z_0)\right)$, the minimizers of the integral (3.20) is the solution of the 2×2 system of linear algebraic equations

$$ak_j^{(\gamma)}(z_0) + bt_j^{(\gamma)}(z_0) = \int_{\widehat{\kappa}}^{\overline{\kappa}} \frac{\partial_z^\gamma \widetilde{v}_j(0,\kappa)}{\kappa} d\kappa, \tag{3.21}$$

$$bk_j^{(\gamma)}(z_0) + ct_j^{(\gamma)}(z_0) = \int_{\widehat{\kappa}}^{\overline{\kappa}} \frac{\partial_z^\gamma \widetilde{v}_j(0,\kappa)}{\kappa^2} d\kappa, \tag{3.22}$$

where

$$a = \int_{\widehat{\kappa}}^{\overline{\kappa}} \frac{d\kappa}{\kappa^2} = \frac{1}{\widehat{\kappa}} - \frac{1}{\overline{\kappa}},\ b = \int_{\widehat{\kappa}}^{\overline{\kappa}} \frac{d\kappa}{\kappa^3} = \frac{1}{2\widehat{\kappa}^2} - \frac{1}{2\overline{\kappa}^2},\ c = \int_{\widehat{\kappa}}^{\overline{\kappa}} \frac{d\kappa}{\kappa^4} = \frac{1}{3\widehat{\kappa}^3} - \frac{1}{3\overline{\kappa}^3}.$$

The determinant of the system (3.21), (3.22) does not vanish. With vectors $V(z_0) := (k_1(z_0), ..., k_N(z_0))/\overline{\kappa}, V'(z_0) := (k_1'(z_0), ..., k_N'(z_0))/\overline{\kappa}$ computed, we can minimize the functional $J_\lambda^1(a_1(\kappa))$ for the first layer. Functions $p_j(z_1,\kappa)$, $p_j'(z_1,\kappa)$ and $p_j''(z_1,\kappa)$ can be evaluated once the solution is obtained.

Step 2. Consider the second layer $z \in [z_1, z_2]$. Denote $k_j^{(0)}(z_1) = k_j(z_1), t_j^{(0)}(z_1) = t_j(z_1)$. From (3.15) and (3.16)

$$\partial_z^\gamma \widetilde{v}_j(z_1,\kappa) = \frac{k_j^{(\gamma)}(z_1)}{\kappa} + \frac{t_j^{(\gamma)}(z_1)}{\kappa^2},\ z \in [z_{i-1}, z_i),\ \kappa \in [\widehat{\kappa}, \overline{\kappa}],\ \gamma = 0,1,2.$$

The same procedure can be applied to find the approximate values of $k_j^{(\gamma)}(z_1), t_j^{(\gamma)}(z_1)$, i.e., we minimize the least squares functional in $L^2(\widehat{\kappa}, \overline{\kappa})$,

$$\min_{k_j^{(\gamma)}(z_1), t_j^{(\gamma)}(z_1)} \int_{\widehat{\kappa}}^{\overline{\kappa}} \left[\partial_z^\gamma \widetilde{v}_j(z_1,\kappa) - \frac{k_j^{(\gamma)}(z_1)}{\kappa} - \frac{t_j^{(\gamma)}(z_1)}{\kappa^2}\right]^2 d\kappa$$

and obtain a system similar to (3.12), (3.22). Once the numbers $k_j^{(\gamma)}(z_1), t_j^{(\gamma)}(z_1)$ are found, tails $V(z_1)$ and their derivatives $V'(z_1), V''(z_1)$ are calculated from (3.21), (3.22) as

$$V^{(\gamma)}(z_1) = \frac{(k_1(z_0), ..., k_N(z_0))}{\overline{\kappa}}, \gamma = 0,1,2.$$

Other layers are treated similarly.

4 Comparative Analysis

In order to fully investigate the numerical performance of the second implementation of the convexification algorithm, we conduct in this section a comparative study on ten aspects of this algorithm [4]. It is carried out with three configurations for the coefficient inverse problem. Recall that we consider the case when mine-like inclusions are located in a dry soil (subsection 3.1). The simplest case is with the homogeneous background medium without mines. One realistic configuration is with a single mine, the one-mine case. The other is with two inclusions and we consider a stone and a mine as the inclusions, the stone-mine case. So, our result below show that we can differentiate between stones and mines on our images. The stone and mine are of the circular shape with different radius, $r_{stone} = 4.5$cm and $r_{mine} = 5$cm. Assuming that the stone is "more wet" than the dry soil, we model the stone with the same relative dielectric permittivity as the wet soil with 5% moisture (Figure 3), thus, $\varepsilon_r^{stone} = 4$. For the case with a single mine, the center of the mine is located at the point $P_m(30cm, 7.5cm)$, whereas for the stone-mine case, the centers of the mine and the stone are at the point $P_m(40cm, 7.5cm)$ and the point $P_s(-40cm, 7.5cm)$, respectively.

4.1 Efficiency

All our computation was performed on a workstation with the CPU of AMD Athlon(tm) 64 Processor 3500+, 2.2 GHz clock speed, 4 GB of RAM, 512 KB cache size, running Novell Client for Linux v1.0. The code is written in C, optimized up to three levels, and the compiler is gcc-3.4.6. To demonstrate the efficiency of the convexification algorithm with our new implementation, we consider the two realistic configurations. For the case with a single mine, we use 35 cubic B-splines for functions $\phi_j(x)$ with layer size $\delta z = 0.005$, $\kappa \in [9, 10]$ and apply Legendre polynomials of degree 5 for pseudo-frequency approximation, and add 2% noise in the input data. The code is run up to 16 layers and the iteration stops when the gradient of the objective function J drops below the threshold $\delta = 0.01$. The computational time for the run is 1 minute and 14 seconds. For the configuration with a stone and a mine, we apply 39 cubic B-splines for functions $\phi_j(x)$ and all other parameters share their corresponding values in the previous case with a single mine. It takes 1 minute and 38 seconds for the code to run up to 16 layers. Thus, the total depth underneath the ground is 8 cm, which is a reasonable depth for antipersonnel land mines.

On each generic Layer #i, the error of the minimizer $\bar{\mathbf{a}}_i$ from the minimization procedure is bigger than that with a tight threshold, e.g., $\delta = 0.001$, or $\delta = 0.0001$. However, the reconstructed unknown coefficient ε_r for each configuration is still good, which is shown in Figure 4. We should point out that although our computations were performed on a computer with a large memory, i.e., 4GB of RAM, the compiled code, which is rather small, can be run on a computer with normal amount of memory, e.g., 512 Mb of RAM, or even smaller size, e.g., 256 Mb of RAM. The memory requirement for the code to run is rather low. The numbers of degrees of freedom for the two cases are 210 and 234, respectively. This points towards a possibility for the convexification to work in *real time* to detect and image

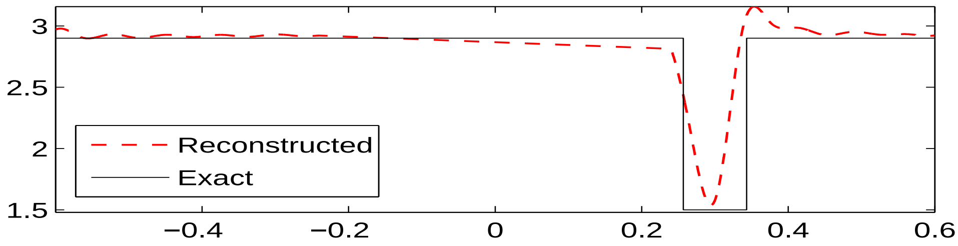

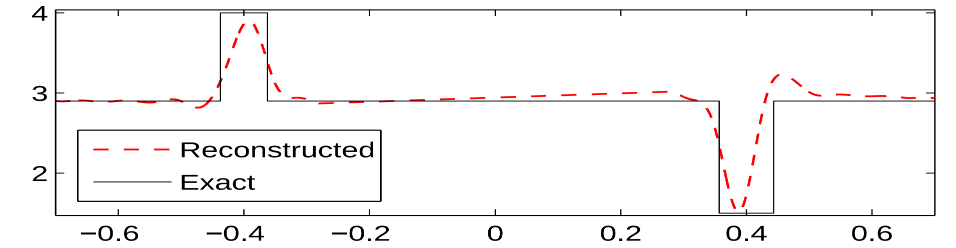

Figure 4: Reconstructed ε_r for the efficiency study at z =4.75 cm, top: the configuration with a single mine, bottom: the configuration with a stone and a mine.

antipersonnel land mines in the field.

The solution of the forward problem has a singularity at the point $x_0 = (0, -10cm)$, where the source is located. This influences the sensitivity region for the inverse problem. Numerical experiences show that the reconstructed unknown coefficient ε_r is not sensitive near the singularity, i.e., near the center of the domain. We have also investigated the case when the central part is imaged [5]. In this case the resulting image has a small dent in the center by the presence of the singularity near the source location. We have explained this dent in [5]. Figure 5 represents a typical image when the central part is in. Unless otherwise mentioned explicitly, each graph below, is the cross-sectional view of the reconstructed unknown coefficient ε_r along x-axis without the central part at a specific value in z direction.

4.2 Stopping Criterion

On each generic Layer #i, the steepest descent method is applied to find the unique minimizer of the weighted least squares objective function J_λ^i. The iterative solver has the form

$$\mathbf{a}_i^{(n+1)} = \mathbf{a}_i^{(n)} - \alpha_i^{(n)} \nabla J_\lambda^i \left(\mathbf{a}_i^{(n)} \right),$$

where $\alpha_i^{(n)} > 0$ is the step size at n-th iteration. The iteration is terminated when the gradient of the function drops below a prescribed threshold, i.e., $\left| \nabla J_\lambda^i \left(\mathbf{a}_i^{(n)} \right) \right| \leq \delta$. We

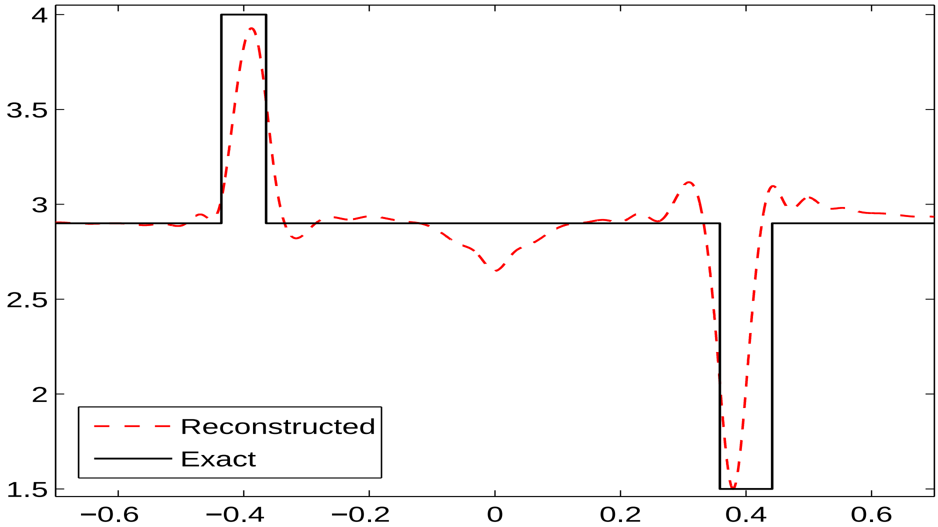

Figure 5: Reconstructed coefficient ε_r, the case with a stone and a mine, z=4.75 cm. The dent in the center is clearly seen and was explained in [5].

consider three thresholds $\delta = \{1 \times 10^{-2}, 1 \times 10^{-3}, 1 \times 10^{-4}\}$ with the homogeneous case and run the code up to 16 layers. The lower and upper limit of the pseudo-frequency is $\kappa_0 = 9$ and $\bar{\kappa} = 10$, respectively, i.e., $\kappa \in [9, 10]$. For this range of pseudo-frequency, Legendre polynomials of degree 5 give the best approximation, which is used as the basis for κ approximation in this run. Value for the parameter λ associated with the Carleman Weight Function is $\lambda = 200$. We use 39 splines on the interval $x \in [-A, A] = [-0.6, 0.6]$ with uniform layer size $\delta z = 0.005$. Unless otherwise noted explicitly, this uniform layer size has been used throughout the subsequent comparative studies. Figure 6 shows the result of the reconstruction for the case $\varepsilon_r \equiv 2.9$, i.e., in the absence of the inclusion. From the graph with normal scale, the relative dielectric permittivity ε_r is reconstructed successfully for all stopping criteria though with very small deviations from the exact value. The difference with the three stopping criteria is self-evident from the blow-up view. The stringent threshold $\delta = 1 \times 10^{-4}$ does not give us a better accuracy. Rather, it introduces more oscillations compared with the relatively loose threshold $\delta = 1 \times 10^{-3}$.

This is due to the ill-posed feature of coefficient inverse problems. Accumulated round-off error also contributes this since more iterations are involved to reach the stringent criterion. It is a delicate issue to choose an appropriate stopping criterion. If it is too loose, i.e., δ is relatively big, then the minimizer $\bar{\mathbf{a}}_i$ from the steepest descent method will be rather far from its true solution $\mathbf{a}_i^*$. This will result in degraded accuracy of the reconstructed unknown coefficient, which is shown in the blow-up view for the threshold $\delta = 1 \times 10^{-2}$. One has to take into account the error with spatial approximation, the error with pseudo-frequency κ

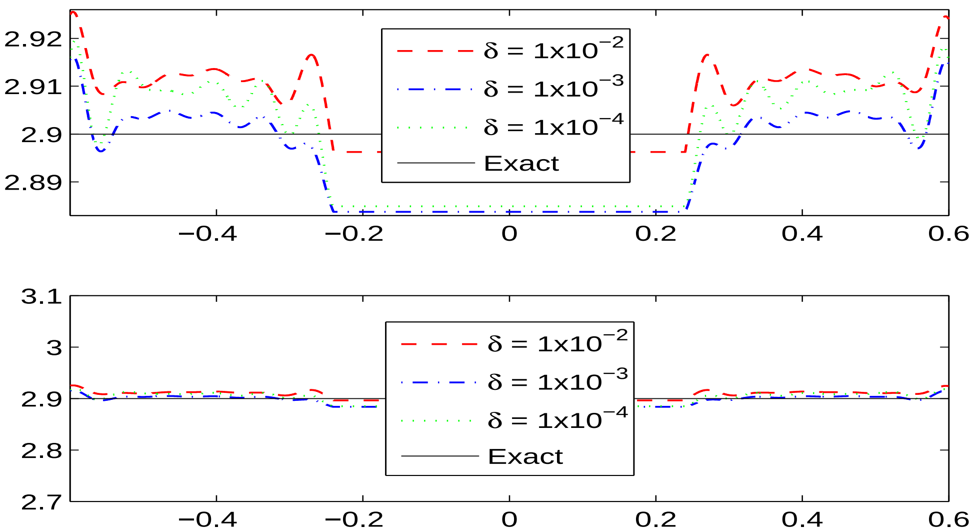

Figure 6: Comparison of three different thresholds at z=8 cm, top: blow-up view, bottom: normal scale view.

integration and layer size δz in selection of a proper stopping criterion.

4.3 Layer Size

We consider three different layer sizes $\delta z = \{2.5\times10^{-3}, 5\times10^{-3}, 1\times10^{-2}\}$ for the configuration with no inclusion, i.e., $\varepsilon_r \equiv 2.9$. The other parameters are the same as in the previous section on stopping criterion with $\delta = 1\times10^{-3}$. The codes run up to 32, 16 and 8 layers for the three layer sizes considered, respectively. We show the cross-sectional view of the reconstructed ε_r at $z = 0.08$ along x-axis, i.e., 8 cm underneath the ground and at the end of the last layer for each run. The comparison is shown in Figure 7. On the graph with normal scale, the three curves are close to each other and ε_r is reconstructed very accurately for each layer size considered. From the blow-up view, one can appreciate the difference - the thinner the layer, the less the oscillations, thus, the better accuracy. This is understandable since the quadratic approximation of function $p_j(z,\kappa)$ with respect to z has more accuracy with layer size decreased. The initial values of $\mathbf{a}^0_{i+1}, \mathbf{b}^0_{i+1}, \mathbf{c}^0_{i+1}$ for the next layer also have less errors with smaller δz.

4.4 Parameter λ

We study the impact of the parameter λ associated with the Carleman Weight Function on the accuracy of the reconstructed ε_r. We consider $\lambda = \{100, 200, 1000\}$ and the stopping criterion $\delta = 1\times10^{-3}$. The rest of the parameters share the same values as those in the section

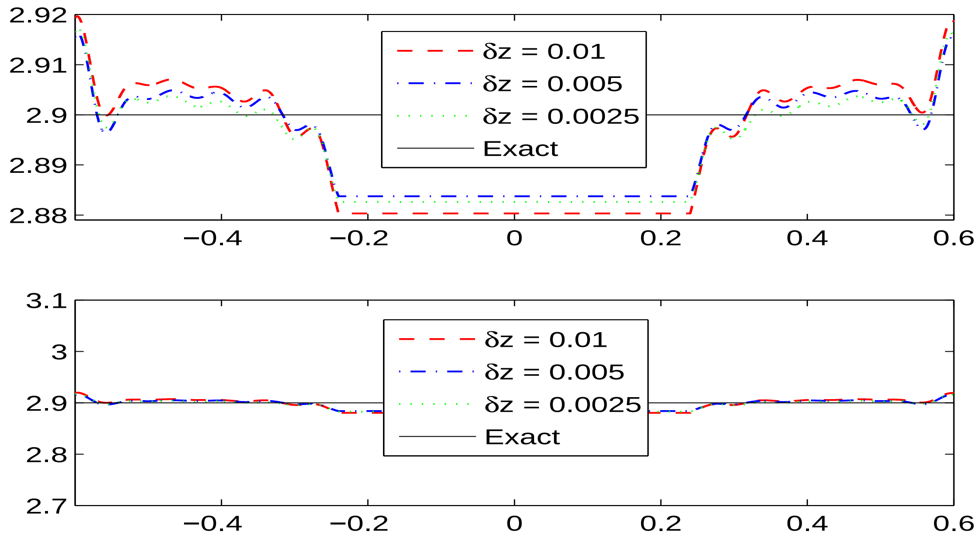

Figure 7: Comparison of three different layer sizes δz at z =8 cm, top: blow-up view, bottom: normal-scale view.

on stopping criterion. Again, we work with the homogeneous situation where $\varepsilon_r \equiv 2.9$. The result is shown in Figure 8. The relative dielectric permittivity ε_r is reconstructed with a good accuracy for all values of λ considered. The difference shows up on the blow-up view. Smaller value of λ generates more oscillations and larger value of λ tends to create less oscillations. This does not necessarily mean that the larger value of λ will have a better accuracy for the reconstructed ε_r. The overall performance for $\lambda = 200$ seems to be better than that for $\lambda = 1000$. The goal of the introduction of the Carleman Weight Function Ψ^i_λ is to ensure the weighted least squares objective function J^i_λ to be strictly convex on each generic layer. Certainly the parameter λ has impact on the solution $\bar{\mathbf{a}}_i$ from the minimization procedure, thus affecting the reconstructed ε_r.

From the results shown in Figure 8, we conclude that the objective function J^i_λ has a unique minimizer when parameter λ varies in a large range. Furthermore, the results conform to the error estimate (2.34), which means that the algorithm is very robust. With all other parameters fixed, there is an unique, optimal value of the parameter λ^*. Actually, we have employed the implicit rule $\lambda \times \delta z = 1$, i.e., taking the inverse of layer size δz as its value for this parameter in the rest of our comparative study. Computational results for various realistic configurations show that this choice works quite well.

4.5 Dimension of the Basis for κ Approximation

An orthonormal basis on the interval $\kappa \in [\kappa_0, \bar{\kappa}]$ has been applied to approximate functions $\mathbf{p}(z, \kappa)$ and $\mathbf{p}_z(z, \kappa)$ with respect to pseudo-frequency κ. We choose Legendre polynomials

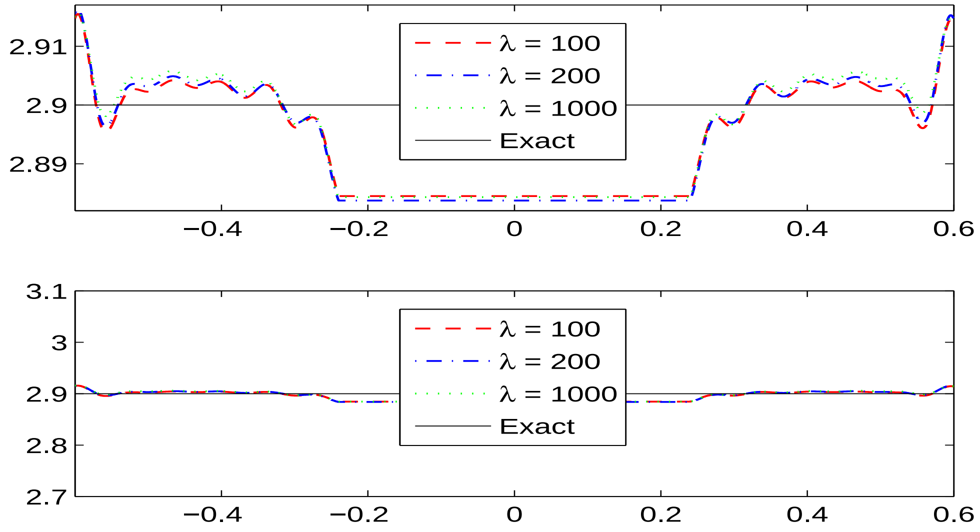

Figure 8: Comparison of three different values for the parameter λ at z=8 cm, top: blow-up view, bottom: normal-scale view.

up to degree K as the basis $\{l_i(\kappa)\}_{i=0}^{K}$. One advantage of introducing such a basis is that all the terms involving κ-integration in the weighted least squares objective function J_λ^i can be computed explicitly in contrast to the composite Simpson's or trapezoidal rules. Functions of the orthonormal basis are defined as

$$l_i(\kappa) := \sqrt{\frac{2i+1}{\bar{\kappa}-\kappa_0}} L_i\left(\frac{2\kappa-(\kappa_0+\bar{\kappa})}{\bar{\kappa}-\kappa_0}\right), \quad i = 0, 1, \cdots, K,$$

where $L_i(\xi)$ is the classical Legendre polynomial of degree i defined on [-1,1] and has the property

$$\int_{-1}^{1} L_i^2(\xi)d\xi = \frac{2}{2i+1}.$$

The orthonormal basis share the property

$$\int_{\kappa_0}^{\bar{\kappa}} l_i(\kappa)l_j(\kappa)d\kappa = \delta_{ij},$$

where δ_{ij} is the Kronecker delta. On the pseudo-frequency interval $\kappa \in [\kappa_0, \bar{\kappa}] = [9, 10]$, Legendre polynomials of degree 5 have the best approximation of functions $\mathbf{p}(0,\kappa)$ and $\mathbf{p}_z(0,\kappa)$ compared with other degrees. Indeed for degree 5 polynomial approximation,

the maximum absolute and maximum relative errors are very small for both functions: $|\delta \mathbf{p}|^{K=5}_{abs,\infty}(0,\kappa) = 9.08 \times 10^{-10}$, $|\delta \mathbf{p}|^{K=5}_{rel,\infty}(0,\kappa) = 2.73 \times 10^{-7}$; $|\delta \mathbf{p}_z|^{K=5}_{abs,\infty}(0,\kappa) = 1.50 \times 10^{-9}$, $|\delta \mathbf{p}_z|^{K=5}_{rel,\infty}(0,\kappa) = 2.76 \times 10^{-7}$. This is in sharp contrast with quadratic polynomial approximation: $|\delta \mathbf{p}|^{K=2}_{abs,\infty}(0,\kappa) = 9.89 \times 10^{-7}$, $|\delta \mathbf{p}|^{K=2}_{rel,\infty}(0,\kappa) = 4.24 \times 10^{-4}$; $|\delta \mathbf{p}_z|^{K=2}_{abs,\infty}(0,\kappa) = 1.72 \times 10^{-6}$, $|\delta \mathbf{p}_z|^{K=2}_{rel,\infty}(0,\kappa) = 3.62 \times 10^{-4}$. We want to investigate if there is any pronounced difference in the reconstructed unknown ε_r with these two polynomial approximations. For the comparison, we consider one realistic configuration, the one-mine case. The center of the mine is located at the point $P_m(0.3m, 0.075m) = P_m(30cm, 7.5cm)$. We use 43 splines for spatial approximation and the threshold $\delta = 0.001$ for the stopping criterion.

Figure 9 shows the comparison result. The mine and the background medium have been clearly identified for both polynomial approximations. On the graph with normal scale, the two curves are very close to each other. From the two blow-up views, one can recognize the difference though not too much. Degree 5 gives relatively better overall performance than degree 2. Compared with the big, several orders' difference in approximation of functions $\mathbf{p}(0,\kappa)$ and $\mathbf{p}_z(0,\kappa)$, the discrepancy of ε_r is rather small with the two different polynomial degrees. This is due to the fact that the tail function $\chi(x,z)$ dominates the contribution for the function $\tilde{v}(x,z,\kappa)$, and therefore we could take a very short interval $\kappa \in [9,10]$ for the pseudo-frequency integration. On this interval the approximation errors with Legendre polynomials of degree 2 and 5 are all very small. Thus, this small error propagates through the minimization procedure and exerts a slight influence on the final reconstructed unknown coefficient.

4.6 Noisy Data

We consider the perturbed input data by adding different noise levels to the input data $\varphi_2(x,\kappa)$ and $\psi_2(x,\kappa)$. In principle, we should add noise to the original data φ and ψ in (3.6) and then use a regularization procedure to differentiate functions φ_1 and ψ_1 in (2.14) with respect to κ. Regularization can be done, for example similarly to subsection 6.1 of [34]. However, to avoid additional complications, instead of considering $\varphi(x,\kappa)$ and $\psi(x,\kappa)$, in this study we introduce multiplicative noise in the input data $\varphi_2(x,\kappa)$ and $\psi_2(x,\kappa)$. For every discrete value $x_i \in [-A, A]$ and $\kappa_j \in [\kappa_0, \bar{\kappa}]$, each of the function $\varphi_2(x_i,\kappa_j)$ and $\psi_2(x_i,\kappa_j)$ is a matrix. The elements in the two matrices are perturbed by

$$\overline{\varphi}_2(x_i,\kappa_j) = \varphi_2(x_i,\kappa_j)\left(1+\zeta_{i,j}\right), \quad \overline{\psi}_2(x_i,\kappa_j) = \psi_2(x_i,\kappa_j)\left(1+\eta_{i,j}\right),$$

where $\zeta_{i,j}$ and $\eta_{i,j}$ are normally distributed pseudo-random numbers with zero means. The standard deviations are selected to create noise levels of 2%, 5% and 10% for the input data $\varphi_2(x,\kappa)$ and $\psi_2(x,\kappa)$. The sample number is taken to be 200 for each noise level. The parameters for this setup are the same as those in the previous subsection with polynomials of degree 5 for pseudo-frequency approximation. The results with the perturbed, noisy input data are shown in Figure 10.

For the reconstructed unknown coefficient ε_r, higher noise level creates more oscillations and there is small undershoots near the mine with the noise level of 10%. Nevertheless,

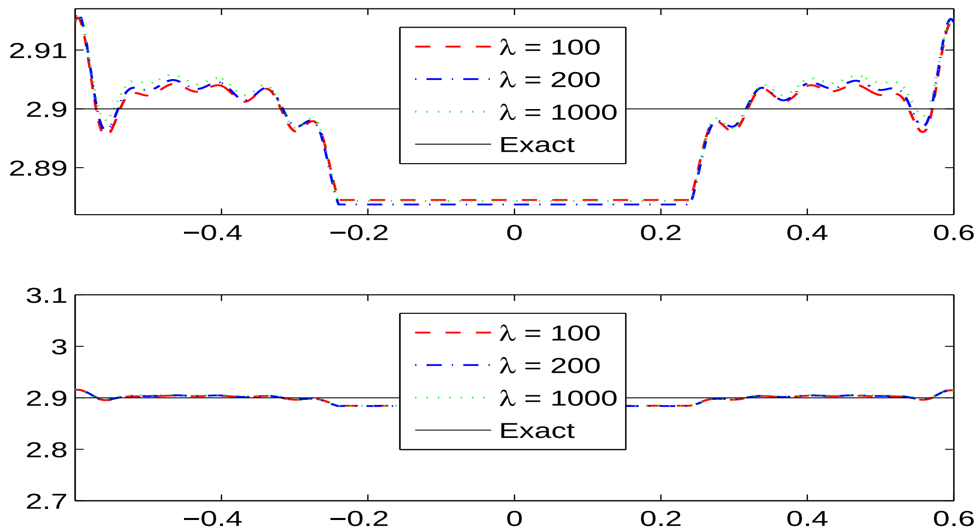

Figure 9: Comparison of polynomial approximations with degree 2 and 5 at z=5.5 cm, top: normal-scale view, middle: blow-up view of the upper portion, bottom: blow up view near the mine.

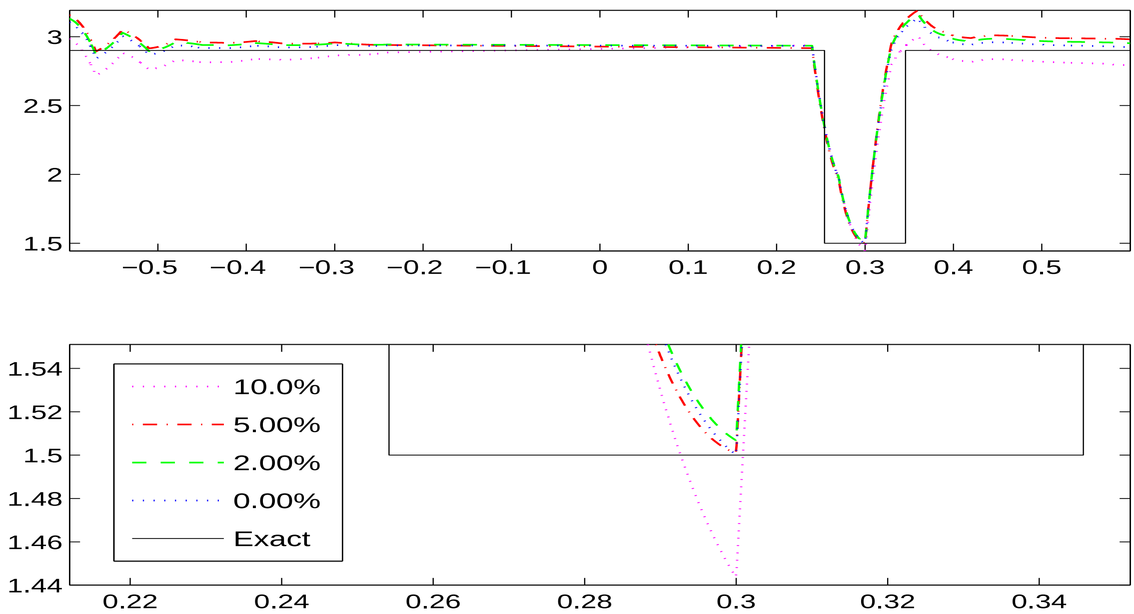

Figure 10: Comparison of three different noise levels at z=5.5 cm, top: normal-scale view, bottom: blow-up view near the mine.

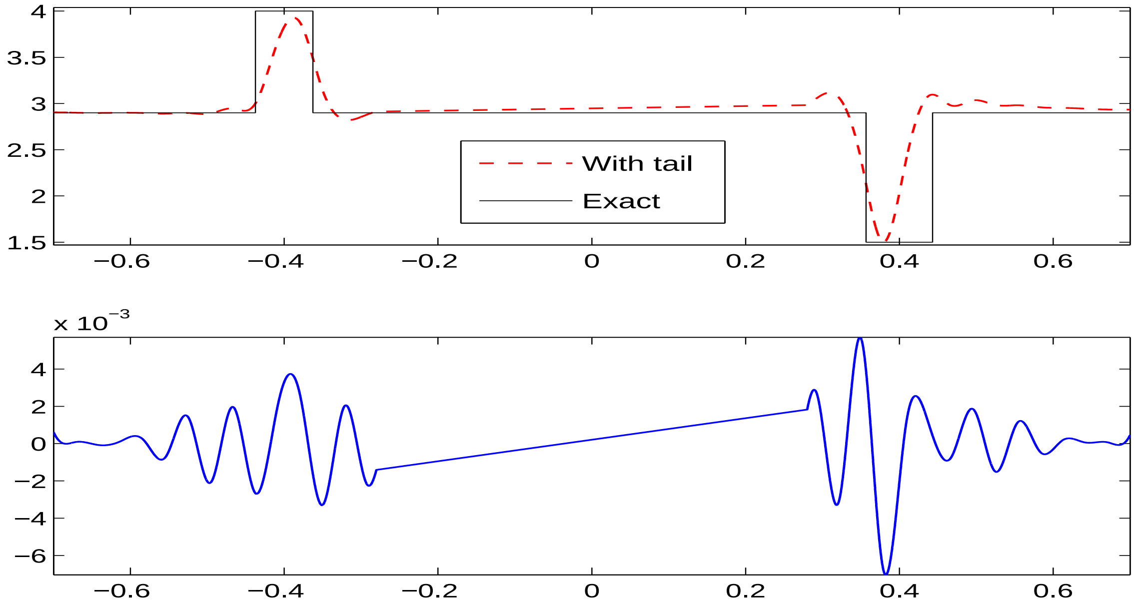

Figure 11: Comparison between the case with the tail and the tail-free case at z=4.75 cm, top: with tail, bottom: tail-free.

the overall performance with all the noise levels are still good and, both the mine and the background medium have been clearly identified in terms of their material property ε_r.

4.7 Tail $V(x)$

As we have pointed out before, the tail function $V(x)$ dominates the contribution in the pseudo-frequency κ integration. We compare the reconstructed unknown coefficient ε_r for the case with tails and the case without tails, the tail-free case and consider the stone-mine realistic configuration. The center of the stone is located at the point $P_s(-0.4m, 0.075m) = P_s(-40cm, 7.5cm)$, i.e., the same depth 7.5 cm underneath the ground as the mine, whose center is at the point $P_m(0.4m, 0.075m) = P_m(40cm, 7.5cm)$. The x-interval for the inverse problem is $\Omega_x := [-A, A] = [-0.7, 0.7]$. Each computation is performed with 51 splines with uniform layer size $\delta z = 0.005m = 0.5cm$ and $\delta = 1 \times 10^{-4}$ as the threshold for the stopping criterion. The lower limit for κ integration is $\kappa_0 = 8$ and degree 6 for Legendre polynomial basis. The comparison is presented in Figure 11. The tail-free case essentially gives us nothing on the reconstructed ε_r, i.e., it could not determine the material property (ε_r) of the heterogeneous media, let alone distinguish the stone and the mine from their background medium. Yet, the variation of ε_r for the tail-free case still indicates the locations of the stone and the mine.

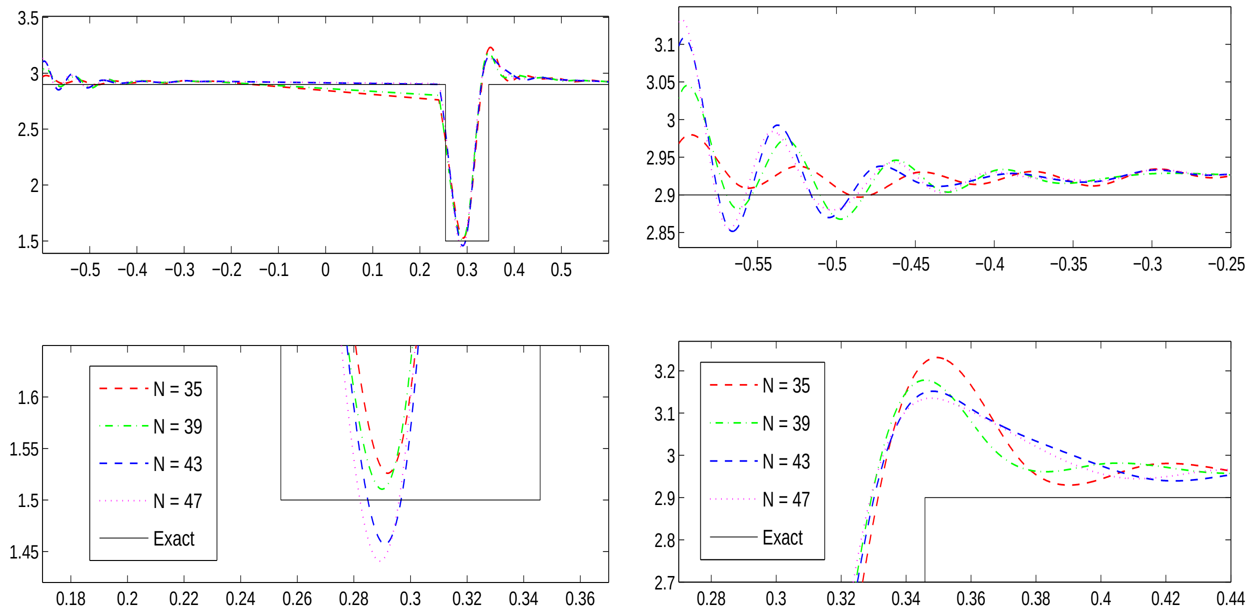

Figure 12: Comparison of four different number of splines at z=5.5 cm, top: normal-scale view, second row: blow up view near the mine, third row: blow-up view of the left portion, bottom: blow-up view for $x \in [0.32, 0.44]$.

4.8 Dimension of the Basis for x Approximation

To approximate function $q(x, z, \kappa)$ and its partial derivatives with respect to spatial variable x, we introduce cubic B-splines: $\left\{\phi_j\left(x\right)\right\}_{j=-1}^{n+1}$. Each spline function is piecewise defined on a subset of the entire interval $[a, b]$, yet globally the interpolating function $\tilde{f}(x)$ has the property $\tilde{f}(x) \in C^2[a, b]$. It is well known that it has the desirable approximation property, i.e., if $f \in C^4[a, b]$, then

$$\|f - \tilde{f}\|_\infty \leq \frac{5}{384}\|f^{(4)}\|_\infty h^4,$$

where h is the distance between two consecutive evenly-spaced knots. We study the effect of the dimension N of the basis on the resolution of the final reconstructed ε_r, i.e., whether using more splines will give us better accuracy of ε_r. The parameters share the same values as in Subsection 4.5 and for κ approximation, we choose $K = 5$ and $\kappa \in [9, 10]$. The results are shown on Figure 12. On the graph with the normal scale, all the 4 curves are close to each other, but from the 3 blow-up views, one can identify the difference. Near the mine, there is small undershoot of ε_r for $N = \{43, 47\}$. In this local region, the best performance seems to be the case with $N = 39$.

At the left portion of the graph, there are mild oscillations for $N = \{43, 47\}$, and the oscillation for $N = 35$ is rather small. The performance with $N = 39$ is in-between the performances for $N = 35$ and $N = 43$. The best resolution of ε_r in this local area is for

the case with $N = 35$. From the blow-up view for $x \in [0.32, 0.44]$ and near the interface of singularity, overshoots exist for all the cases with the four different splines numbers. The curve for $N = 35$ shows the maximum overshoot while the minimum overshoot exhibits on the curve for $N = 47$. The best overall performance in this short interval seems to be for $N = 39$. Thus, on the whole interval $x \in [-0.6, 0.6]$, the highest accuracy of the reconstructed ε_r is for the case with $N = 39$. The main reason why further more splines does not improve the accuracy of the reconstructed ε_r is due to the inherent ill-posed nature of coefficient inverse problems. Accumulated round-off error also contributes but to a less degree. Another disadvantage with more number of spline approximation is the increased computational load, i.e., more running time and more required memory of the machine. This might be a problem for detecting the land mines in real time.

4.9 Lower Limit κ_0

Once $\bar{\kappa}$ is decided using the asymptotic behavior of function $w(\mathbf{x}, s)$ as $s \to \infty$, there is an arbitrariness in selecting the lower limit κ_0 for pseudo-frequency integration. Theoretically, κ_0 should be as small as possible in order to have better accuracy for κ integration. The problem with smaller value of κ_0 is that the dimension of the Legendre polynomial basis will also have to be correspondingly higher. For example, if we take $\kappa_0 = 1$, Legendre polynomials of degree 17 give the best approximation of functions $\mathbf{p}(0, \kappa)$ and $\mathbf{p}_z(0, \kappa)$. This is in a sharp contrast with the case for $\kappa_0 = 8$, where the degree 6 gives the best approximation for both functions. Here we want to study the impact of different values of κ_0, i.e., $\kappa_0 = 8$ and $\kappa_0 = 9$ on the resolution of our reconstructed ε_r. We record the maximum absolute and maximum relative errors with degree 6 polynomial approximations for both functions: $|\delta\mathbf{p}|^{K=6}_{abs,\infty}(0, \kappa) = 1.43 \times 10^{-9}$, $|\delta\mathbf{p}|^{K=6}_{rel,\infty}(0, \kappa) = 3.47 \times 10^{-7}$; $|\delta\mathbf{p}_z|^{K=6}_{abs,\infty}(0, \kappa) = 2.45 \times 10^{-9}$, $|\delta\mathbf{p}_z|^{K=6}_{rel,\infty}(0, \kappa) = 3.29 \times 10^{-7}$. Each error is on the same order as its corresponding one with degree 5 approximation for $\kappa_0 = 9$, though a little larger. For this study, we consider a realistic configuration, the stone-mine case. The rest of parameters are the same as those in subsection 4.7. Figure 13 shows the results for the comparison.

The two curves are almost inappreciable from the graph with normal scale, and there is no overshoot near the stone, nor undershoot near the mine. The stone, the mine and the background medium have been correctly and sharply identified. The difference shows up on both blow-up views. The performance of the reconstructed ε_r is a little better with $\kappa_0 = 8$. This is due to the extra information with κ integration for $\kappa \in [8, 9]$, in the presence with the case for $\kappa_0 = 8$ and lost in the case for $\kappa_0 = 9$.

4.10 Initial Guess $\mathbf{a}_1^0$

To start the layer stripping procedure, we need to have the initial guess $\mathbf{a}_1^0$ for the first layer $z \in [0, \delta z]$. There are two ways to obtain $\mathbf{a}_1^0$. The first approach needs one more datum $w_{zz}(x, 0, \kappa)$ besides the two given Cauchy data, $w(x, 0, \kappa)$ and $w_z(x, 0, \kappa)$. This extra datum can be obtained by solving the forward problem. In order to distinguish from the

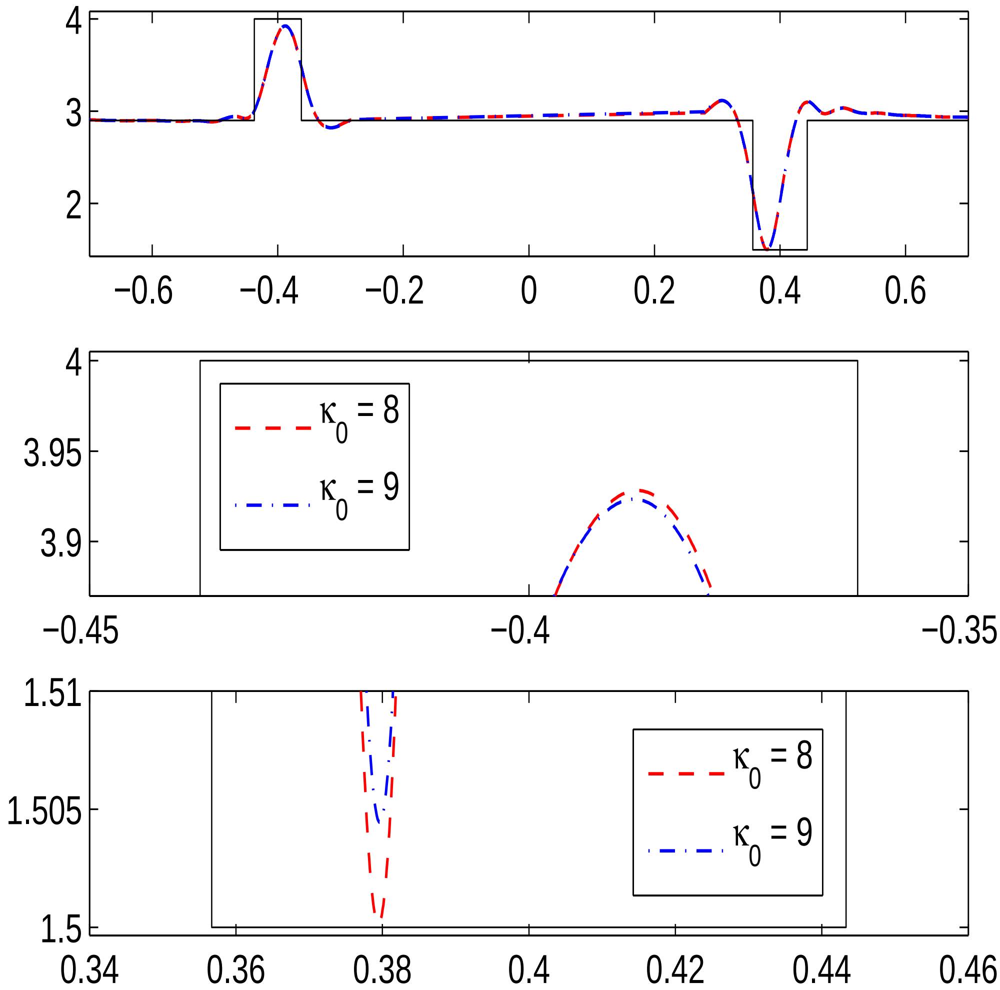

Figure 13: Comparison of two different values of $\kappa_0$at z=4.75 cm, top: normal-scale view, middle: blow up view near the stone, bottom: blow-up view near the mine.

other method, we term this approach as "External data" for the obvious reason. The second method is by utilizing equation (2.27). For the first layer and at $z=0$, by the quadratic approximation of $\mathbf{p}(z,\kappa)$ in (2.27), we have $\mathbf{p}(0,\kappa)=\mathbf{c}_1$, $\mathbf{p}'(0,\kappa)=\mathbf{b}_1$, and $\mathbf{p}''(0,\kappa)=\mathbf{a}_1$. Plugging these expressions into equation (2.27) and re-arranging the second term on the left hand side yields

$$B\mathbf{a}_1=\mathbf{f}\left(\mathbf{c}_1,\mathbf{b}_1,\int_{\kappa}^{\bar{\kappa}}\mathbf{c}_1\left(z_0,\tau\right)d\tau,\int_{\kappa}^{\bar{\kappa}}\mathbf{b}_1\left(z_0,\tau\right)d\tau,\chi(z_0),\chi'(z_0),\kappa\right).$$

The vector-valued function $\mathbf{f}$ can be evaluated since all its arguments are known. As matrix B is non-singular, we could solve the above linear equation for $\mathbf{a}_1$ to get the initial guess $\mathbf{a}_1^0$ for the first layer. We name this method "By formula". For this run, the parameters take the same values as their corresponding ones in subsection 4.7 for the case with tail. The comparison results are shown in Figure 14. On the graph with normal scale, the two curves are nearly indistinguishable.

From the blow-up view, one can tell the difference: the by-formula method is a little better than the approach with external data in terms of resolution of the reconstructed unknown coefficient ε_r. The convergence history for Layer #10 shows that the by-formula method converges a little slower than the approach with external data. The former needs 33 iterations compared with 29 iterations for the latter to reach the stopping criterion $\left|\nabla J_{10}^{(n)}\right|\leq 1\times10^{-4}$. The iteration number between the two approaches differs only slightly. We consider this comparison is a testimony of the fact that the convexification algorithm is indeed a globally convergent method.

5 Summary and Conclusions of Comparative Studies

A systematic comparative study of the globally convergent convexification algorithm has been carried out. Below is a summary of our findings.

- An appropriate stopping criterion for the iteration of gradient-like method is central to the accuracy of the reconstructed unknown coefficient. A stringent criterion does not necessarily guarantee better accuracy. To choose a proper threshold, one needs to consider the errors of spatial approximation, of pseudo-frequency integration and layer size. With a known configuration and by trial and error, one can calibrate the threshold and apply it to other unknown realistic situations. Our numerical studies show that for realistic configurations, the difference of the reconstructed unknown coefficient ε_r between a stringent and a loose threshold is small. On the other hand, the stringent threshold requires much more computational time. This means that with a loose threshold, we can still generate a good image of the unknown coefficient, and more importantly, the efficiency study shows that it is possible to run the algorithm in *real time* for identification and imaging of antipersonnel land mines in the field.

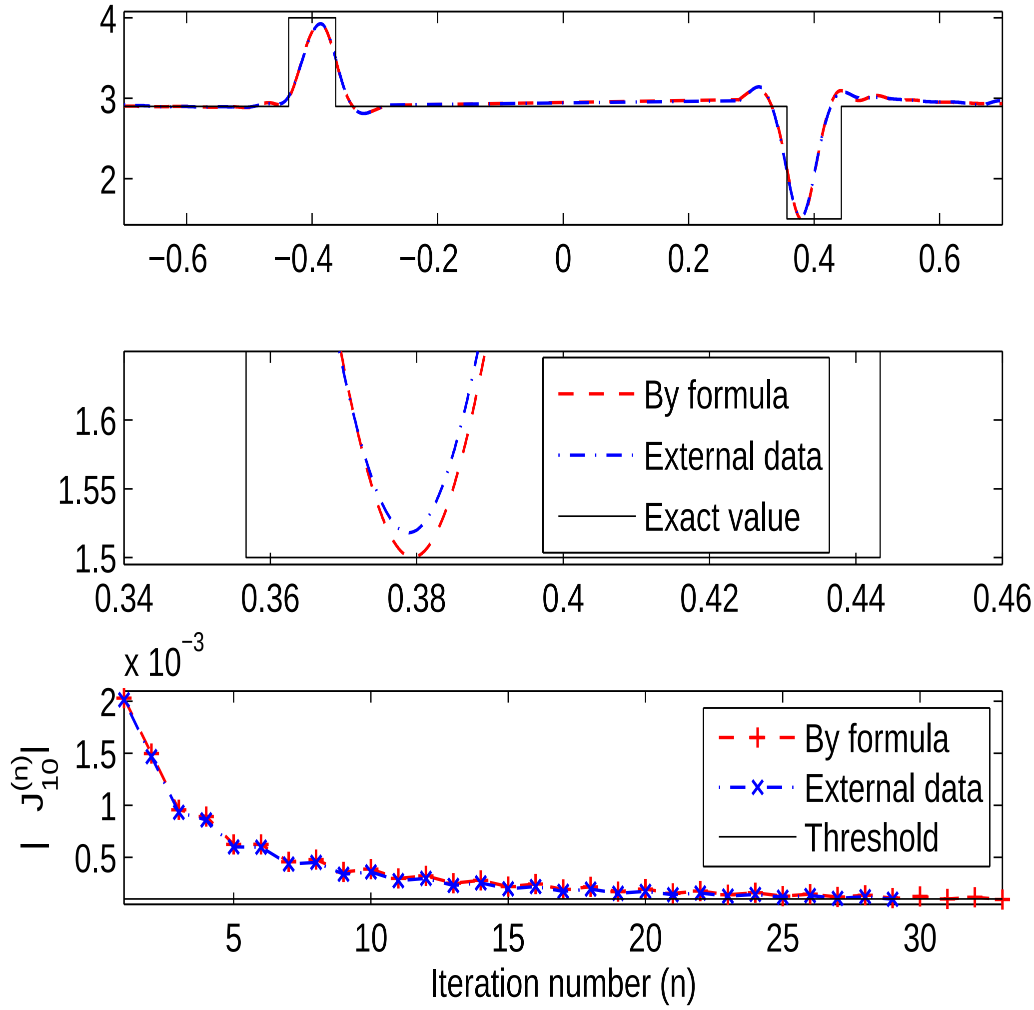

Figure 14: Comparison of two different initial guesses of a_1^0 at z=4.75 cm, top: normal-scale view, middle: blow-up near the mine, bottom: convergence history for layer #10.

- Thinner layer size has better resolution of the reconstructed unknown coefficient ε_r, which provides a numerical confirmation of the estimate (2.35).
- The weighted least squares objective function is strictly convex for the parameter λ associated with the Carleman Weight Function varies in a large range. As long as λ varies in this range, its influence on the accuracy of the reconstructed ε_r is not pronounced, which confirms the error estimate (2.34). The inverse of the layer size can be a good choice for the value of this parameter.
- A basis of low dimension can be applied for the pseudo-frequency approximation and generate good accuracy on ε_r. This is due to the dominance of the tails in the pseudo-frequency integration.
- A higher noise level affects more severely the quality of the reconstruction of the unknown coefficient ε_r. Up to the 10% noise level, the quality of the reconstructed ε_r is still good.
- For each specific problem, there is an appropriate dimension of the basis for spatial x approximation. Due to the inherent ill-posed nature of coefficient inverse problems, basis with even higher dimension does not further improve quality of the reconstructed unknown coefficient.
- The lower bound of the pseudo-frequency may be selected quite close to the upper bound due to the fact that tails dominate pseudo-frequency integration. Small change of the lower limit has negligible impact on the reconstructed unknown coefficient.
- Fitting the correct tails is crucial for the algorithm to work properly and efficiently.
- The initial guesses obtained by the methods of "External data" and "By formula" differ only slightly in terms of resolution of reconstructed unknown coefficient and speed of convergence. This conforms well with the theoretically established strict convexity of the functional J_{λ}^{i}.
- Overall, the comparative study demonstrates the robustness of the convexification algorithm. Efficiency with the new implementation shows the possibility for the algorithm to be applied in *real time* to detect and image antipersonnel land mines in the field.

The above comparative analysis provides valuable references to further development of the convexification algorithm for a broad class of CIPs.

6 Convexification Method for an Inverse Problem for an Elliptic Equation

In [7] we have also considered the inverse problem for the elliptic equation (6.1) in the case when the running pseudo frequency of the above case is replaced by the running source

x^s. The source is running along a line. This corresponds to the constant current in the case of search of e.g., land mines and underground bunkers using the method of Electrical Impedance Tomography (EIT). The soil is probed by the constant current then. In the case of EIT the function $u(x, x_s)$ in (6.1) is the voltage at the point x generated by the constant current at the source point x^s. In the case of optical imaging of diffuse media this corresponds to the so-called Constant Wave (CW) light. The optical imaging through the diffuse media can be applied to image targets on battlefields through smogs and flames, as well as to medical optical imaging. Interestingly, the diffuse-like propagation of light in the battlefield application would even be helpful, because even if the direct laser beam would "miss" the target, one might still image it because photons would still "sense" that target due to the diffusion of light. A simplified version of the convexification for this inverse problem was considered in [9] and was reported in the annual 2006 report on this project [21].

The reason why the above scheme of the convexification works well for the case of frequency/time dependent data is that there exists a "proper" asymptotic behavior (2.11) of the solution of the corresponding elliptic equation when the pseudo-frequency tends to the infinity in this case. However, in the case of the source dependent data a "proper" asymptotic behavior as the source position tends to the infinity is unknown. This means that we need a special treatment of the so-called "tail". The tail is unknown *a priori* and appears due to the truncation of an improper integral with respect to the source position, see (6.11). In order to apply our layer stripping procedure, we need to approximate the tail. Thus, we use a heuristic approach of approximating the tail. At the same time, we point out that if the tail is given, then the global convergence of our layer stripping procedure is rigorously guaranteed.

6.1 Statement of the Inverse Problem and Applications

6.1.1 The Inverse Problem

For the sake of generality we consider the 3-D case with $x = (x_1, x_2, z) \in \mathbb{R}^3$. The 2-D case, for which our numerical experiments are conducted, is both simpler and similar. Let the function $a(x) \geq const. > 0, a \in C^1(\mathbb{R}^3)$ and $a(x) = k^2 = const. > 0$ for $x \in \{|x| > R\}$, where R is a positive number. Let the function $u(x, s)$, where s is a parameter, satisfies the following elliptic equation

$$\Delta_x u - a(x)u = -\delta(x - x^s) \text{ in } \mathbb{R}^3 \tag{6.1}$$

with the conventional condition at the infinity

$$\lim_{|x|\to\infty} u(x, s) = 0, \forall s \in \mathbb{R}. \tag{6.2}$$

The source position is at the point x^s and when s is changing, the source is running along the line $l = \{x = (x_1, 0, z_m)\}$, where $z_m = const. > 0$. We also assume that

$$a(x) = k^2 \text{ in } l_\varepsilon, \tag{6.3}$$

where l_ε is a small neighborhood of the line l.

If the function $a(x) \equiv k^2$, then the fundamental solution of the equation (6.1) with the condition (6.2) is

$$u_0(x,s) = \frac{\exp\left(-k\left|x - x^s\right|\right)}{4\pi\left|x - x^s\right|}.$$

Hence, we seek the solution of the problem (6.1), (6.2) in the form $u = u_0 + \widehat{u}$, where the function $\widehat{u} \in C^2\left(\mathbb{R}^3\right)$ and satisfies the following conditions

$$\Delta_x \widehat{u} - a(x)\widehat{u} = \left(a(x) - k^2\right) u_0 \text{ in } \mathbb{R}^3, \tag{6.4}$$

$$\lim_{|x|\to\infty} \widehat{u}(x, x^s) = 0. \tag{6.5}$$

Uniqueness and existence results of the problem (6.1), (6.2) for functions

$u \in C^{2+\alpha}\left(\mathbb{R}^3 \diagdown \{|x - x_0| < \varepsilon\}\right)$ follow from the classic theory of elliptic equations, see, e.g., []. Here $\varepsilon > 0$ is an arbitrary number, $\alpha \in (0,1)$ and $C^{2+\alpha}$ are Hölder spaces.

Let $\Omega \subset \mathbb{R}^3$ be a rectangular prism

$$\Omega = \left\{x : -A < x_1, x_2 < A, z \in (z_0, z_m - \theta)\right\},$$

where A and L are positive numbers. Denote $\Gamma = \Omega \cap \{z = z_0\}$. We are not setting $\theta := 0$ because we want to avoid working with the line l, where the singularities of the function u occur. We consider the following

Inverse Problem. Suppose that the function $a(x)$ is unknown inside of the domain Ω, known outside of it, and it is also known in $\Omega \cap \{z \in (z_m - \theta, z_m)\}$. Determine the function $a(x)$ in $\Omega \cap \{z \in (z_0, z_m - \theta)\}$ given the following functions φ and ψ

$$u\left(x,s\right) = \varphi\left(x,s\right), u_z\left(x,s\right) = \psi\left(x,s\right), \text{ for } x \in \Gamma, s \in \left[s_0, \overline{s}\right], \tag{6.6}$$

where s_0 and $\overline{s}$ are two numbers. Thus, functions φ and ψ represent the Dirichlet and Neumann data caused by the transmitted signal.

6.1.2 Applications

In applications discussed below it would be more natural to consider equation (6.1) either in a bounded domain or in the half-space $\{z < z_m\}$. In principle, these cases can also be incorporated in the scheme of the convexification. However, this would create some additional difficulties in the forward problem solution near the boundary. Thus, we consider the forward problem (6.1), (6.2) in the entire space, for brevity.

1. Electrical Impedance Tomography

One of applications of the EIT is in the search of land mines and underground bunkers via probing the ground by the constant current at different source locations. Let $v(x,s)$ be the voltage generated by the source of the constant current located at $(s, 0, z_m)$ and let $\sigma(x)$

be the electric conductivity of the medium, $\sigma(x) \geq const. > 0$. Then the function $v(x,s)$ satisfies the following equation

$$\nabla \cdot (\sigma(x)\nabla v) = -\delta\left(x_1 - s, x_2, z - z_m\right)$$

and

$$\lim_{|x|\to\infty} v(x,s) = 0.$$

Replacing the function v with the function $u = v\sqrt{\sigma}$ and assuming that $\sigma\left(x_1, 0, z_m\right) = 1$, we obtain equation (6.1) with

$$a(x) = \frac{\Delta\left(\sqrt{\sigma}\right)}{\sqrt{\sigma}}. \tag{6.7}$$

Hence, assuming that the function $\sigma(x)$ is known near the surface Γ, we arrive at the above inverse problem with the unknown coefficient in the form (6.7).

2. Optical Diffusion Tomography

In Optical Diffusion Tomography, lasers with the CW (constant wave) light are used as light sources. The first application of the Optical Diffusion Tomography is in optical medical imaging of tumor-like abnormalities both in human organs and small animals using Near Infrared (NIR) light with the wavelength of light somewhere between 500 and 1000 nanometers. The second feasible application is in optical imaging of targets on battlefields via smogs and flames. Both cases of transmitted and back reflected light are feasible for both applications. The light source should move along a straight line and the output light should be measured at a part of a surface.

Let $u(x, x^s)$ be the light intensity at the point x due to the light source located at the point x^s. It can be derived from the well known literature sources (see, e.g., [31]) that the function $u(x, x^s)$ is the solution of the problem (6.1), (6.2) with the coefficient $a\left(x\right)$ as

$$a\left(x\right) = 3\left(\mu_s' \mu_a\right)\left(x\right), \tag{6.8}$$

where μ_s' is the reduced scattering coefficient and μ_a is the absorption coefficient of the medium. Both coefficients are measured in [1/cm]. The reduced scattering coefficient μ_s' is assumed constant here. This is reasonable because in NIR applications the coefficient μ_s' usually changes quite slowly with respect to x for this spectrum of light waves, whereas the coefficient μ_a changes significantly. Furthermore, μ_a can be used for the diagnostics. In the case of imaging of targets through flames these targets are usually impenetrable for light, meaning that $\mu_a = \infty$ in them. However, one can model those targets as ones with finite, though large values of μ_a, i.e., the ones having large contrasts with the surrounding.

6.2 The Convexification

Let $x^s = \left(s, 0, z_m\right)$, where the running parameter s characterizes the changing source position of the source. Below we consider the function $u(x,s)$ and all related functions only in the

above domain of interest Ω. By the maximum principle $u(x, s) > 0$. Hence, similarly with section 2 we consider the function

$$v(x, s) = \ln u(x, s).$$

By (6.1)

$$\Delta v + (\nabla v)^2 = a(x) \text{ in } \Omega. \tag{6.9}$$

To remove the unknown coefficient $a(x)$ from (6.9), differentiate (6.9) with respect to s and denote $q(x, s) = \partial_s v(x, s)$. Hence,

$$\Delta q + 2\nabla q \cdot \nabla v = 0. \tag{6.10}$$

We now need to express the function v via the function q. This expression is obviously given by

$$v(x, s) = -\int_s^{\overline{s}} q(x, \tau) d\tau + v\left(x, \overline{s}\right). \tag{6.11}$$

We set $\overline{s}$ to be a large number. We call the function $v\left(x, \overline{s}\right)$ "tail". In the frequency dependent case the function $v\left(x, \overline{s}\right)$ was dropped, for $\overline{s} >> 1$ because $v\left(x, \overline{s}\right) \approx 0$ in that case. However, the latter is not true in our case. Hence, we need a special treatment to approximate the tail. We focus now on an approximation of the function q. Substituting (6.11) in (6.9), we obtain

$$\Delta q - 2\nabla q \cdot \int_s^{\overline{s}} q(x, \tau) d\tau + 2\nabla q \cdot \nabla v\left(x, \overline{s}\right) = 0. \tag{6.12}$$

Also, conditions (6.6) imply that

$$q(x, s) = \varphi_1(x, s), q_z\left(x, s\right) = \psi_1\left(x, s\right), \text{ for } x \in \Gamma, s \in \left[s_0, \overline{s}\right], \tag{6.13}$$

where

$$\varphi_1(x, s) = \partial_s \ln \varphi(x, s), \psi_1\left(x, s\right) = \frac{\psi_s}{\varphi}(x, s) - \left[\frac{\varphi_s}{\varphi^2}\psi\right](x, s).$$

Although the calculation of the derivative with respect to s is an ill-posed procedure, but it can be handled via a regularization method, see, e.g., [34] for a simple method.

We have obtained the Cauchy problem for the nonlinear integral-differential elliptic Partial Differential Equation (6.12) with the Cauchy data (6.13). Its numerical treatment was similar with the one described in section 2. As to the basis functions in (2.21),we have chosen trigonometric functions. As to the tail, we have used the asymptotic formula for the solution of the forward problem (6.1), (6.2) and the available data to get an approximate value of the tail. Interestingly, we have discovered that it is sufficient to have only three (3) source positions for the tail and only two (2) source position for the subsequent reconstruction via the convexification.

6.3 Some details of numerical experiments

We now describe some ideas of numerical experiments. For the forward problem, we calculate the solution of the diffusion equation

$$\Delta u - a(x,z)u = -\delta\left(x - s, z - z_m\right) \tag{6.14}$$

with the conventional condition at the infinity

$$\lim_{|(x,z)|\to\infty} u(x,z,s) = 0, \tag{6.15}$$

where the physics of the function $a(x,z)$ is defined in (6.8). We have considered a medical application. However, the above application to imaging of targets on battlefields can also be considered after a proper re-scaling. Consider the rectangle Ω,

$$\Omega = \left\{(x,z) : 5cm < x < 15cm, 5cm < z < 10cm\right\}.$$

We assume that

$$a(x,z) = k^2 = const. > 0 \text{ in } \mathbb{R}^2 \diagdown \Omega. \tag{6.16}$$

We assume that in (6.14) the source position (s, z_m) is running along the right side of Ω, i.e., $z_m = L = 10cm$. Also, consider a bigger rectangle

$$\Omega_0 = \{(x,z) : 0cm < x < 20cm, 0cm < z < 15cm\}.$$

The reason why we consider the rectangle Ω_0 along with the rectangle Ω is that it is natural to approximate the solution of the problem (6.14), (6.15) in the infinite domain by the solution of equation (6.14) in Ω_0 with Robin boundary conditions at $\partial\Omega_0$. We have established numerically that for the range of parameters we use the solution of the problem (6.14), (6.15) is close in Ω to the solution of equation (4.1) in the bigger rectangle Ω_0 with the Robin boundary conditions at its sides.

The light sources are located in several positions $(x_i, z) = (s_i, 10)$ along the right-hand side of the smaller rectangle Ω, and receivers are located at the left-hand side of Ω. However, we have found in our numerical experiments that only three farthest away sources are typically useful for the reconstruction. We use three (3) sources to construct an approximation of the tail functions to be described below. Next, we use two (2) sources for the above layer stripping procedure both in the s-derivative and the s-integral. Although it is possible to use more data or light source positions, but our numerical experiments showed no significant improvement. We have also introduced the multiplicative random noise in the data.

Following the convexification method described above, we divide the domain Ω along the z axis into 30 layers within the interval $z \in [z_0, z_m - \theta]$. In each layer we then approximate the vector function $p(z,s)$ along the z-axis by interpolations using quadratic polynomials (2.14). Coefficients $b_i(s)$ and $c_i(s)$ are determined by the values of solutions from the previous layer. The unknown coefficient $a_i(s)$ is determined by solving equation (2.33) with the contractive

mapping operator, see Theorem 2.1 in section 2. In our case we take only two values s_1 and $s_2 = \overline{s}$, $s_1 < s_2$ and assume that

$$b_i(s) = b_i(s_1), c_i(s) = c_i(s_1), a_i(s) = a_i(s_1) \text{ for } s \in [s_1, s_2]\,.$$

In x-direction we approximate the solution using Fourier series. Although this is not completely justifiable (because the boundary conditions are not periodical), it does provide a reasonable approximation in our problem. We first tried the number 65 of terms in Fourier series (2.21), or 32 Fourier modes involving

$$\sin(\frac{\pi m x}{5}) \text{ and } \cos(\frac{\pi m x}{5}) \text{ for } m = 0, ..., 32.$$

However, this case was unstable. To explain the latter, we note that the problem (2.22), (2.23) inherited the instability of the original Cauchy problem for the nonlinear integral differential equation (2.20a) with the Cauchy data (2.20b). It is well known that the Cauchy problem for an elliptic equation is unstable. Hence, in our case the numerical error will be increasing with the number of Fourier modes. In order to reduce the numerical noise generated by the layer stripping reconstruction, we need to reduce the number of modes in our truncated Fourier series.

Because of the latter, we start our calculations with five (5) Fourier modes in the first layer and end up with two (2) Fourier modes at the 30^{st} layer (the right edge). To do this, we change initial conditions in each layer as follows

$$\widetilde{b}_{im}(s) := b_{im}(s)\left(1 - \frac{(i-1)h}{30}\right), \widetilde{c}_{im}(s) := c_{im}(s)\left(1 - \frac{(i-1)h}{30}\right),$$

where $b_{im}(s)$ is the component of the vector $b_i(s)$, which corresponds to either of functions

$$\sin(\frac{\pi m x}{5}) \text{ or } \cos(\frac{\pi m x}{5}), m = 3, 4, 5.$$

The coefficient $c_{im}(s)$ is defined similarly.

6.4 Tails $\widehat{v}(\mathbf{x}, \overline{s})$ in (6.11)

A crucial issue in our problem is to find a good quality approximation of the function $\widehat{v}(\mathbf{x}, \overline{s})$ in (6.11) for a large value of $\overline{s}$. In the case of inverse problems for time dependent equations this can be done using a clear asymptotic behavior of the Laplace transform of the solution of the forward problem. In our case, however, the free parameter s is the location of the light source. For real world applications, the source location cannot be too far from the inclusion, both due to the restriction in size and the limit of the light intensity. We have undertaken a substantial effort to understand the behavior of solutions when locations of light sources move at realistic scales.

First, we consider the fundamental solution of the problem (6.14), (6.15) for the case $a(x,z)/D \equiv k^2$. This solution is

$$u_0 = \frac{1}{2\pi} K_0(k|(x-s, z-z_m)|),$$

where $K_0(z)$ a modified Bessel function. It is well known that the asymptotic behavior of this function is

$$K_0(z) = \sqrt{\frac{\pi}{2|z|}} e^{-k|z|} \left(1 + O\left(\frac{1}{|z|}\right)\right), |z| \to \infty. \tag{6.17}$$

Represent now solution of the problem (6.14), (6.15) with the condition (6.16) as the solution of the following integral equation

$$u(x,z,s) = \frac{1}{2\pi} K_0(k|(x-s, z-z_m)|) \tag{6.18}$$

$$-\frac{1}{2\pi} \int\limits_{\Omega} K_0\left(k\sqrt{(x-\xi)^2 + (z-\eta)^2}\right) \left[a(\xi,\eta) - k^2\right] u(\xi,\eta,s)\, d\xi d\eta.$$

Let $S(x,z,s) = |(x,z) - (s,z_m)|$. Introducing the function

$$U(x,z,s) = 2\sqrt{2\pi S} e^{kS} \cdot u(x,z,s)$$

and taking into account (6.17) and (6.18), we obtain that

$$u(x,z,s) = \frac{1}{2\sqrt{2\pi S}} e^{-kS} \left[1 + \tilde{g}(x,z) + O\left(\frac{1}{S}\right)\right], S \to \infty.$$

The function $\tilde{g}(x,z)$ is unknown and is independent of S as $S \to \infty$. Hence, we obtain for the function $v = \ln u$

$$v(x,z,s) = -kS - \ln S + g(x,z) + O\left(\frac{1}{S}\right), S \to \infty \tag{6.19}$$

where the unknown function $g(x,z) \neq \tilde{g}(x,z)$.

We approximate the function $g(x,z)$ by two different methods and the final answer is the average of two. We start at $z = z_0$ where the boundary values are known. We decompose the boundary values of v into

$$v(x,z_0,s) = \sum_{m=0}^{5} \left[b_m^{(1)}(s) \cos\left(\frac{m\pi}{5}x\right) + b_m^{(2)}(s) \sin\left(\frac{m\pi}{5}x\right)\right], \tag{6.20a}$$

$$v_z(x,z_0,s) = \sum_{m=0}^{5} \left[b_{zm}^{(1)}(s) \cos\left(\frac{m\pi}{5}x\right) + b_{zm}^{(2)}(s) \sin\left(\frac{m\pi}{5}x\right)\right]. \tag{6.20b}$$

Hence,

$$b_m^{(1)}(s) = \frac{1}{\sqrt{5}} \int_5^{15} v(x, z_0, s) \cos\left(\frac{m\pi}{5}x\right) dx, \tag{6.21a}$$

$$b_m^{(2)}(s) = \frac{1}{\sqrt{5}} \int_5^{15} v(x, z_0, s) \sin\left(\frac{m\pi}{5}x\right) dx. \tag{6.21b}$$

Therefore it follows from (6.19) that the asymptotic expansions for functions $b_m^{(1)}(s)$ are

$$\begin{aligned} b_m^{(1)}(s) &= \frac{1}{\sqrt{5}} \int_5^{15} -\left[kS(x, z_0, s) + \ln S(x, z_0, s)\right] \cos\left(\frac{m\pi}{5}x\right) dx + \widetilde{b}_m^{(1)} \\ &+ O\left(\frac{1}{S(x, z_0, s)}\right). \end{aligned}$$

The function $g(x, z_0)$ can be approximated by a truncated Fourier series with coefficient $\widetilde{b}_m^{(1)}(s)$ and $\widetilde{b}_m^{(2)}(s)$ and similarly for $g_z(x, z_0)$. To approximate numbers $\widetilde{b}_m^{(1)}$, we take three measurements ranging for source locations s_1,s_2, s_3 that are far enough and set

$$\widetilde{b}_m^{(1)} = \frac{1}{3} \sum_{k=1}^{3} \left[b_m^{(1)}(s_k) + \frac{1}{\sqrt{5}} \int_5^{15} \left(kS(x, z, s_k) + \ln S(x, z, s_k)\right) \cos\left(\frac{m\pi}{5}x\right) dx \right], \tag{6.22}$$

where numbers $b_m^{(1)}(s_k)$ are calculated by (6.21a,b). We do similarly for other coefficients in (6.20a,b). Note that in (6.20a,b) and (6.22) one should actually put "$\approx$" sign instead of "$=$". The number of light sources $N = 3$ is taken in all our experiments when we approximate the function g.

However, the above procedure (6.19)-(6.22) gives us the value of the tail function $\widehat{v}\,(x, z, \overline{s})$ and its derivative $\widehat{v}_z\,(x, z, \overline{s})$ in (6.11) only at $z := z_0$, i.e., $\widehat{v}\,(x, z_0, \overline{s})\,, \widehat{v}_z\,(x, z_0, \overline{s})\,.$ Equation (6.19) provides an approximation for all $(x, z) \in \Omega$ if we simply set $g(x, z, s) = g(x, z_0, s)$. In our numerical experiments we found that this is insufficient. Hence, we use the measurement data from a different angle, which enhances our numerical results. We obtain a similar tail function using the measurement data at the lower edge of Ω, i.e., at $x = 5cm$. We have decomposed the boundary values $v\,(5, z, s)$ and $v_z\,(5, z, s)$ into a Fourier series of z and got a second tail function using the idea similar with the above. Thus, we have approximated $v\,(5, z, \overline{s})\,, v_z\,(5, z, \overline{s})\,.$ Finally we set for the tail

$$\widehat{v}\,(x, z, \overline{s}) := \frac{1}{2}\left[\widehat{v}\,(x, z_0, \overline{s}) + \widehat{v}\,(5, z, \overline{s})\right], \tag{6.23}$$

$$\widehat{v}_z\,(x, z, \overline{s}) := \frac{1}{2}\left[\widehat{v}_z\,(x, z_0, \overline{s}) + \widehat{v}_z\,(5, z, \overline{s})\right], \tag{6.24}$$

In our numerical experiments we have used the value of $\lambda = 50$. We have attempted to use the tail function alone from (6.23), (6.24) for the reconstruction of $a(x,z)$. The tail function has provided most of the information about locations of the inclusions. These locations were reconstructed precisely. However the peak value of the reconstructed coefficient within inclusions was is about 30% off the original. To overcome that, we follow the following four steps procedure:

Step 1. Use the tail function to obtain an initial guess $\mu_{a0}(x,z)$ for the unknown coefficient $\mu_a(x,z)$.

Step 2. Re-scale $\mu_{a0}(x,z)$ linearly to a commonly acceptable biological value. In our case, we set $\mu_{a1}(x,z) = \mu_{a0}(x,z)$ if $\mu_{a0}(x,z) < \widehat{\mu}$, below the threshold and $\mu_{a1}(x,z) = \alpha\mu_{a0}(x,z)$ if $\mu_{a0}(x,z) > \widehat{\mu}$, where $\widehat{\mu}$ is a threshold value. The scaling constant α in our problem is chosen such that the maximum of $\mu_{a1}(x,z) = 0.3$ which is the maximum value of the actual coefficient. In problems where the actual $\mu_a(x,z)$ is unknown, we use biologically well-known coefficient for that specific kind of medical application. The value of $\widehat{\mu}$ ranges from 0.14 to 0.16 in numerical examples we calculated.

Step 3. Re-calculate the forward problem using re-scaled $a_1(x,z)$ as the coefficient. The function $v(x,z,\overline{s})$ resulting from the calculated solution is used then as the tail function instead of (6.23)-(6.24).

Step 4. After we have obtained the function $u(x,z,s)$ at the measurement surface at $z=0$ and obtain consequently $v = \ln u$ at $s = s_1,\ s_2$, where $s_2 > s_1$, we set $\overline{s} := s_2$. Then we calculate the function $q(x,z,s_1)$ as

$$q(x,z_0,s_1) = \frac{v(x,z_0,s_2) - v(x,z_0,s_1)}{s_2 - s_1}.$$

Similarly for the derivative $q_z(x,z_0,s_1)$. This way we obtain initial values $b_0(s_1), c_0(s_1)$. In all follow up calculations on all layers we set $q(x,z,s) := q(x,z,s_1)$ for $s \in [s_1,s_2]$. In each layer we have solved equation (2.33) with the contractive mapping operator. After we obtain $q(x,z,s_1)$ for all z, we update $v(x,z,s_1) = \widehat{v}(x,z,s_2) - q(x,z,s_1)(s_2 - s_1)$

Step 5. Reconstruct the coefficient $\mu_a(x,z)$ from the function $v(x,z,s_1)$ using a finite element code of [10].

Figures 15 and 16 display some results of reconstruction from the transmitted data in the 2-D case with $\mathbf{x} = (x,z)$. That is, the source was running along the line $\{x_1, z_m\}, z_m = const. > 0, x \in [c,d]$ and the data were given at the line $\{x, z_0\}, z_0 = const. < z_m, x \in [c,d]$, as well as at the line $\mathbf{x} = \{c, z\}, z \in [z_0, z_m]$, where the data at the second line were used to get an approximate value for the tail function.

6.5 Conclusions

Although the case of the running source is not covered by the original theory of the convexification, especially the issue of tails, we were capable to adapt the convexification scheme to this case. Applications include imaging of land mines by the Electrical Impedance Tomography, optical imaging of targets on battlefields covered by smogs and flames and medical optical imaging.

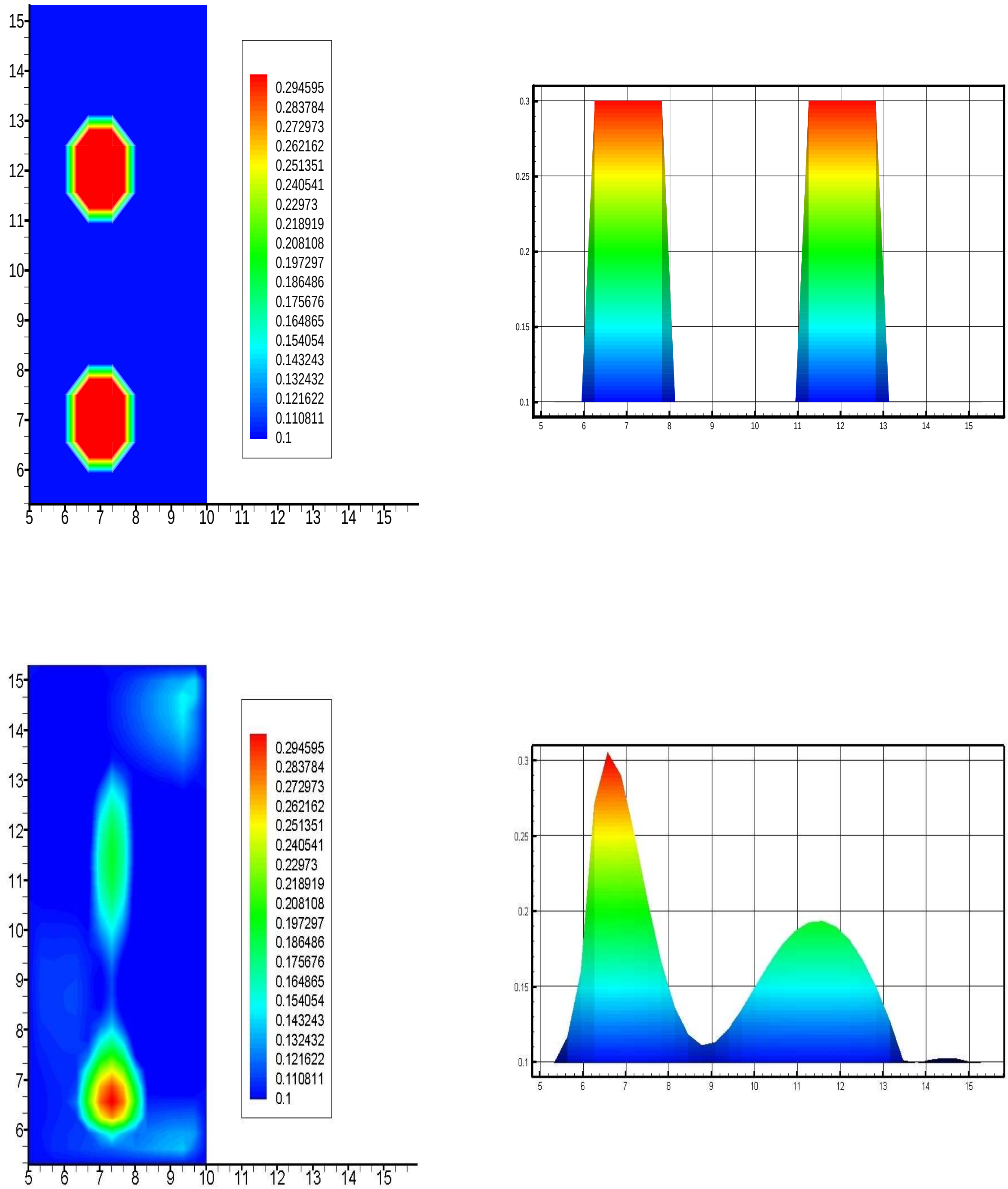

Figure 15: The original function $a(x,z)$ (top left) and its 1-d cross-section (top right) via the centerline of inclusions. Other 1-d cross-sections of Figs. 15 and 16 are by the same line. The bottom figures display the reconstruction for the noiseless data.

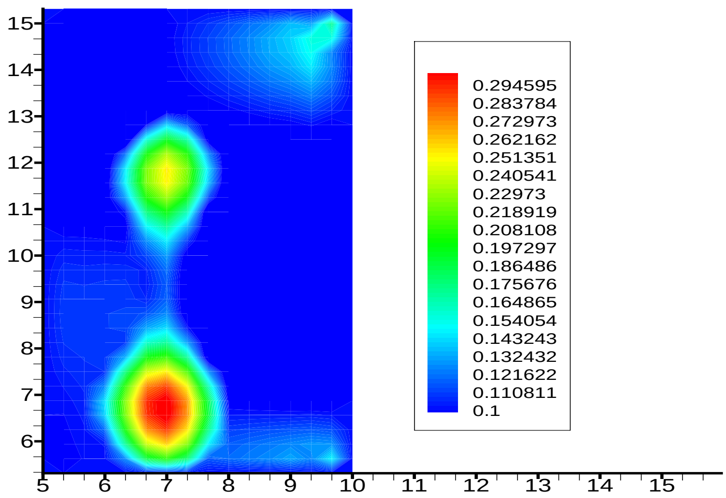

Figure 16: Reconstruction of the medium of Figure 15 (top) with 2% noise in the data.

7 Convexification via the Cauchy-Riemann-like System of the First Order

The work of this section was performed by Dr. A. Timonov, who was working during 2007 under a subcontract as a faculty of University of South Carolina Upstate. He has proposed the idea of replacing the second order PDE (2.20a) with the Cauchy-Riemann-like system of PDEs of the first order.

Consider again the Cauchy problem (2.20a,b). To simplify the presentation, consider the "tail free" case, although tails were incorporated in the numerical scheme. We rewrite it now in the 2-Dimensional case as follows

$$q_{zz}+q_{xx}+2s^2q_z\left[-\int\limits_s^{\bar{s}}q_z\left(x,z,\tau\right)d\tau\right]+2s^2q_x\left[-\int\limits_s^{\bar{s}}q_x\left(x,z,\tau\right)d\tau\right]$$

$$+2s\left[\int\limits_s^{\bar{s}}q_x\left(x,z,\tau\right)d\tau\right]^2+2s\left[\int\limits_s^{\bar{s}}q_z\left(x,z,\tau\right)d\tau\right]^2=0. \tag{7.1}$$

In addition, the following Cauchy data are given

$$q\left(x,0,s\right)=\varphi_2\left(x,s\right),\ q_z\left(x,0,s\right)=\psi_2\left(x,s\right), \tag{7.2}$$

$$\text{for }\ (x,s)\in(-A,A)\times(s_0,\bar{s}).$$

Equation (7.1) contains only derivatives of the function q. Hence, introduce two new functions $u(x,z,s)$ and $v(x,z,s)$ as

$$u(x,z,s) := q_z(x,z,s), v(x,z,s) := q_x(x,z,s). \tag{7.3}$$

Then (7.1) leads to

$$u_z + v_x + 2s^2 u\left[-\int_s^{\bar{s}} u(x,z,\tau)\,d\tau\right] + 2s^2 v\left[-\int_s^{\bar{s}} v(x,z,\tau)\,d\tau\right] \tag{7.4}$$

$$+2s\left[\int_s^{\bar{s}} v(x,z,\tau)\,d\tau\right]^2 + 2s\left[\int_s^{\bar{s}} u(x,z,\tau)\,d\tau\right]^2 = 0.$$

In addition, since $q_{xz} = q_{zx}$, then (7.3) implies that

$$v_z - u_x = 0. \tag{7.5}$$

And by (7.2)

$$u(x,0,s) = \psi_2(x,s), v(x,0,s) = \varphi_{2x}(x,s). \tag{7.6}$$

We have obtained the first order system (7.4), (7.5) with the initial conditions (7.6). If integrals would be absent, then (7.4), (7.5) would be exactly the classic Cauchy-Riemann equations known from the complex analysis for real and imaginary parts of an analytic function.

To solve the problem (7.4)-(7.6), we apply an analogue of the convexification method of section 2. However, instead of using quadratic polynomials on each layer, we use linear functions with respect to z: because of the first order derivatives.

Convergence Theorem. A stability and convergence theorem similar with the above Theorem 2.1 can be proven.

It is natural to first test the case of the 1^{st} order equation in the 1-dimensional case. Three algorithms were tested for the case of imaging of land mines: (a) the original convexification algorithm for the 2^{nd} order PDE, (b) the above new version of the convexification for the 1^{st} order PDE, and (c) another version of the convexification, which is based on the introduction of a new norm using the Carleman Weight Function; this version was tested for the 1^{st} order PDE. Figure 14 displays some of obtained numerical results. Since the performance of versions (a) and (b) is very similar, results for the version (a) are not displayed on Figure 17.

Conclusion. The original version of the convexification for the 2^{nd} order PDE (section 2) and two new versions for the 1^{st} order PDE provide very similar numerical results in the 1-d case. Therefore, the activity of this section was not pursued in 2008.

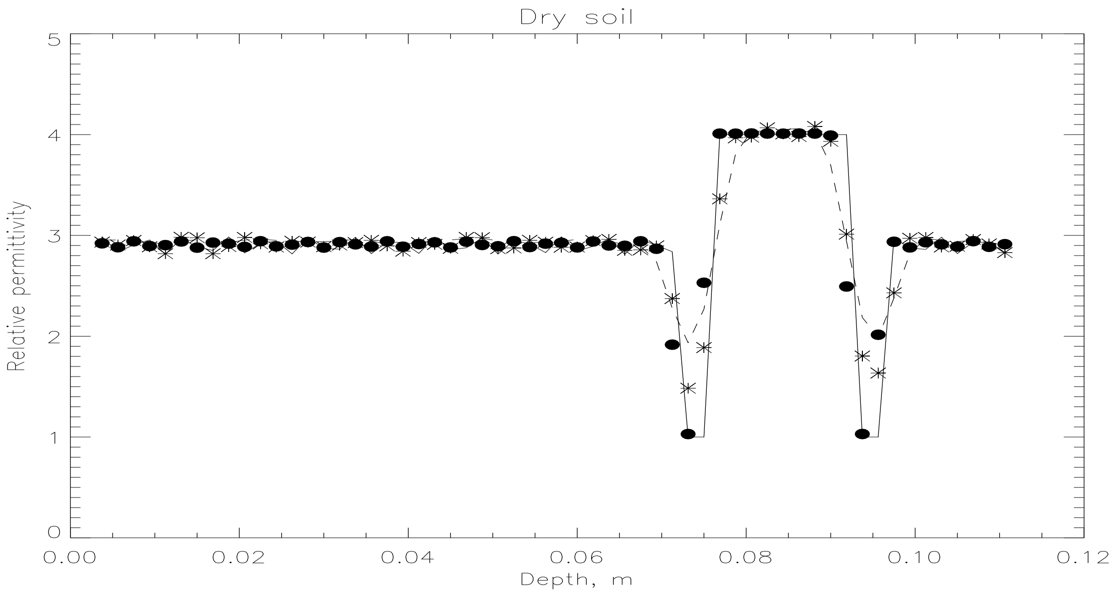

Figure 17: Numerical comparison of the performance of the convexification in the 1-d case for the first order equation. Solid line: true solution. Bullets: numerical reconstruction using the first order PDEs described in this subsection. Stars: numerical reconstruction using the re-normalization and the first order PDEs. Very similar results were obtained by the original version of the convexification for the second order PDE.

8 Numerical Solution of the Inverse Problem of Thermoacoustic Tomography

Results of subsections 8.1 and 8.2 are obtained jointly by Dr. C. Clason (Austria) and the PI and are published in [10]. Results of subsection 8.3 are obtained jointly by the graduate student Mr. A. V. Kuzhuget, Drs. S. I. Kabanikhin, D.V. Nechaev (Russia) and the PI, and are published in [11]. The PI is the thesis advisor of Mr. Kuzhuget and Kuzhuget was partially supported by this grant.

8.1 Theory

Thermoacoustic computed tomography is a new imaging method that uses different modalities for the illumination of the target and measurement of its response. The target is subjected to a short electromagnetic impulse, which is absorbed, leading to a temperature increase and hence to expansion. This induces a pressure wave in the target, which can be measured as a change in the acoustic field outside the sample. If the absorption of the electromagnetic energy is spatially varying, the resulting wave field will carry the signature of that inhomogeneity. The problem is hence to calculate this absorption of the target from time dependent acoustic measurements outside it. the mathematical statement of the problem is to find initial condition of the wave equation given time dependent measurements of both its solution and its normal derivative at a surface.

The propagation of the resulting acoustic pressure field $u(x,t)$ in $\mathbb{R}^3$ is governed by the equation

$$\frac{1}{c^2(x)} u_{tt} = \Delta u, (x,t) \in \mathbb{R}^3 \times (0,T) \tag{8.1}$$

with the initial conditions

$$u(x,0) = f_1(x), u_t(x,0) = f_2\left(x\right), \tag{8.2}$$

where the function $f_1(x) = \alpha\left(x\right) k$, where $\alpha(x)$ is the spatially varying absorption coefficient, which is unknown, the positive constant k is known, so as the spatially varying sound speed $c(x)$. In applications to thermoacustic tomography $f_2\left(x\right) \equiv 0$ and only the function $f_1(x)$ is unknown. However, our numerical scheme of subsections 8.1 and 8.2 does not rely on any knowledge of functions $f_1\left(x\right), f_2\left(x\right)$ and actually determines both of them simultaneously. We consider the following

Inverse Problem. Let $\Omega \subset \mathbb{R}^3$ be a bounded domain with the piecewise smooth boundary $\partial\Omega$. And let $\Gamma \subseteq \partial\Omega$ be a part of the boundary. Denote $\Gamma_T = \Gamma \times (0,T)$. Determine functions $f_1\left(x\right), f_2\left(x\right)$ in Ω assuming that the following lateral Cauchy data $\varphi_0(x,t)$ and $\varphi_1(x,t)$ are known

$$u \mid_{\Gamma_T} = \varphi_0(x,t), \partial_n u \mid_{\Gamma_T} = \varphi_1(x,t). \tag{8.3}$$

Denote $Q_T = \Omega \times (0,T)$, $S_T = \partial\Omega \times (0,T)$. Suppose that there exists a function $g(x,t) \in H^2(Q_T)$ satisfying boundary conditions (8.3), i.e.,

$$g\mid_{\Gamma_T} = \varphi_0(x,t), \partial_n g\mid_{\Gamma_T} = \varphi_1(x,t). \tag{8.4}$$

Denote

$$w(x,t) = u(x,t) - g(x,t), L = \frac{1}{c^2(x)}\partial_t^2 - \Delta,$$
$$\Phi(x,t) = -L(g)(x,t).$$

Then (8.1)-(8.4) imply that

$$Lw = \Phi(x,t) \text{ in } Q_T, \tag{8.5}$$
$$w\mid_{\Gamma_T} = \partial_n w\mid_{\Gamma_T} = 0. \tag{8.6}$$

If we find the function w from conditions (8.5), (8.6), then we can easily find unknown initial conditions $f_1(x) = w(x,0) + g(x,0)$, $f_2(x) = w(x,0) + g(x,0)$. Hence, we now focus on obtaining a good approximation of the function $w(x,t)$ from conditions (8.5), (8.6). Clearly, the problem (8.5), (8.6) is a non-classical one. We first formulate a Lipschitz stability estimate for this problem, which is Theorem 8.1. This theorem is proven via a Carleman estimate for the operator L.

Theorem 8.1 [10]. *Assume that*

$$c_{\max} > c(x) > c_{\min} > 0, \forall x \in \overline{\Omega},$$

there exists a point $x_0 \in R^3$ *such that*

$$\frac{1}{2} + \left\langle \nabla\left(c^{-2}(x), x - x_0\right)\right\rangle \geq 0, \forall x \in \overline{\Omega}.$$

Let $r = \max_{x\in\overline{\Omega}} |x - x_0|$. *Choose a number* $\beta > 0$ *such that*

$$\sqrt{\beta} < \frac{1}{4\left(c_{\min}^{-4} + r\left|\nabla c^{-2}(x)\right|\right)}, \forall x \in \overline{\Omega}$$

and

$$\beta < \frac{c_{\min}^2}{3}.$$

If $c \equiv$ *const.* > 0, *then these conditions reduce to* $c > \beta$. *Suppose that the observation time* $T >$ *diameter* $(\Omega)/\sqrt{\beta}$. *Then there exists a positive constant* $C = C(Q_T, x_0, c_{\min}, c_{\max})$ *such that the following Lipschitz stability estimate holds*

$$\|v\|_{H^1(Q_T)} \leq C\left[\|Lv\|_{L_2(Q_T)} + \|v\mid_{S_T}\|_{H^1(S_T)} + \|v\mid_{S_T}\|_{L_2(S_T)}\right], \forall v \in H^2(Q_T).$$

This theorem guarantees stability of the numerical method proposed below for the case $\Gamma_T = S_T$. To solve the problem (10.5), (10.6) numerically, consider the Tikhonov functional $J_\varepsilon(w)$,

$$J_\varepsilon(w) = \frac{1}{2}\|Lw - \Phi\|_{L_2(Q_T)}^2 + \frac{\varepsilon}{2}\|w\|_{QR}^2, \tag{8.7}$$

where $\varepsilon > 0$ is the regularization parameter and

$$\|w\|_{QR}^2 := \|w\|_{L_2(Q_T)}^2 + \|w_{tt}\|_{L_2(Q_T)}^2 + \|\Delta w\|_{L_2(Q_T)}^2 .$$

Denote $\langle , \rangle_{QR}$ the scalar product corresponding the norm $\|.\|_{QR}^2$. We consider this functional over the space $H_0^2(Q_T)$, where

$$H_0^2(Q_T, \Gamma_T) = \left\{ w \in H^2(Q_T, \Gamma_T) : w \mid_{\Gamma_T} = \partial_n w \mid_{\Gamma_T} = 0 \right\}.$$

By the variational principle the minimizer w_ε of the functional $J_\varepsilon(w)$ satisfies the following integral identity

$$\int_{Q_T} L w_\varepsilon L v dq + \varepsilon \langle w_\varepsilon, v \rangle = \int_{Q_T} \Phi L v dq, dq := dxdt, \forall v \in H_0^2(Q_T, \Gamma_T). \tag{8.8}$$

Hence, we need to solve (8.8). First, we formulate the existence, stability and convergence theorems for (8.8). Theorem 2 follows from the classic Riesz theorem.

Theorem 8.2 [10]. *For any function $\Phi \in L_2(Q_T)$ and any $\varepsilon > 0$ there exists unique solution $w_\varepsilon \in H_0^2(Q_T, \Gamma_T)$ of the problem (10.8) and*

$$\|w_\varepsilon\|_{H_0^2(Q_T, \Gamma_T)} \leq \frac{C}{\sqrt{\varepsilon}} \|\Phi\|_{L_2(Q_T)},$$

where a positive constant C independent on $\varepsilon, w_\varepsilon$ and Φ.

However, Theorem 8.2 does not guarantee existence of the solution of the original problem (9.5), (9.6). To formulate convergence and stability result, we assume first, that $\Gamma_T = S_T$. Also, we assume by the Tikhonov principle [37] that there exists an exact solution $w^* \in H_0^2(Q_T, S_T)$ of the problem (8.5), (8.6) with the "ideal" non-noisy data Φ^*. In addition, we assume that the actual data $\Phi := \Phi^\delta$ are given with an error, i.e.,

$$\left\|\Phi^\delta - \Phi^*\right\|_{L_2(Q_T)} \leq \delta,$$

where $\delta > 0$ is a small number characterizing the level of the error in the data. Let w_ε^δ be the solution of the problem (8.8) with $\Phi := \Phi^\delta$. Theorem 8.3 guarantees convergence of the regularized solution w_ε^δ to the exact solution w^* as $\varepsilon := \delta^2 \to 0$. Theorem 8.3 follows from Theorem 8.1.

Theorem 8.3 [10]. *Suppose that conditions of Theorem 8.1 hold and $\Gamma_T = S_T$. Then there exists a positive constant $B = B(Q_T, x_0, c_{\min}, c_{\max})$ such that the following estimate holds*

$$\left\|w_\varepsilon^\delta - w^*\right\|_{H^1(Q_T)} \leq B\left[\delta^2 + \varepsilon \|w^*\|_{H^2(Q_T)}^2\right].$$

8.2 Numerical Solution

To test the above method in the 2-D case, we took $\Omega = (-3,3) \times (-3,3)$ and $T = 7$ in all numerical experiments below. We have used the Riesz-Galerkin approximation of the function $w(x,y,t)$ via cubic B-splines, which provides necessary smoothness. In other words, we take certain partition of each of intervals

$$x \in [-3,3], y \in [-3,3], t \in [0,7]$$

represent the function $w(x,y,t)$ as

$$w(x,y,t) = \sum_{i,j=1}^{N} \sum_{k=1}^{P} a_{ijk} B_i(x) B_j(y) B_k(t)$$

with unknown coefficients a_{ijk}. As test functions v in (8.8) we took products of cubic B-splines,

$$v_{i_1 j_1 k_1}(x,y,t) = B_{i_1}(x) B_{j_1}(y) B_{k_1}(t).$$

This gave us a linear algebraic system $Ma = F$ with respect to the vector $a = (a_{ijk})$. We have solved this system to a tolerance of 10^{-6} by a stabilized biconjugate gradient method (BICGSTAB, provided by MATLAB). Due to the matrix being diagonally dominant, we employ Jacobi prescaling, i.e., solving $DMDa = DF$ with the diagonal matrix $D_{ii} = M_{ii}^{-1/2}$. This has proved more efficient than specialized preconditioners, since the matrix is diagonally dominant.

To test the stability of our method with respect to the random noise in the data, we introduce noise in calculated spline coefficients

$$a_{ijk}^{\delta} = a_{ijk} \left(1 + \delta \xi_{ijk}\right) a_{ijk},$$

where $\delta \geq 0$ is the noise level and ξ is the random variable uniformly distributed over $[-1,1]$

For simulations of forward problems we took $f_2(x,y) = 0$ in all our tests. We test our algorithm for the case of the reconstruction of the initial condition $f_1(x,y)$ in (8.2) of the form

$$f_1(x,y) = \sin(3x)\sin(3y)\exp\left[-x^2 - y^2\right],$$

which is negligibly small outside of the test domain Ω. Denote

$$f_{\varepsilon}(x,y) = w_{\varepsilon}(x,y,0) + g(x,y,0).$$

Test 1. Constant coefficient c. We take $\Gamma_T = S_T$ and $c(x) \equiv 1$. Figure 18 shows the slice $f_{\varepsilon}(x,0)$ for $\varepsilon = 10^{-3}$ for various noise level δ ranging from 0 to 3. One can see that even at 300% noise level the reconstruction is quite good, which is in a good agreement with the previous publication [10]. The Lipschitz stability estimate of Theorem 2 provides an explanation of such a stability.

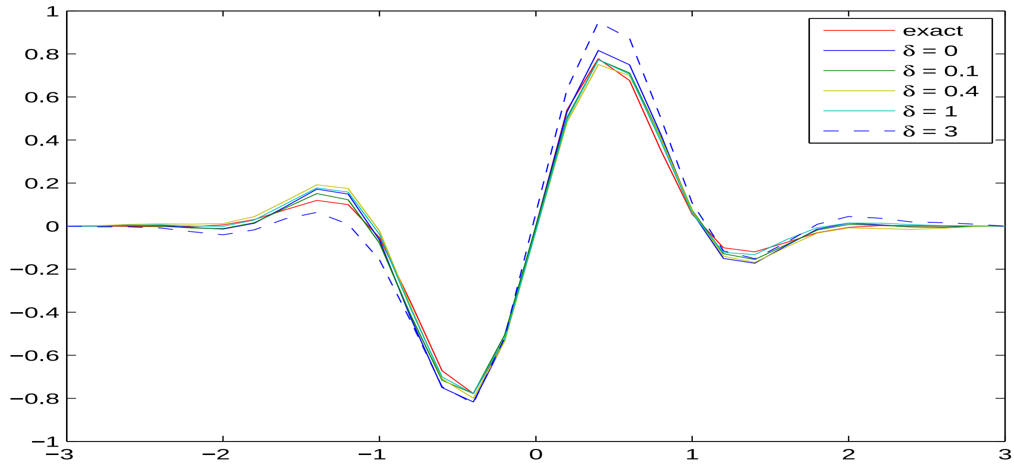

Figure 18: Comparison of the reconstructed initial condition $f_{1\varepsilon}(x, y)$ with the exact one (solid line) in a homogeneous medium for test 1 for various noise levels $\delta \in [0, 3]$, i.e., from 0% to 300% noise. The regularization parameter $\delta = 10^{-3}$. Slices of $f_{1\varepsilon}(x, y)$ are shown.

Test 2. Non-constant coefficient $c(x, y)$. We take

$$\frac{1}{c^2(x, y)} = \frac{5}{2} - \frac{1}{12}\left(x^2 + y^2\right). \tag{8.9}$$

This coefficient satisfies conditions of Theorem 8.1. By this theorem we should take $\sqrt{\beta} < 1/197$, which leaves us with $T = 1672$. However, we still take $T = 7$, since we believe that the estimate of Theorem 8.1 is a pessimistic one. Figure 19 displays the slice $f_\varepsilon(x, 0)$ for $\varepsilon = 10^{-3}$ for various noise level δ ranging from 0 to 3. One can see again that even at 300% noise level the reconstruction is quite good. **Test 3. Limited boundary data with** $\Gamma_T \neq S_T$. Again we take a heterogeneous medium with the coefficient $c(x, y)$ in (8.9). We take $T = 14$ and

$$\Gamma = \{(x, y) \in \partial\Omega : \{x = -3\} \cup \ \{y = -3\}\}. \tag{8.10}$$

Uniqueness of the solution can still be proven. Figure 20 shows numerical results for various noise levels $\delta \in [0, 1]$.

8.3 The case of a smaller observation time

We now consider the same Inverse Problem as in subsection 8.1 but under assumption that at least one initial condition at $t = 0$ is known, whereas the second one is unknown. We show that the required observation time T can be lowered by the factor of 2 in the case when in (8.1) $c \equiv 1$. In numerical experiments we consider the case of unbounded domain. Specifically, quadrant. It was shown in [11] that this case can be reduced, under certain

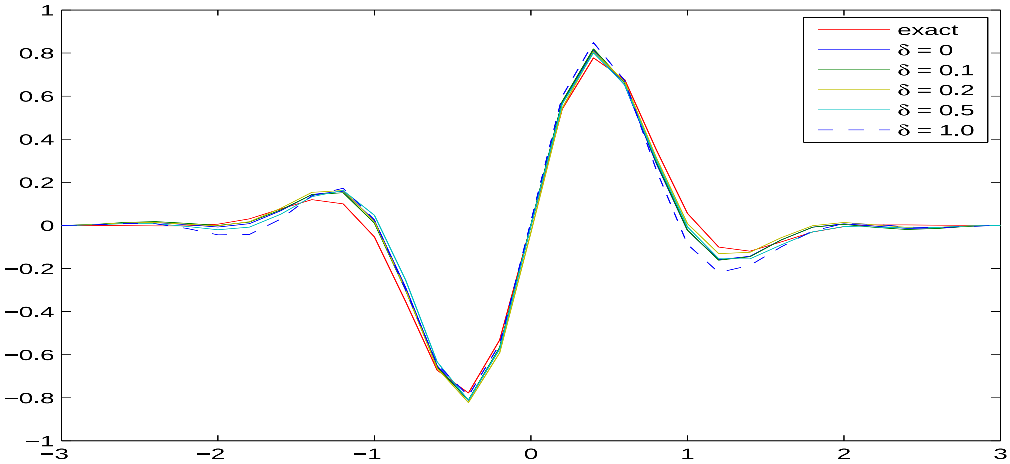

Figure 19: Comparison of the reconstructed initial condition $f_{1\varepsilon}(x, y)$ with the exact one (solid line) in a homogeneous medium for test 1 for various noise levels $\delta \in [0, 1]$. The regularization parameter $\delta = 10^{-3}$. Slices of $f_{1\varepsilon}(x, y)$are shown.

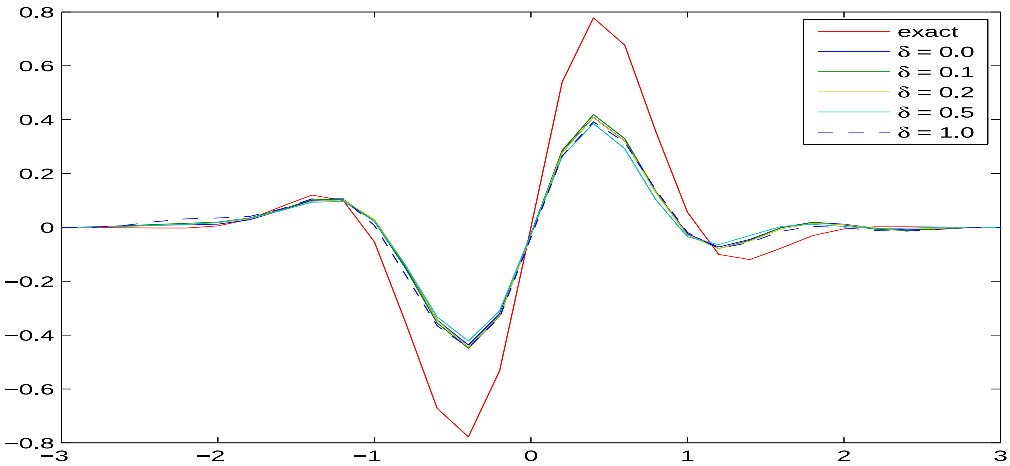

Figure 20: Results for the case of incomplete boundary data at the boundary Γ in (8.10). The heterogeneous medium (8.9) was considered. Slices of $f_{1\varepsilon}(x, y)$ are shown. Due to the energy loss at the rest of the boundary $\partial\Omega \diagdown \Gamma$ the resulting solution has a lower amplitude. The shape, however, is preserved.

conditions, to the situation of a bounded domain. The second significant difference with the above is that instead of using finite elements of subsection 8.2, we use in our numerical implementation finite differences. This enables us to image narrow peaks, which model δ-function. The latter was impossible when using finite elements of the previous subsections, because of their over-smoothness.

Let $\Omega \subset \mathbb{R}^n$ be a convex domain with a piecewise smooth boundary $\partial\Omega$ and $2R$ be the diameter of $\Omega, 2R = \max_{x,y\in\Omega} |x-y|$. Let $T = const. > R$. Denote $Q_T = \Omega \times (0,T)$. Consider the elliptic operator $L(x,t)$ of the form

$$L(x,t)u = \Delta u + \sum_{j=1}^{n} b_j(x,t)\, u_j + b_0(x,t)\, u_t + c(x,t)\, u,$$

where $u_j := \partial_{x_j} u$. We assume that all coefficients of the operator L belong to $C\left(\overline{Q}_T\right)$. Let the function $u \in H^2(Q_T)$ be a solution of the hyperbolic equation in the cylinder Q_T,

$$u_{tt} = L(x,t)u + F(x,t) \text{ in } Q_T, \tag{8.11}$$

$F \in L_2(Q_T)$ with initial conditions

$$u(x,0) = \varphi(x), u_t(x,0) = \psi(x), \varphi \in H^1(\Omega), \psi \in L_2(\Omega). \tag{8.12}$$

In this subsection we consider

Inverse Problem 1. Let one of functions φ or ψ be known and another one be unknown. Determine that unknown function assuming that the following functions f and g are given

$$u \mid_{S_T} = f(x,t), \ \frac{\partial u}{\partial \nu} \mid_{S_T} = g(x,t), \ S_T = \partial\Omega \times (0,T), \tag{8.13}$$

where ν is the unit outward normal vector at $\partial\Omega$. We call the problem of the determination of the function φ the "$\varphi-$problem" and the problem of the determination of the function ψ the "$\psi-$problem".

It follows from Theorem 8.1 that in the case $T > 2R$ one should not assume that one of functions φ or ψ is known. So, we are interested here in the case $T \in (R, 2R)$. We now specify conditions of our numerical study. Suppose that equation (8.11) is homogeneous with $F(x,t) \equiv 0$ and it is satisfied in $D_T^3 = \mathbb{R}^2 \times (0,T)$. Consider the quadrant $QU = \{x_1, x_2 > 0\}$. And also consider the square $SQ \subset QU$,

$$SQ(a) = \{0 < x_1, x_2 < a\}.$$

Suppose that

$$\varphi(x) = \psi(x) = 0 \text{ outside of } SQ(a). \tag{8.14}$$

Then the energy estimate implies that

$$u(x,t) = 0, \forall (x,t) \in \{x \mid x \in QU, dist(x, SQ(a)) > T\} \times (0,T). \tag{8.15}$$

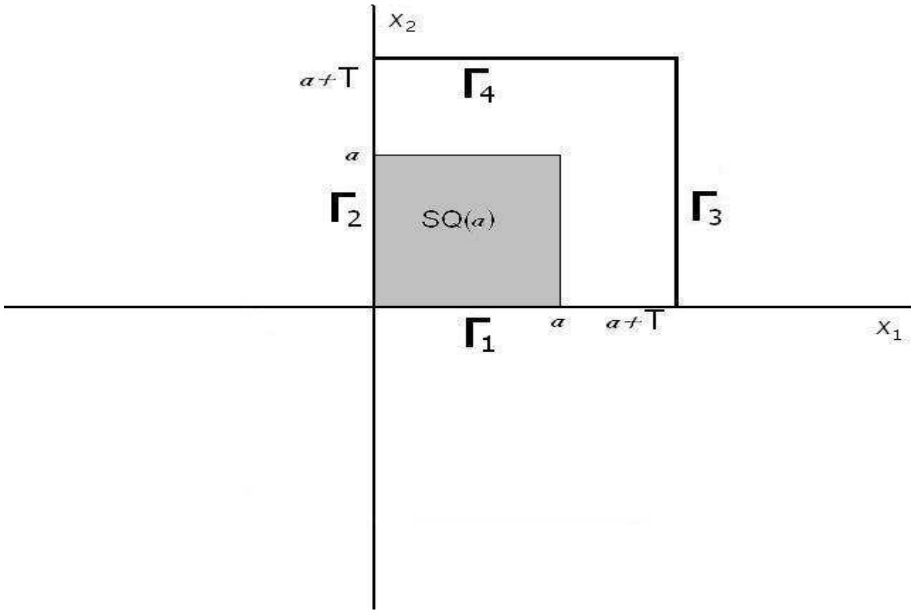

Figure 21: Geometry for the case of quadrant (Inverse Problem 2).

Denote

$$\Gamma_{1T} = \{x_1 \in (0, a+T), x_2 = 0\} \times (0,T),$$
$$\Gamma_{2T} = \{x_2 \in (0, a+T), x_1 = 0\} \times (0,T),$$
$$\Gamma_{3T} = \{x_1 = a+T, x_2 \in (0, a+T)\} \times (0,T),$$
$$\Gamma_{4T} = \{x_2 = a+T, x_1 \in (0, a+T)\} \times (0,T),$$

see Figure 21. Then by (8.15)

$$u = \frac{\partial u}{\partial \nu} = 0 \text{ on } \Gamma_{3T} \cup \Gamma_{4T}. \tag{8.16}$$

Hence, we focus our numerical study on

Inverse Problem 2. Let equation (8.11) be satisfied in D_T^3 with initial conditions (8.12) satisfying (8.14). In this case $\Omega := SQ(a+T)$. Suppose that one of these initial conditions is zero. Determine the second initial condition, assuming that functions f and g are known, where

$$u \mid_{\Gamma_{1T} \cup \Gamma_{2T}} = f(x,t), \ \frac{\partial u}{\partial \nu} \mid_{\Gamma_{1T} \cup \Gamma_{2T}} = g(x,t). \tag{8.17}$$

It was proven in [11] that if

$$T > \frac{a\sqrt{2}}{2-\sqrt{2}} \tag{8.18}$$

and one of functions φ or ψ equals zero, then the following Lipschitz stability estimate is valid

$$\|u\|_{H^1(G_T)} \leq C\left(\|f\|_{H^1(\Gamma_T)} + \|g\|_{L_2(\Gamma_T)}\right), \tag{8.19}$$

where $\Gamma_T = \Gamma_{1T} \cup \Gamma_{2T}$ and $\|f\|_{H^1(\Gamma_T)} = \|f\|_{H^1(\Gamma_{1T})} + \|f\|_{H^1(\Gamma_{2T})}$.

We consider Inverse Problem 1, because it is more general than Inverse Problem 2. Denote $Mu = u_{tt} - Lu$. To solve the Inverse Problem 1 numerically, consider the Tikhonov regularizing functional

$$\begin{gathered} J_\varepsilon(u) = \|Mu - F\|^2_{L_2(Q_T)} + \varepsilon\|u\|^2_{H^2(Q_T)} \\ + \left\|D^\beta u\mid_{S_T} - D^\beta f\right\|^2_{L_2(S_T)} + \|u_\nu\mid_{S_T} - g\|^2_{L_2(S_T)} \\ +\chi_\varphi\|u_t(x,0) - \psi\|^2_{L_2(\Omega)} + \chi_\psi\|u(x,0) - \varphi\|^2_{H^1(\Omega)}, \forall u \in H^2(Q_t). \end{gathered} \tag{8.20}$$

Here $\varepsilon > 0$ is the regularization parameter,

$$u_\nu\mid_{S_T} := \frac{\partial u}{\partial \nu}\mid_{S_T}$$

and $D^\beta, |\beta| \leq 1$ is the operator of (x,t) derivatives with, where x-derivatives are those, which are taken in directions orthogonal to the normal vector. Also,

$$\chi_\psi = \left\{\begin{array}{l} 1 \text{ for the } \psi - \text{problem} \\ 0 \text{ for the } \varphi - \text{problem}\end{array}\right\}, \chi_\varphi = \left\{\begin{array}{l} 1 \text{ for the } \varphi - \text{problem} \\ 0 \text{ for the } \psi - \text{problem}\end{array}\right\}.$$

Hence, $\chi_\varphi\chi_\psi = 0, \chi_\varphi + \chi_\psi = 1$. In subsection 8.2 and in all previous works on the QRM terms in the second line of (8.20) were absent because of subtracting off boundary conditions from the original function u. Terms in the third line of (8.20) were absent also, and they are incorporated now to emphasize the knowledge of one of initial conditions.

To find the minimizer of $J_\varepsilon(u)$, we set the Fréchet derivative of this functional to zero and obtain for all $v \in H^2(Q_T)$

$$\begin{gathered} \int\limits_{Q_T} MuMvdxdt + \int\limits_{S_T}\left(D^\beta v D^\beta u + vu\right)\mid_{S_T} dS + \int\limits_{S_T}(v_\nu u_\nu)\mid_{S_T} dS \\ +\chi_\psi\int\limits_\Omega [\nabla u\nabla v + uv](x,0)\,dx + \chi_\varphi\int\limits_\Omega u_t(x,0)v_t(x,0)dx + \varepsilon[u,v] \\ = \int\limits_{Q_T} FMvdxdt + \int\limits_{S_T}\sum_{|\beta|\leq 1}\left(D^\beta v\mid_{S_T}\right)D^\beta f dS + + \int\limits_{S_T}(v_\nu\mid_{S_T})\cdot g dS \\ +\chi_\psi\int\limits_\Omega[\nabla\varphi\nabla v(x,0) + \varphi v(x,0)]\,dx + \chi_\varphi\int\limits_\Omega \psi v_t(x,0)dx. \end{gathered} \tag{8.21}$$

Riesz theorem and (8.21) imply

Lemma 8.4. *For any vector function* $(F, f, g) \in L_2(Q_T) \times H^1(S_T) \times L_2(S_T)$ *there exists unique solution* $u_\varepsilon \in H^2(Q_T)$ *of the problem (3.2) and*

$$\|u_\varepsilon\|_{H^2(Q_T)} \leq \frac{C}{\sqrt{\varepsilon}} \Big(\|F\|_{L_2(Q_T)} + \|f\|_{H^1(S_T)} + \|g\|_{L_2(S_T)} + \chi_\psi \|\varphi\|_{H^1(\Omega)} + \chi_\varphi \|\psi\|_{L_2(\Omega)} \Big).$$

Setting in (8.21) $v := u$, we obtain that the unique minimizer of the functional $J_\varepsilon(u)$ satisfies the following estimate

$$\begin{gathered} \|Mu\|^2_{L_2(Q_T)} + \chi_\psi \|u(x,0)\|^2_{H^1(\Omega)} + \chi_\varphi \|u_t(x,0)\|^2_{L_2(\Omega)} \\ + \|u\ |_{S_T}\|^2_{H^1(S_T)} + \|u_\nu\ |_{S_T}\|^2_{L_2(S_T)} \\ \leq \|F\|^2_{L_2(Q_T)} + \|f\|^2_{H^1(S_T)} + \|g\|^2_{L_2(S_T)} + \chi_\psi \|\varphi\|^2_{H^1(\Omega)} + \chi_\varphi \|\psi\|^2_{H^1(\Omega)}. \end{gathered} \tag{8.22}$$

To prove convergence of our method, we need to derive from (8.22) the Lipschitz stability estimate for the function u in the $H^1(Q_T)$-norm.

Theorem 8.5 [11]. *Let* $\Omega \subset \mathbb{R}^n$ *be a convex bounded domain with the piecewise smooth boundary and let* $T > R$. *Suppose that the function* $u \in H^2(Q_T)$ *satisfies the inequality*

$$\begin{gathered} \|Mu\|_{L_2(Q_T)} + \chi_\psi \|u(x,0)\|_{H^1(\Omega)} + \chi_\varphi \|u_t(x,0)\|_{L_2(\Omega)} \\ + \|u\ |_{S_T}\|_{H^1(S_T)} + \|u_\nu\ |_{S_T}\|_{L_2(S_T)} \leq K, \end{gathered}$$

where $K = const. > 0$. *Then*

$$\|u\|_{H^1(Q_T)} + \chi_\varphi \|u(x,0)\|_{H^1(\Omega)} + \chi_\psi \|u_t(x,0)\|_{L_2(\Omega)} \leq CK.$$

Theorem 8.5 enables us to prove convergence of our method. Following the Tikhonov concept for ill-posed problems [50], we first introduce an "ideal" exact solution of either φ or ψ problem without an error in the data. Next, we assume the existence of the error in the boundary data f and g and prove that our solution tends to the exact one as the level of error in the data tends to zero. We consider the more general Inverse Problem 1. Let $f^* \in H^1(S_T)$ and $g^* \in L_2(S_T)$ be the exact boundary data (8.13), $F^* \in L_2(Q_T)$ be the exact right hand side of equation (8.11) and φ^* and ψ^* be exact initial conditions. We assume that there exists an exact function $u^* \in H^2(Q_T)$ satisfying

$$u^*_{tt} = L(x,t)u^* + F^*(x,t) \text{ in } Q_T,$$

with initial conditions

$$u^*(x,0) = \varphi^*(x), u^*_t(x,0) = \psi^*(x), \varphi^* \in H^1(\Omega), \psi^* \in L_2(\Omega),$$

$$u^*\ |_{S_T} = f^*(x,t), \frac{\partial u^*}{\partial \nu}\ |_{S_T} = g^*(x,t),$$

where φ^* and ψ^* are exact initial conditions. We assume that the real boundary data in (8.13) have an error, so as the given initial condition. In other words, we assume that

$$\|f - f^*\|_{H^1(S_T)} + \|g - g^*\|_{L_2(S_T)} + \|F - F^*\|_{L_2(Q_T)}$$

$$+\chi_\psi \|\varphi - \varphi^*\|_{H^1(\Omega)} + \chi_\varphi \|\psi - \psi^*\|_{L_2(\Omega)} \leq \delta,$$

where $\delta > 0$ is a small number. The following convergence theorem holds

Theorem 8.6 [11]**.** *Suppose that $T > R$. Let $u_{\varepsilon\delta} \in H^2(Q_T)$ be the solution of the QRM problem (8.21), which is guaranteed by Lemma 2.1. Let conditions (5.1)-(5.4) be satisfied. Then the following estimate is valid*

$$\|u - u^*\|_{H^1(Q_T)} + \chi_\varphi \|\varphi - \varphi^*\|_{H^1(\Omega)} + \chi_\psi \|\psi - \psi^*\|_{L_2(\Omega)} \leq C\left(\delta + \sqrt{\varepsilon}\right).$$

In our numerical study we have considered the Inverse Problem 2. To generate the data for the inverse problem, we have solved the Cauchy problem

$$u_{tt} = \Delta u, (x,t) \in \mathbb{R}^2 \times (0,T), \tag{8.23}$$

$$u(x,0) = \varphi(x), u_t(x,0) = \psi(x). \tag{8.24}$$

In our numerical experiments $\psi(x) \equiv 0$ for the $\varphi-$problem, and $\varphi(x) \equiv 0$ for the $\psi-$problem. Because of (8.15) and the finite speed of propagation, we use in our solution of the forward problem zero Dirichlet boundary condition at the boundary of the rectangle $(-T, a+T) \times (-T, a+T)$ (Figure 18). Hence, we solve initial boundary value problem inside of this rectangle for equation (8.23) with initial conditions (8.24) and zero Dirichlet boundary condition. In all our calculations we took $a = 1, T = 3$. The square $SQ(a)$ is $SQ(a) = SQ(1) = (0,1) \times (0,1)$, the domain Ω is

$$\Omega := (0,4) \times (0,4)$$

and in all tests

$$\varphi(x) = \psi(x) = 0 \text{ for } x \notin SQ(1).$$

We have solved the Cauchy problem (6.1), (6.2) via finite differences using the uniform grid. To find the minimizer of the functional J_ε, we have also used finite differences and have minimized the resulting functional $\widetilde{J}_\varepsilon$ with respect to the vector $\{u_{kmn}\}$, which approximates values of the function u at grid points. Here $\widetilde{J}_\varepsilon$ means the functional J_ε, which is expressed via the finite differences. The norms $\|u_{x_1}(x,0)\|_{L_2(\Omega)}$, $\|u_{x_2}(x,0)\|_{L_2(\Omega)}$ in $\|u(x,0)\|_{H^1(\Omega)}$ in the $\psi-$problem were calculated via finite differences. As to the term $\left\|D^\beta u\,|_{S_T} - D^\beta f\right\|^2_{L_2(S_T)}$ in (8.20), we have used only $\beta = 0$, thus ending up with $\|u\,|_{S_T} - f\|^2_{L_2(S_T)}$ (in the discrete sense).

To minimize the functional $\widetilde{J}_\varepsilon$, we have used the conjugate gradient method. Derivatives with respect to variables u_{kmn} where calculated in closed forms, using the following formula

$$\frac{\partial u_{kmn}}{\partial u_{\overline{k}\overline{m}\overline{n}}} = \delta_{k\overline{k}}\delta_{m\overline{m}}\delta_{n\overline{n}},$$

where $\delta_{k\overline{k}}$ is the Kronecker symbol. This formula can be conveniently used to obtain closed form expressions for derivatives

$$\frac{\partial \widetilde{J}_{\varepsilon}(u)}{\partial u_{kmn}}.$$

We have always used the regularization parameter $\varepsilon = 10^{-6}$. Larger values of ε such as 10^{-5} brought lower quality results. In our numerical experiments we have imaged both smooth slowly varying functions and the finite difference analogue of the $\delta-$ function. Let $(x_{1k}, x_{2r}) \in \Omega$ be a fixed grid point. To obtain the finite difference analogue of $\delta(x_1 - x_{1k}, x_2 - x_{2r})$, we consider the following grid points (x_{1n}, x_{2m}) and model the function $\delta(x_{1n} - x_{1k}, x_{2m} - x_{2r})$ as

$$\delta(x_{1n} - x_{1k}, x_{2m} - x_{2r}) = \frac{3}{4h_{x_2}h_{x_1}}\delta_{nk}\delta_{mr},$$

where the multiplier at $\delta_{nk}\delta_{mr}$ is chosen such that the volume of the pyramid based on (x_{1k-1}, x_{2r-1}), (x_{1k-1}, x_{2r+1}), (x_{1k+1}, x_{2r+1}), (x_{1k+1}, x_{2r-1}) equals to 1. Hence, the support of the function $\delta(x_{1n} - x_{1k}, x_{2m} - x_{2r})$ is limited only to the point (x_{1n}, x_{2m}).

Test. *The $\varphi-$problem with two $\delta-$functions.* We now consider the Inverse Problem 2 with the domain Ω as with $\psi(x) \equiv 0$. The data for the forward problem were simulated for the case of two $\delta-$functions

$$\varphi(x_1, x_2) = \delta(x_1 - 0.4, x_2 - 0.4) + \delta(x_1 - 0.7, x_2 - 0.7) \tag{8.25}$$

with the above described finite difference analogue of the $\delta-$ function. Figure 19 displays the resulting image of the function (8.25) for the case of 50% of the noise in the boundary data, scatter plot mode was used, squares show exact height. Very similar results (not shown) were obtained for the $\psi-$problem with exactly the same $\delta-$ functions as ones in (8.25).

9 An Inverse Problem for a Nonlinear Parabolic Equation with Applications in Population Dynamics and Magnetics

Results of this section are obtained jointly with Dr. B. Kaltenbacher, University of Stuttgart, Germany [14]. We formulate uniqueness theorem, outline a numerical method and present some numerical results.

Nonlinear parabolic PDEs arise in a large variety of applications ranging from combustion theory via environmental pollution, population dynamics and nonlinear magnetics to the theory of the economic growth. Since the coefficient depending nonlinearly on the solution of the PDE is often not accessible to direct measurements, its determination from boundary measurements is an important task.

We consider the question of the identifiability, i.e., whether this coefficient function can be uniquely determined from the given data. While there exist results on the situation that the coefficient depends on values of the solution (as it is relevant, e.g., in nonlinear heat

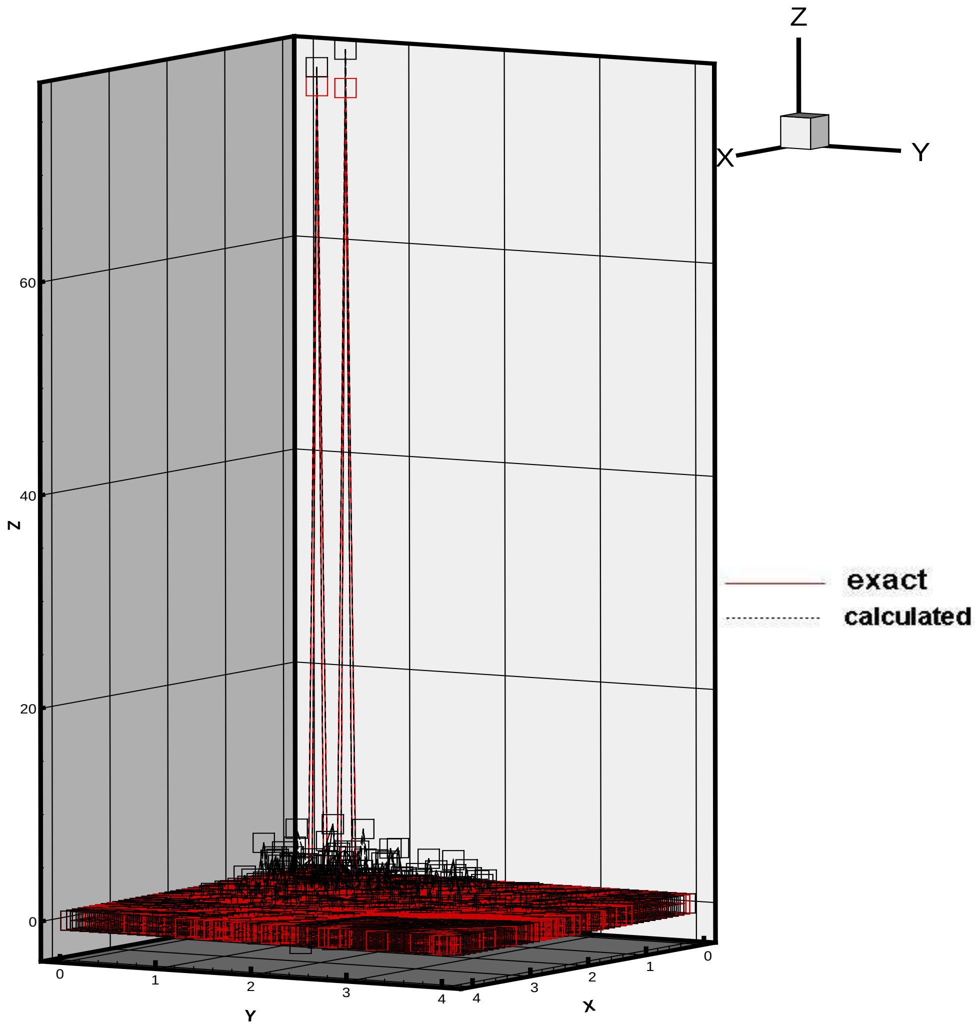

Figure 22: Test of subsection 8.3. Exact (red) and calculated (black) function φ with 50% noise in the boundary data. The function χ_{φ}=1 in (8.20). Scatter plot mode. Squares show heights. Correct heights are achieved.

conduction), we here concentrate on the problem when this coefficient is a function of the derivative of the solution (as typical for nonlinear magnetics, (cf., e.g., [25]) or where the equation is in non-divergence form (e.g., in diffusion models for population dynamics, cf. [24]).

To prove our uniqueness theorem, we apply the above mentioned method of Carleman estimates. The majority of works on this method is concerned with linear equations in which unknown coefficients depend on spatial variables. Nonlinear parabolic equations were treated by this technique in [32], [45], [46] and Chapter 4 of the book [41]. Our inverse problem is a problem with the data resulting from a single measurement event. In the case of multiple measurements uniqueness theorems for inverse problems for nonlinear parabolic equations with unknown coefficients depending on solutions and their first derivatives were proven in [36]. The case of single measurement data for such equations was considered in e.g., [32], [41], [45], [46]. However, in these works the unknown coefficient depends on the solution of the original parabolic equation (as well as on some spatial variables in the multidimensional case). The case of the dependence on derivatives of the solution was not considered. Thus, it is an important new element here that the unknown coefficient $k\left(u_x\right)$ is involved together with its first derivative.

9.1 Statement of the Problem and Uniqueness Theorem

The forward problem is

$$u_t = \left(k\left(u_x\right)u_x\right)_x, \ (x,t) \in (0,L) \times (0,T), \tag{9.1}$$

$$u\left(x,0\right) = r(x), \ x \in (0,L), \tag{9.2}$$

$$u\left(0,t\right) = f_0\left(t\right), \ u(L,t) = f_1\left(t\right), \ t \in (0,T), \tag{9.3}$$

or with $v(x,t) = u_x(x,t)$, i.e., $u(x,t) = \int_0^x v(\xi,t)\, d\xi + f_0(t)$

$$v_t = \left(k\left(v\right)v\right)_{xx}, \ (x,t) \in (0,L) \times (0,T), \tag{9.4}$$

$$v\left(x,0\right) = r'(x), \ x \in (0,L), \tag{9.5}$$

$$(k(v)v)_x(0,t) = f_0'(t), \ (k(v)v)_x(L,t) = f_1'(t), \ t \in (0,T), \tag{9.6}$$

which results from the previous setting by the differentiation with respect to the space variable. Naturally, it is assumed that the function $k(z) \in C^1\left(\mathbb{R}\right)$ and

$$k\left(z\right) \geq k_0 = const. > 0, \forall z \in \mathbb{R}. \tag{9.7}$$

It is well known that it is difficult to investigate the question of uniqueness of coefficient inverse problems for parabolic equations unless one assumes that the solution of the forward problem is known at $t = \varepsilon \in (0,T)$. In the latter case, however, one does not need to assume the knowledge of the initial condition at $\{t = 0\}$, see, e.g., subsections 3.3.1 and 3.3.2 in [41]. In other words, one needs to assume that the knowledge of the initial condition (9.2)

is replaced with the knowledge of the function $u(x,\varepsilon)$ for an arbitrary $\varepsilon \in (0,T)$; also see below for a physical interpretation. Because of this, we formulate the inverse problem as

Inverse Problem. Assume that equation (10.1) is satisfied for $(x,t) \in (0,L) \times (-c,T)$, where $c \in (0,T]$ is an arbitrary number, the function $u(x,0) = r(x)$ in (10.2) is known, so as boundary conditions $f_0(t)$ and $f_1(t)$ for $t \in (-c,T)$. Also, assume that the following two functions $g_0(t)$ and $g_1(t)$ are given

$$u_x(0,t) = g_0(t), u_x(L,t) = g_1(t), t \in (-c,T). \tag{9.8}$$

Let the interval (a,b) be the range of the function $u_x(x,t)$ for $(x,t) \in (0,L) \times (-c,T)$, i.e., $a \leq u_x(x,t) \leq b$. Determine the interval (a,b), as well as the unknown coefficient $k(z)$ for $z \in (a,b)$.

The following uniqueness theorem holds.

Theorem 9.1 [14]**.** *Let the conditions of the statement of the Inverse Problem be satisfied. Suppose that there exist two functions $k_1(z)$ and $k_2(z)$ satisfying condition (10.7) and such that*

$$zk_i'(z) + k_i(z) \geq const. > 0, \forall z \in \mathbb{R}, i = 1,2.$$

Let $u_1(x,t)$ and $u_2(x,t)$ be two functions satisfying (10.1) and (10.3) for $t \in (-c,T)$, as well as the same Neumann boundary conditions (10.8) and such that (see (10.2)) $u_1(x,0) = u_2(x,0) = r(x)$ and

$$D_t^s D_x^j u_i \in C([0,L] \times [-c,T]) \text{ for } s = 0,1; j = 0,1,2,3; i = 1,2.$$

Assume also that in $(0,L) \times (-c,T)$

$$D_x^2 u_i \geq \alpha = const. > 0,\ i = 1,2.$$

In addition, let

$$g_0'(t) \geq 0, t \in (-c,T),$$

$$g_1(t) \equiv const. = \widetilde{g}, t \in (-c,T)$$

and

$$k_1(z) = k_2(z), z \in (g_0(-c), g_0(\varepsilon)),$$

where $\varepsilon \in (0,T)$ is an arbitrary number. Denote $a = g_0(-c), b = \widetilde{g}$. Then the range of both functions u_{1x} and u_{2x} coincides with the interval (a,b) and $k_1(z) = k_2(z)$ for $z \in (a,b)$.

9.2 Application Examples

9.2.1 A Diffusion Model in Population Dynamics

In this section we discuss the assumptions of Theorem 9.1 for an example from population dynamics, given in the form (10.4). Aronson in [24] has proposed the diffusion model

$$v_t = (\phi(v)v)_{xx} \tag{9.9}$$

in the absence of drift, where $v(x,t)$ is the population density at location x and time t and the diffusion coefficient $\phi(v)$ is the population density dependent limit (as the minimal individual step length tends to zero) of the second moment of the transition probability between different locations. The function ϕ plays the role of k in the setting of Theorem 9.1. With $u(x,t) = \int_0^x v(\xi,t)\,d\xi + f_0(t)$ and an integration with respect to the space variable this can be rewritten as

$$u_t - (\phi(u_x)u_x)_x = c \tag{9.10}$$

with c depending on time only, which without loss of generality we can set to zero, which yields

$$u_t = (\phi(u_x)u_x)_x \tag{9.11}$$

so that with $k = \phi$ we get the PDE considered in Theorem 9.1. The boundary and initial data as well as the conditions imposed on them have the following interpretation in the context of this example:

- $u(x,0) = r(x)$, i.e., $v(x,0) = r'(x)$ means that the population density is known everywhere at time $t = 0$, e.g., from a census at that instance of time.
- $u(0,t) = f_0(t)$ is satisfied by our setting of the integration constants.
- $u(L,t) = f_1(t)$, i.e., $\int_0^L v(\xi,t)\,d\xi = f_1(t) - f_0(t)$ means that the total population density is known at each time instance, e.g., by observation of the in- and outflow at the boundary.
- $u_x(0,t) = v(0,t) = g_0(t)$ with $g' \geq 0$: The population density at location $x = 0$ is observed for all time instances and it increases with time.
- $u_x(L,t) = v(L,t) = g_1(t) = \tilde{g}$ and $[g_0(\varepsilon), \tilde{g}]$ is the interval on which k can be identified according to Theorem 9.1: The population density at location $x = L$ is observed for all time instances and is constant in time, where this constant should be as large as possible, e.g., equal to some saturation value.
- $u_{xx} = v_x \geq \alpha > 0$: The population density increases from left to right.

9.2.2 Nonlinear Magnetics

Quasistationary magnetic fields can be described by a subset of Maxwell's equations, which leads to the system of PDEs

$$\gamma \mathbf{u}_t + \nabla \times (\nu \nabla \times \mathbf{u}) = J_{imp}$$

for the magnetic vector potential $\mathbf{u}$, where γ is the electric conductivity, μ the magnetic reluctivity, J_{imp} the impressed current density and the magnetic flux density $\mathbf{B}$ as well as the magnetic field intensity can be expressed as

$$\mathbf{B} = \nabla \times \mathbf{u}\,, \quad \mathbf{H} = \nu \mathbf{B}\,.$$

In the situation of high magnetic fields, the parameter ν is not constant but depends on the magnetic flux density, i.e.,

$$\mathbf{H} = \nu(\mathbf{B})\mathbf{B}\,.$$

Assuming an appropriate geometry (flat, ring shaped probe with large interior radius) we can restrict our attention to the spatially one-dimensional model problem

$$\gamma u_t - (\nu(u_x)u_x)_x = 0\,,$$

i.e., with $k = \frac{1}{\gamma}\nu$ we arrive at the PDE considered in Theorem 9.1. An interpretation of the conditions of Theorem 9.1 in the context of this example can be made as follows:

- Neumann boundary data $u_x(0,t) = g_0(t)$, $u_x(L,t) = g_1(t)$ here have the meaning of a magnetic flux density, which can be extracted from measurements of the magnetic flux through two coils positioned on both sides of the material strip, i.e., at the endpoints of the interval $[0,L]$. The magnetic flux can be controlled via the impressed current through these coils such that it is monotonically nondecreasing (and small) at the left endpoint as well as constant (and large) at the right endpoint to achieve $g_0' \geq 0$, $g_1' = 0$, and a wide interval (a,b).

- Via the relation $\mathbf{u}_t = \mathbf{E}$ with $\mathbf{E}$ the electric field, one can obtain the initial and boundary data of u by time integration of electric field measurements.

The conventional measurement setup for determining ν consists of just an excitation (and measurement) coil wound around the probe and does not enable to collect all the data required from the point of view of our uniqueness theorem (especially not electric field measurements inside the probe which would be required for giving initial data for u). In this sense, there is a gap between theory and practice. Still, the model problem considered in this paper gives important insight, since the correct form of the PDE with a coefficient depending on the space derivative of u is considered.

9.3 Numerical results

In this subsection, we shortly outline a numerical method for determining the coefficient k and provide some computational results.

Here we make use of a special time discretization based on trigonometric polynomials, i.e., in a complex valued setting, time harmonic functions $t \mapsto \exp(\imath nt)$. This leads to a so called multiharmonic formulation of the forward (cf., e.g., [25], [35], [37]) problem as follows: We think of the boundary data as extended periodically and sufficiently smoothly to the larger interval $[0,\bar{T}] = [0, T+T_1]$ with some $T_1 > 0$, and make an ansatz

$$u(x,t) \approx u^N(x,t) := \sum_{n=-N}^{N} \exp(\imath n\omega t)\hat{u}_n(x)\,,$$

with $\omega = 2\pi/\bar{T}$. (Note that continuation of the boundary values beyond T, by the causality of the problem does not influence u for $t < T$.) Inserting into the PDE, we get

$$\sum_{j=-N}^{N} e^{\imath j\omega t}\left(\imath\omega j\hat{u}_j - \left(k(\sum_{n=-N}^{N} e^{\imath n\omega t}\hat{u}_{n\,x})\hat{u}_{j\,x}\right)_x\right) = 0\,.$$

Testing this with the functions

$$t \mapsto \frac{1}{\bar{T}}\, e^{-\imath l\omega t}$$

and using the orthonormality

$$\frac{1}{\bar{T}}\int_0^{\bar{T}} e^{-\imath l\omega t}e^{\imath j\omega t}\; dt = \delta_{lj} \tag{9.12}$$

where δ_{lj} is the Kronecker Symbol, yields

$$\begin{aligned}\imath\omega l\hat{u}_l - \tfrac{1}{\bar{T}}\textstyle\int_0^{\bar{T}}\sum_{j=-N}^{N} e^{\imath(j-l)\omega t}\left(k(\sum_{n=-N}^{N} e^{\imath n\omega t}\hat{u}_{n\,x})\hat{u}_{j\,x}\right)_x dt \;&= 0\\ \forall l \in \{-N,\ldots,N\}\,&.\end{aligned} \tag{9.13}$$

To eliminate the time integral, we use an appropriate approximation for k that enables to take advantage of the orthogonality (9.12). For this purpose we make use of a polynomial ansatz

$$k(z) \approx \sum_{p=1}^{P} \alpha_p z^p\,,$$

which is justified by the fact that in the applications we have in mind, k is typically a smooth function. Since the multinomial theorem yields

$$\left(\sum_{n=-N}^{N} e^{\imath n\omega t}\hat{u}_{n\,x}\right)^p = \sum_{\substack{\mathbf{p}\,=\,(p_{-N},\ldots,p_N)\,\in\,\mathbb{N}_0^{2N+1}\\ \sum_{n=-N}^{N} p_n = p}} \begin{pmatrix} p\\ \mathbf{p}\end{pmatrix} \prod_{m=-N}^{N} (e^{\imath m\omega t}\hat{u}_{m\,x})^{p_m}\,,$$

with the multinomial coefficients

$$\begin{pmatrix} p\\ (p_{-N},\ldots,p_N)\end{pmatrix} = \frac{p!}{p_{-N}!\cdots p_N!}\,,$$

by (9.12) one arrives at a system of space dependent PDEs

$$\imath\omega l\hat{u}_l - \left(\sum_{n=-N}^{N}\sum_{p=0}^{P} \alpha_p \vec{c}^{\,p}_{l-n}\hat{u}_{n\,x}\right)_x = 0 \quad l \in \{-N,\ldots,N\}\,, \tag{9.14}$$

where

$$\bar{c}_s^p = \sum_{\mathbf{p}\in\mathcal{I}(p,s)} \begin{pmatrix} p \\ \mathbf{p} \end{pmatrix} \prod_{m=-N}^{N} (\hat{u}_{m\,x})^{p_m} ,$$

$$\mathcal{I}(p,s) = \{\mathbf{p} = (p_{-N},\dots,p_N) \subseteq \mathbb{N}_0^{2N+1} \mid \sum_{n=-N}^{N} p_n = p \ \wedge \ \sum_{n=-N}^{N} np_n = s\} ,$$

i.e., the coefficients $\bar{c}_{l-n}^p$ depend nonlinearly on $(\hat{u}_{-N\,x},\dots,\hat{u}_{N\,x})$. The boundary conditions and measurements become

$$\hat{u}_{l\,x}(0) = \hat{g}_{0\,l},\ \hat{u}_{l\,x}(L) = \hat{g}_{1\,l}, \quad l \in \{-N,\dots,N\} \tag{9.15}$$
$$\hat{u}_l(0) = \hat{f}_{0\,l},\ \hat{u}_l(L) = \hat{f}_{1\,l}, \quad l \in \{-N,\dots,N\}$$

with

$$\hat{f}_{i\,l} = \frac{1}{\bar{T}} \int_0^{\bar{T}} \exp(-\imath l\omega\tau) f_i(\tau)\ d\tau ,$$

and analogously for g_i, $i = 0,1$. Note that we consider the Neumann data as boundary conditions (and the Dirichlet data as measurement) in our numerical tests below in order to be able to directly prescribe a monotonically increasing g_0 and a constant g_1. To avoid singularity of the system due to the elliptic Neumann problem for index $l = 0$, we make the additional normalization assumption $\hat{u}_0 = \frac{1}{\bar{T}} \int_0^{\bar{T}} u^N(\cdot,t)\, dt = 0$. Physically, this corresponds to the fact that in experiments only higher harmonics (i.e. multiples $n\omega$ with $|n| \geq 1$ of the basic frequency ω) appear. From a mathematical point of view this normalization corresponds to a $\bar{T}$ periodicity assumption on the antiderivative of u^N, while the multiharmonic ansatz implies periodicity of u^N itself. To keep compatibility, we add this assumption of vanishing time integral also to the conditions imposed on the periodic extension of the boundary values f_0, f_1, g_0, g_1.

Since k is real-valued, we expect to get a real-valued solution and therefore additionally stipulate

$$\hat{u}_{-n} = \overline{\hat{u}_n} . \tag{9.16}$$

The inverse problem of reconstructing k from boundary measurements of u in this kind of discretization amounts to determining the polynomial coefficients $\alpha_0,\dots,\alpha_p$ from boundary data of $\hat{u}_l$, $l = 0,\dots,N$. Writing this as a system of equations

$$F_N^P(\alpha) = y$$

where $F_N^P : \alpha \mapsto (\hat{u}_{n\,x}(0), \hat{u}_{n\,x}(L))_{n=0^N}$ with $(\hat{u}_n)_{n=0}^N$ solving (9.13), (9.15), (9.16), we can apply Newton's method

$$\alpha^{m+1} = \alpha^m + \theta\beta \text{ with } F_N^{P\prime}(\alpha^m)\beta = y - F_N^P(\alpha^m) ,$$

to iteratively recover α. In here θ is an appropriately chosen stepsize that guarantees strictly monotone decrease of the residual. Keeping in mind the fact that the original infinite dimensional inverse problem of recovering k is ill-posed in the sense of instability, we here rely

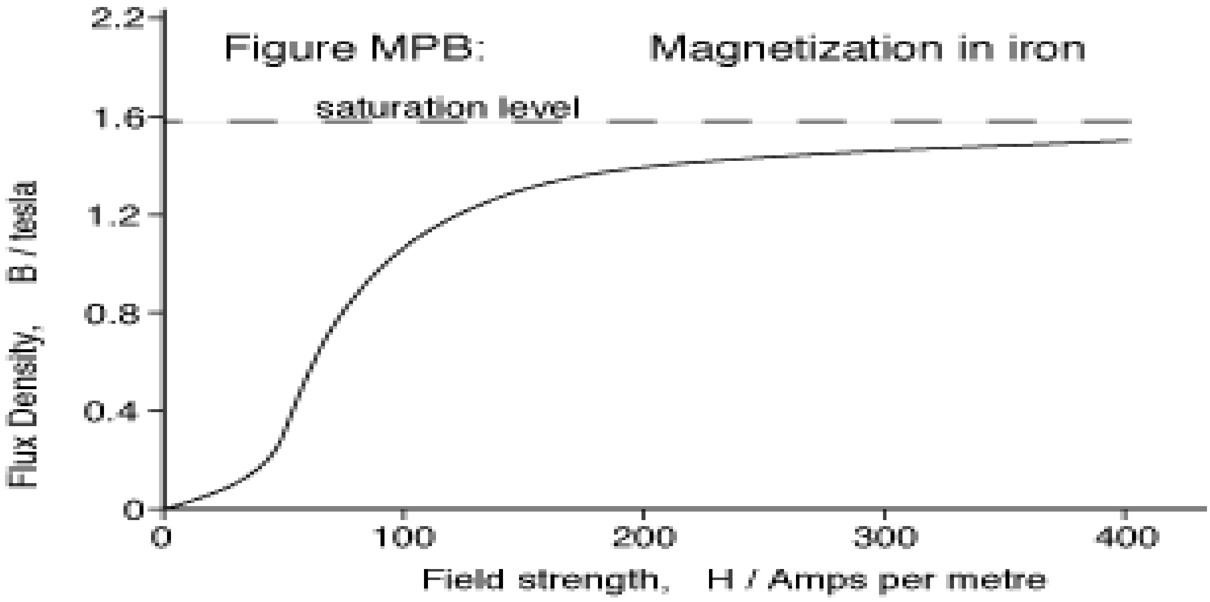

Figure 23: A typical B-H curve for iron.

on the regularizing effect of discretization. More precisely, we stabilize the problem by projection in data space, since our special time discretization corresponds to an L^2 projection in data space to the subspace spanned by the first $2N+1$ trigonometric polynomials. These L^2 projections converge pointwise to the identity due to the fact that $\{t \mapsto \frac{1}{\sqrt{\bar{T}}} e^{\imath j \omega t} \mid j \in \mathbb{Z}\}$ forms a complete orthonormal system in $L^2_{\mathbb{C}}(0, \bar{T})$. To fully discretize this method, it remains to define a space discretization of the space dependent functions $\hat{u}_l$, which we do by using finite elements on a uniform grid.

The application we have in mind here is nonlinear magnetics, where the nonlinearity is usually considered in terms of the B-H curves a where $a^{-1}(z) = k(z)z$. B-H curve means a plot of the magnetic flux density $\mathbf{B}$ over the magnetic field intensity $\mathbf{H}$. A typical B-H curve for iron is displayed in Figure 23, where the ratio between the slope at $B = 0$ and the slope at $B = B_{sat}$ amounts to the relative reluctivity $\mu_{rel} \sim \frac{1}{5000}$. For testing the proposed method, we constructed two test problems with similar behavior. Upon renormalization to $B_{sat}^{norm} = 1$, $\nu_{rel}^{norm} = \frac{1}{10}$, the values $H_{sat}^{norm} = 3.6$ and $H_{sat}^{norm} = 2.4$ as appearing in the synthetic test example in Figure 24 indeed turn out to be in a realistic range.

For the test example of Figure 20, Figure 21 shows the iteration history of the proposed method for exact and for randomly perturbed data with a noise level of one per cent, as compared to the true curve a_{ex} in black. Note that in our numerical tests, the starting value for k is just a constant function, corresponding to the fact that in practice the constant reluctivity coefficient for small magnetic fields is typically known.

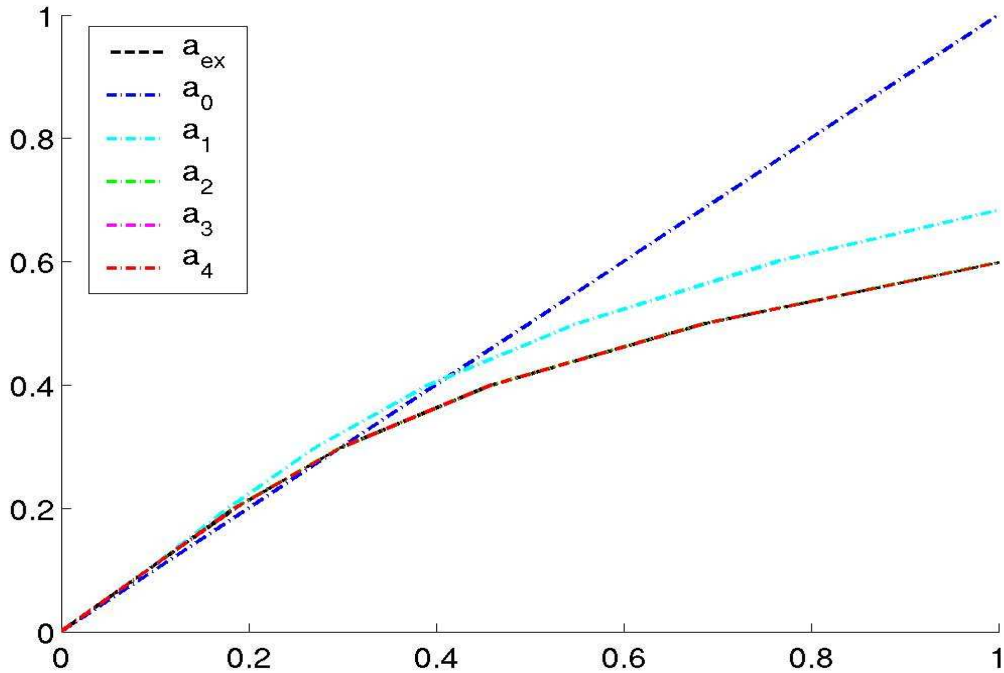

Figure 24: Starting value a_0 and Newton iterations a_1, a_2, a_3, a_4 for a, where $a^{-1}(z) = zk(z)$.

10 The First Result on the Second Generation of Globally Convergent Numerical Methods

This activity is an ongoing joint effort of Dr. L. Beilina (Norway) and the PI [12]. Prior to this activity Dr. Beilina has developed (with co.-authors) the so-called adaptivity technique for inverse problems [26-28]. The idea is to develop the second generation of globally convergent numerical methods. The first step of such methods is the same as in the convexification: the transformation procedure which leads to the nonlinear integral differential equation (2.20a). However, the question of numerical solution of this equation is the **most challenging** one in the entire approach. Thus,the main difference with the convexification is in the solution of this equation. Instead of using the layer stripping procedure with respect to a spatial variable, we now use the layer stripping with respect to the pseudo frequency s via going from the truncation high pseudo frequency in the downward direction. On each small s-layer we solve the Dirichlet boundary value problem for an elliptic equation via the FEM. Since the derivative with respect to s is not a part of the differential operator (unlike derivatives with respect to spatial variables of the convexification), we expect a better stability of this second generation methods. Further, the Dirichlet boundary value problem presumes that the "measurements" are taken over the entire boundary. At the same time, in problems of the interest to the Army only back reflected data are given. Nevertheless, it seems that this new approach can be extended to this case. To do this, one should impose radiation-like boundary conditions (i.e., Robin conditions actually) on the rest of the boundary. In this case one should replace the Dirichlet boundary problems with "mixed" boundary value problems. In other words, Dirichlet conditions will be assigned on the "accessible" part of the boundary and Robin conditions on the rest. However, the latter development is a matter of future effort, since only the first result in this direction is obtained so far [12].

Another essentially new and important element here is the presence of s-dependent Carleman Weight Functions (CWFs) in the numerical scheme. s-dependent CWFs are present in our numerical scheme. Until now CWFs have been widely used for proofs of unique continuation and conditional stability results for ill-posed Cauchy problems for PDEs, as well as for multidimensional CIPs with the single measurement data, see, e.g. [29,30,32,38,39,41,45]. In this capacity CWFs were dependent on spatial variables, since they have provided weighted estimates for differential operators. In the convexification CWFs also depend on the spatial variable z. However, CWFs of this new method are used for integral Volterra-like operators, they are involved in the numerical scheme and depend on the pseudo frequency s, rather than on a spatial variable.

We now state the inverse problem a little bit differently than in section 2. Namely, we use only one boundary condition at the entire boundary. And also we do not require that the domain Ω be a rectangular prism.

Inverse Problem. Let $\Omega \subset R^3$ be convex bounded domain with the boundary $\partial\Omega \in C^2$. Suppose that one of coefficients of the equation (2.9a) is unknown in Ω and known in $\mathbb{R}^3 \diagdown \Omega$ and all other coefficients are known everywhere. Determine that unknown coefficient for $x \in \Omega$, assuming that the following two function $\varphi(x, s)$ is known for a single source position

$x_0 \notin \overline{\Omega}$

$$w(x,,s) = \varphi(x,s), \text{ for } (x,s) \in -\partial\Omega \times [s_0, \overline{s}], \tag{10.1}$$

where s_0 and $\overline{s}$ are certain positive numbers.

Denote

$$\psi(x,s) = \frac{\partial}{\partial s}\left(\frac{\ln \varphi(x,s)}{s^2}\right)$$

10.1 Layer Stripping With Respect to the Pseudo Frequency

We approximate the function $q(x,s)$ in (2.20a) as a piecewise constant function with respect to the pseudo frequency s. That is, we assume that there exists a partition $\underline{s} = s_N < s_{N-1} < ... < s_1 < s_0 = \overline{s}$ of the interval $[\underline{s}, \overline{s}]$ with the sufficiently small grid step size $h = s_{i-1} - s_i$ such that $q(x,s) = q_n(x)$ for $s \in (s_n, s_{n-1}]$. Hence,

$$\int\limits_{s}^{\overline{s}} \nabla q(x,\tau)\, d\tau = (s_{n-1} - s)\nabla q_n(x) + h\sum_{j=1}^{n-1} \nabla q_j(x), s \in (s_n, s_{n-1}].$$

We approximate the boundary condition (10.1) as a piecewise constant function,

$$q_n(x) = \overline{\psi}_n(x), x \in \partial\Omega, \tag{10.2}$$

where

$$\overline{\psi}_n(x) = \frac{1}{h}\int\limits_{s_n}^{s_{n-1}} \psi(x,s)\, ds.$$

Hence, for $s \in (s_n, s_{n-1}]$ the equation (2.20a) can be rewritten as

$$\begin{aligned} \widetilde{L}_n(q_n) := \Delta q_n - 2\left(s^2 - 2s(s_{n-1} - s)\right)\left(h\sum_{j=1}^{n-1}\nabla q_j(x)\right)\nabla q_n \\ +2\left(s^2 - 2s(s_{n-1} - s)\right)\nabla q_n \nabla V(x) \\ = 2(s_{n-1} - s)\left[s^2 - s(s_{n-1} - s)\right](\nabla q_n)^2 - 2sh^2\left(\sum_{j=1}^{n-1}\nabla q_j(x)\right)^2 \\ +4s\nabla V(x)\left(h\sum_{j=1}^{n-1}\nabla q_j(x)\right) - 2s|\nabla V(x)|^2, s \in (s_{n-1}, s_n] \end{aligned} \tag{10.3}$$

The equation (10.3) is nonlinear, and it depends on the parameter s, whereas the function $q_n(x)$ is independent on s. This discrepancy is due to the approximation of the function $q(x,s)$ by a piecewise constant function. Although it seems that the equation (10.3) is over-determined because the function $q_n(x)$ is not changing with the change of s, variations of

s-dependent coefficients of (10.3) are small over $s \in [s_n, s_{n-1})$, because this interval is small. This discrepancy is actually helpful for our method, because it enables us to "mitigate" the influence of the nonlinear term $(\nabla q_n)^2$ in (10.3) via introducing the s-dependent CWF.

In addition, we add the term $-\varepsilon q_n$ to the left hand side of equation (10.3), where $\varepsilon > 0$ is a small parameter. We are doing so because, by the maximum principle, if a function $p(x, s)$ is the classical solution of the Dirichlet boundary value problem

$$\widetilde{L}_n (p) - \varepsilon p = f(x, s) \text{ in } \Omega, p \mid_{\partial\Omega}= p_b(x, s),$$

then

$$\max_{\overline{\Omega}} |p| \leq \max \left[\max_{\partial\Omega} |p_b| , \varepsilon^{-1} \max_{\overline{\Omega}} |f| \right], \forall s \in (s_{n-1}, s_n] . \tag{10.4}$$

On the other hand, if $\varepsilon = 0$, then an analogue of the estimate (10.4) would be worse because of the involvement of some other constants. Therefore, it is anticipated that the introduction of the term $-\varepsilon q_n$ should provide a better stability of our process, and we indeed observe this in our computations.

Introduce the s-dependent CWF $\mathcal{C}_{n,\lambda} (s)$ by

$$\mathcal{C}_{n,\lambda} (s) = \exp [-\lambda |s - s_{n-1}|] , s \in (s_n, s_{n-1}] , \tag{10.5}$$

where $\lambda >> 1$ is a parameter. Multiply both sides of (10.3) by this CWF and integrate with respect to s over the interval $[s_n, s_{n-1}]$. We obtain

$$\begin{aligned} L_n (q_n) &:= \Delta q_n - A_{1,n} \left(h \sum_{i=1}^{n-1} \nabla q_i \right) \nabla q_n + A_{1n} \nabla q_n \nabla V - \varepsilon q_n \\ &= 2\frac{I_{1,n}}{I_0} (\nabla q_n)^2 - A_{2,n} h^2 \left(\sum_{i=1}^{n-1} \nabla q_i (x) \right)^2 \\ &+2A_{2,n} \nabla V \left(h \sum_{i=1}^{n-1} \nabla q_i \right) - A_{2,n} (\nabla V)^2 , n = 1, ..., N, \end{aligned} \tag{10.6}$$

where

$$I_0 := I_0 (\lambda, h) = \int_{s_n}^{s_{n-1}} \mathcal{C}_{n,\lambda} (s) \, ds = \frac{1 - e^{-\lambda h}}{\lambda},$$

$$I_{1,n} := I_{1,n} (\lambda, h) = \int_{s_n}^{s_{n-1}} (s_{n-1} - s) \left[s^2 - s (s_{n-1} - s) \right] \mathcal{C}_{n,\lambda} (s) \, ds,$$

$$A_{1,n} := A_{1,n} (\lambda, h) = \frac{2}{I_0} \int_{s_n}^{s_{n-1}} \left(s^2 - 2s (s_{n-1} - s) \right) \mathcal{C}_{n,\lambda} (s) \, ds,$$

$$A_{2,n} := A_{2,n}(\lambda, h) = \frac{2}{I_0} \int\limits_{s_n}^{s_{n-1}} s\mathcal{C}_{n,\lambda}(s)\, ds.$$

Thus, we have obtained a boundary value problem (10.2), (10.6) for a coupled system of nonlinear elliptic PDEs with respect to the vector function $(q_1, ..., q_N)$. In this system the tail function V is also unknown and should be treated differently. An important observation is that

$$\frac{|I_{1,n}(\lambda, h)|}{I_0(\lambda, h)} \leq \frac{4\overline{s}^2}{\lambda}, \tag{10.7}$$

for $\lambda h, \overline{s} \geq 1$. Therefore by taking $\lambda >> 1$, we mitigate the influence of the nonlinear term with $(\nabla q_n)^2$ in (10.6).

In computations the above integrals with the CWF should be calculated in closed forms. This is because the function $\mathcal{C}_{n,\lambda}(s)$ changes rapidly for large λ, which means that the integration step size should be taken too small. In principle, one can decrease the step size h in the s-direction instead of using the CWF. However, the introduction of the CWF provides more flexibility for the choice of parameters for computations, since parameters h and λ are independent, as long as $\lambda h \geq 1$. In addition, taking h too small would increase the computational time, because one would need to compute too many functions q_n then.

10.2 The Algorithm

The above considerations lead to the algorithm described in this section. Below $C^{k+\alpha}\left(\overline{\Omega}\right)$ are standard Hőlder spaces, where $k \geq 0$ is an integer and $\alpha \in (0,1)$. Denote $|f|_{k+\alpha} = \|f\|_{C^{k+\alpha}\left(\overline{\Omega}\right)}, \forall\, f \in C^{k+\alpha}\left(\overline{\Omega}\right)$. Our algorithm reconstructs iterative approximations $c_{n,k}(x) \in C^{\alpha}\left(\overline{\Omega}\right)$ of the function $c(x)$ only inside the domain Ω. On the other hand, to iterate with respect to tails, we need to solve the forward problem (2.9a,b) in the entire space $\mathbb{R}^3$. To do this, we need to extend each function $c_{n,k}(x)$ outside of the domain Ω in such a way that the resulting function $\widehat{c}_{n,k} \in C^{\alpha}(\mathbb{R}^3)$, $\widehat{c}_{n,k} \geq d_1$ in Ω and $\widehat{c}_{n,k} = 2d_1$ outside of Ω. So, we first describe the procedure of such an extension and this procedure is a rather standard one. Choose a smaller convex subdomain $\Omega' \subset \Omega$. Choose a function $\chi(x) \in C^1(\mathbb{R}^3)$ such that

$$\chi(x) = \left\{ \begin{array}{c} 1 \text{ in } \Omega', \\ \text{between 0 and 1 in } \Omega \diagdown \Omega', \\ 0 \text{ outside of } \Omega \end{array} \right\}.$$

The existence of such functions $\chi(x)$ is well known from the Real Analysis course. Define the target extension of the function $c_{n,k}$ as $\widehat{c}_{n,k}(x) := 2d_1(1 - \chi(x)) + \chi(x)\, c_{n,k}(x), \forall x \in \mathbb{R}^3$. Hence, and $\widehat{c}_{n,k}(x) = const. = 2d_1$ outside of the domain Ω and $\widehat{c}_{n,k} \in C^{\alpha}(\mathbb{R}^3)$. Furthermore, if $c_{n,k}(x) \geq d_1$ in Ω, then also $\widehat{c}_{n,k}(x) \geq d_1$ in $\mathbb{R}^3$. Indeed,

$$\widehat{c}_{n,k}(x) - d_1 = (1 - \chi(x))\, d_1 + \chi(x)\,(c(x) - d_1) \geq 0.$$

Step 1^1. Choose an initial tail function $V_{1,1}(x) \in C^{2+\alpha}\left(\overline{\Omega}\right)$. Choose a large parameter $\lambda >> 1$ and a small parameter $\varepsilon \in (0,1)$. To compute the first approximation $q_{1,1}$ for the function q_1 with this tail, solve the following Dirichlet boundary value problem

$$\Delta q_{1,1} + A_{1,1} \nabla q_{1,1} \nabla V_{1,1} - \varepsilon q_{1,1} = -A_{2,1} \left(\nabla V_{1,1}\right)^2,$$

$$q_{1,1} = \overline{\psi}_1(x), x \in \partial\Omega.$$

By the classic Schauder theorem this problem has unique solution $q_{1,1} \in C^{2+\alpha}\left(\overline{\Omega}\right)$. Reconstruct an approximation $c_{1,1}(x) \in C^{\alpha}\left(\overline{\Omega}\right)$ for the unknown coefficient $c(x)$ using the function $q_{1,1}(x)$ and formulas (2.13), (2.18), where $x \in \overline{\Omega}$, $V(x,\overline{s}) := V_{1,1}(x,\overline{s}), \underline{s} := s_1$. Next, construct the function $\widehat{c}_{1,1} \in C^{\alpha}\left(\mathbb{R}^3\right)$.

Step 1^k, $k \geq 2$. Suppose that the function $c_{1,k-1} \in C^{\alpha}\left(\overline{\Omega}\right)$ is reconstructed, $c_{1,k-1}(x) \geq d_1$ in Ω and the function $\widehat{c}_{1,k-1} \in C^{\alpha}\left(\mathbb{R}^3\right)$ is also constructed. Solve the forward problem (2.6), (2.7), where $c(x) := \widehat{c}_{1,k-1}(x)$, $s = \overline{s}$. Let $w_{1,k}(x,\overline{s})$ be the solution of this forward. Update the tail function as

$$V_{1,k}(x) = \frac{1}{\overline{s}^2} \ln w_{1,k}(x,\overline{s}) \in C^{2+\alpha}\left(\overline{\Omega}\right).$$

Next, solve the boundary value problem for the equation

$$\Delta q_{1,k} + A_{1,1} \nabla q_{1,k} \nabla V_{1,k} - \varepsilon q_{1,k} = 2\frac{I_{1,1}}{I_0} \left(\nabla q_{1,k-1}\right)^2 - A_{2,1} \left(\nabla V_{1,k}\right)^2$$

with the boundary condition (10.2) (at $n = 1$). We obtain the function $q_{1,k} \in C^{2+\alpha}\left(\overline{\Omega}\right)$. Reconstruct a new approximation $c_{1,k} \in C^{\alpha}\left(\overline{\Omega}\right)$ for the unknown coefficient similarly with the Step 1^1 in which $V_{1,1}(x,\overline{s})$ is replaced with $V_{1,k}(x,\overline{s})$. In addition, construct the function $\widehat{c}_{1,k-1} \in C^{\alpha}\left(\mathbb{R}^3\right)$. Make several steps $1^1, 1^2, .., 1^{m_1}$. As a result, we obtain functions $q_1, c_1, \widehat{c}_{1,m_1}, V_{1,m_1}$ where

$$q_1 := q_{1,m_1} \in C^{2+\alpha}\left(\overline{\Omega}\right), c_1 := c_{1,m_1} \in C^{\alpha}\left(\overline{\Omega}\right), \widehat{c}_{1,m_1} \in C^{\alpha}\left(\mathbb{R}^3\right), V_{1,m_1} \in C^{2+\alpha}\left(\overline{\Omega}\right).$$

Step n^1. Having functions $q_1, ..., q_{n-1} \in C^{2+\alpha}\left(\overline{\Omega}\right)$ and the tail function $V_{n-1,m_{n-1}} \in C^{2+\alpha}\left(\overline{\Omega}\right)$, set $q_{n,0}(x) := q_{n-1}(x)$ in Ω,

$$V_{n,1}(x) := V_{n-1,m_{n-1}}(x), x \in \overline{\Omega}.$$

Solve the following Dirichlet boundary value problem for the function $q_{n,1}$ (in (10.8), (10.9) the vector function $(q_{n.k}, q_{n,0}, V_{n,k})$ should be replaced with $(q_{n,1}, q_{n,k-1}, V_{n,1})$)

$$\Delta q_{n,k} - A_{1n}\left(h\sum_{j=1}^{n-1} \nabla q_j\right) \nabla q_{n,k} - \varepsilon q_{n,1} + A_{1,n} \nabla q_{n,k} \cdot \nabla V_{n,k}$$

$$= 2\frac{I_{1,n}}{I_0} \left(\nabla q_{n,k-1}\right)^2 - A_{2,n} h^2 \left(\sum_{j=1}^{n-1} \nabla q_j(x)\right)^2 \tag{10.8}$$

$$+2A_{2,n}\nabla V_{n,k}\left(h\sum_{j=1}^{n-1}\nabla q_j(x)\right)-A_{2,n}(\nabla V_{n,k})^2,$$

$$q_{n,1}(x)=\overline{\psi}_n(x), x\in\partial\Omega. \tag{10.9}$$

Hence, we obtain the function $q_{n,1}\in C^{2+\alpha}\left(\overline{\Omega}\right)$. Reconstruct a new approximation $c_{n,1}\in C^{\alpha}\left(\overline{\Omega}\right)$ for the unknown coefficient $c(x)$ using the function $q_{n,1}(x)$, functions $q_1,...,q_{n-1}$ and formulas (2.13), (2.18), where $x\in\overline{\Omega}, V(x):=V_{n,1}(x), \underline{s}:=s_n$. Next, construct the function $\widehat{c}_{n,1}\in C^{\alpha}(\mathbb{R}^3)$.

Step n^k, $k\geq 2$. Suppose that the function $c_{n,k-1}\in C^{\alpha}\left(\overline{\Omega}\right)$ is reconstructed, $c_{n,k-1}(x)\geq d_1$ in Ω and the function $\widehat{c}_{n,k-1}\in C^{\alpha}(\mathbb{R}^3)$ is also constructed. Solve the forward problem (2.9a,b), in which $c(x):=\widehat{c}_{n,k-1}(x)$, $s=\overline{s}$. Let $w_{n,k}(x,\overline{s})$ be the solution of this forward problem. Update the tail function as $V_{n,k}(x)=\overline{s}^{-2}\ln w_{n,k}(x,\overline{s})\in C^{2+\alpha}\left(\overline{\Omega}\right)$. Next, solve the boundary value problem (10.8), (10.9). Reconstruct a new approximation $c_{n,k}\in C^{\alpha}\left(\overline{\Omega}\right)$ for the unknown coefficient similarly with the Step n^1 in which $V_{n,1}(x,\overline{s})$ is replaced with $V_{n,k}(x,\overline{s})$. Make several steps $n^1,n^2,..,n^{m_n}$. As a result, we obtain the functions $q_n, c_n, \widehat{c}_n, V_{n,m_n}$, where

$$q_n:=q_{n,m_n}\in C^{2+\alpha}\left(\overline{\Omega}\right), c_n:=c_{n,m_n}\in C^{\alpha}\left(\overline{\Omega}\right), \widehat{c}_n\in C^{\alpha}\left(\mathbb{R}^3\right), V_{n,m_n}(x)\in C^{2+\alpha}\left(\overline{\Omega}\right).$$

If functions $c_n(x)$ did not yet converge, then proceed with Step $(n+1)^1$, provided that $n<N$. However, if either functions $c_n(x)$ converged, or $n=N$, then stop. The convergence criterion for functions $c_n(x)$, which we have established in our computational experiments, is described in sub-subsection 10.4.2. In principle, however, there might be several convergence criteria, which indicates that a better one might be found. Thus, we do not specify such a criterion here.

10.3 Global convergence theorem

First, we reformulate the Schauder theorem in a way, which is convenient for our case. Assuming that

$$\overline{s}>1,\ \lambda h\geq 1 \tag{10.10}$$

and (10.7) and formulas for numbers $A_{1,n}, A_{2,n}$, we obtain that $|A_{1,n}|\leq 6\overline{s}^2$ and $|A_{2,n}|\leq 2\overline{s}$ for all $n=1,...,N$. Hence,

$$\max_{1\leq n\leq N}\{|A_{1,n}|+|A_{2,n}|\}\leq 8\overline{s}^2. \tag{10.11}$$

Introduce the positive constant $M^*=M^*\left(\|q^*\|_{C^{2+\alpha}\left(\overline{\Omega}\right)\times C^1[\underline{s},\overline{s}]},\overline{s}\right)=M^*(C^*,\overline{s})$ by

$$M^*=2C^*\max\left(8\overline{s}^2,\max_{1\leq n\leq N}\{|A_{1,n}|+|A_{2,n}|\}\right). \tag{10.12}$$

Hence, (10.10)-(10.12) imply that

$$M^* \leq 16C^* \overline{s}^2. \tag{10.13}$$

Consider the Dirichlet boundary value problem

$$\Delta u + \sum_{j=1}^{3} b_j(x) u_{x_j} - d(x) u = f(x),\ x \in \Omega,$$

$$u \mid_{\partial\Omega} = g(x) \in C^{2+\alpha}(\partial\Omega).$$

Assume that the following conditions are satisfied

$$b_j, d, f \in C^{\alpha}\left(\overline{\Omega}\right), d(x) \geq 0;\ \max\left(|b_j|_{\alpha}, |d|_{\alpha}\right) \leq C_1,$$

where C_1 is a positive constant. By the Schauder theorem, there exists unique solution $u \in C^{2+\alpha}\left(\overline{\Omega}\right)$ of this boundary value problem, and with a constant $K = K(C_1, \Omega) > 0$ depending only on the number C_1 and the domain Ω the following estimate holds

$$|u|_{2+\alpha} \leq K\left[\|g\|_{C^{2+\alpha}(\partial\Omega)} + |f|_{\alpha}\right].$$

In the formulation of Theorem 10.1 we provide estimates (10.17)-(10.22) via M^* and also use (10.14) to obtain estimates via $\overline{s}$.

Theorem 10.1. *Let $\Omega \subset \mathbb{R}^3$ be a convex bounded domain with the boundary $\partial\Omega \in C^3$. Suppose that the inequality (10.12) holds. Let the exact coefficient $c^*(x)$ satisfies (2.6),(2.7) and also $c^* \geq 2d$, where the numbers $d_1, d_2 > 0$ are given. For any function $c(x) \in C^{\alpha}(\mathbb{R}^3)$ such that $c(x) \geq d_1$ in Ω and $c(x) = 2d_1$ in $\mathbb{R}^3 \diagdown \Omega$ consider the solution $w_c(x, \overline{s}) \in C^3\left(\mathbb{R}^3 \diagdown \{|x - x_0| < \gamma\}\right), \forall \gamma > 0$ of the problem (2.9a,b). Let $V_c(x) = \overline{s}^{-2} \ln w_c(x, \overline{s}) \in C^{2+\alpha}\left(\overline{\Omega}\right)$ be the corresponding tail function. Suppose that the cut-off pseudo frequency $\overline{s}$ is so large that both for $c^*(x)$ and any such function $c(x)$ the following estimates hold*

$$|V^*|_{2+\alpha} \leq \xi, |V_c|_{2+\alpha} \leq \xi, \tag{10.15}$$

where $\xi \in (0,1)$ is a sufficiently small number. Let $V_{1,1}(x, \overline{s}) \in C^{2+\alpha}\left(\overline{\Omega}\right)$ be the initial tail function and let

$$|V_{1,1}|_{2+\alpha} \leq \xi. \tag{10.16}$$

Denote $\eta := 2(h + \sigma + \xi + \varepsilon)$. Choose an arbitrary constant C_1 independent on other above parameters. Let $K = K(C_1, \Omega) > 0$ be the constant of the Schauder theorem and $\overline{N} \leq N$ be the total number of functions q_n calculated by the above algorithm. Suppose that the number $\overline{N} = \overline{N}(h)$ is connected with the step size h via $\overline{N}(h)\, h = \beta$, where the constant $\beta > 0$ is independent on h. Let β be so small that

$$\beta \leq \min\left(\frac{2}{7}, \frac{1}{16^2 K C^* \overline{s}^4}, \frac{C_1}{16^2 C^* \overline{s}^4}\right) \leq \min\left(\frac{2}{7}, \frac{1}{16KM^*}, \frac{C_1 C^*}{(M^*)^2}\right), \tag{10.17}$$

In addition, let the number η and the parameter λ of the CWF satisfy the following estimates

$$\eta \leq \eta_0 \left(\Omega, M^*, d_1, C_1\right) = \eta_0 \left(\Omega, \|q^*\|_{C^{2+\alpha}\left(\overline{\Omega}\right)\times C^1[\underline{s},\overline{s}]}, d_1, \overline{s}, C_1\right)$$

$$= \min\left(\frac{1}{2}, \frac{1}{4K}, \frac{d_1}{32\cdot 16C^*\overline{s}^4}, \frac{C_1}{8C^*\overline{s}^2}\right) \leq \min\left(\frac{1}{2}, \frac{1}{4K}, \frac{d_1}{32M^*\overline{s}^2}, \frac{2C_1}{M^*}\right), \tag{10.18}$$

$$\lambda \geq \lambda_0\left(C^*, K, \overline{s}, \eta\right) = \max\left(16^4\left(C^*\right)^4\overline{s}^8, 6\cdot 16^2\left(C^*\right)^2 K\overline{s}^4, \frac{1}{\eta^2}\right). \tag{10.19}$$

Then for every integer $n \in \left[1, \overline{N}\right]$ the following estimates hold

$$\left|q_{n,k} - q_n^*\right|_{2+\alpha} \leq 2KM^*\left(\frac{1}{\sqrt{\lambda}} + 3\eta\right) \leq 32C^*K\overline{s}^2\left(\frac{1}{\sqrt{\lambda}} + 3\eta\right), \tag{10.20}$$

$$\left|q_{n,k}\right|_{2+\alpha} \leq 2M^* \leq 32C^*\overline{s}^2, \tag{10.21}$$

$$\left|c_{n,k} - c^*\right|_{\alpha} \leq 8M^*\overline{s}^2\left(\frac{1}{\sqrt{\lambda}} + 3\eta\right) \leq 128C^*\overline{s}^4\left(\frac{1}{\sqrt{\lambda}} + 3\eta\right). \tag{10.22}$$

In addition, functions $c_{n,k}(x) \geq d_1$ in Ω and $\widehat{c}_{n,k}(x) \geq d_1$ in $\mathbb{R}^3$.

Remarks:

1. It often happens in the computational practice of inverse problems that theoretical estimates in convergence theorems are more pessimistic than ones obtained in numerical studies. Our computational experiments show that this is exactly our case in reference to estimates (10.17)-(10.22). For this reason, we use in our computations a stopping rule, which is different from (10.17).

2. By the Tikhonov concept, the constant C^* should be known a priori. It is reasonable to assume that C^* is independent on $\overline{s}$, although we do not use this assumption in our proof.

3. The parameter η characterizes the error both in the data and in our mathematical model. One should have $\eta \to 0$. However, since in the reality it is off its limiting value and we also have some other parameters, it is important to conduct numerical experiments, which would verify this theorem.

4. Truncating integrals at a high pseudo frequency $\overline{s}$ is a natural thing to do, because one routinely truncates high frequencies in physics and engineering. By truncating integrals, we actually come up with a different, although a quite reasonable mathematical model. Consider now the influence of this truncation on the accuracy of the reconstruction. Let, for example $h = \varepsilon = \sigma = \xi$, and $\lambda^{-1/2} = \xi$. Then (10.22) implies that the error of our reconstruction is $O(\xi)$ for $\xi \to 0$. In other words, one of claims of Theorem 10.1 is that the error of the reconstruction of the unknown coefficient is mainly determined by the truncation error, which means the error in our new mathematical model.

5. Conditions (10.15) and (10.16) with a small number ξ are natural ones, because the number $\overline{s}$ is supposed to be sufficiently large, and by (3.4) the function $\widetilde{v}(x, \overline{s})$ tends to zero together with its x-derivatives as $\overline{s} \to \infty$. Therefore, the condition (10.16) does *not* imply

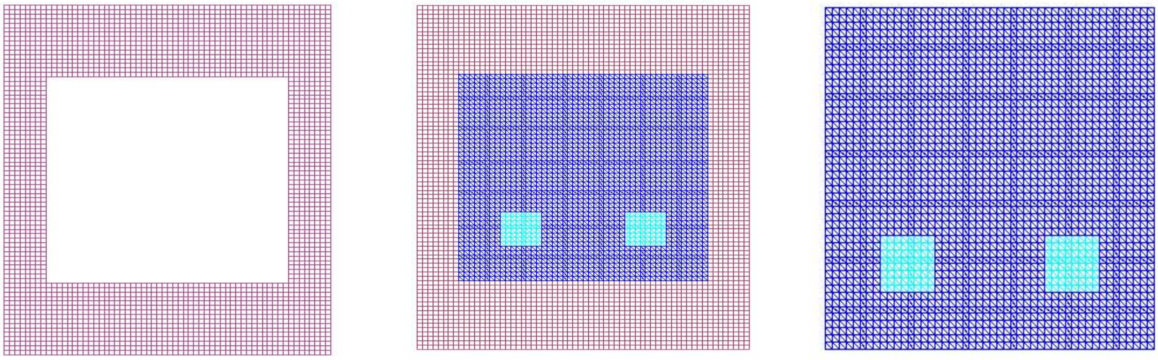

(a) (b) (c)

Figure 25: The hybrid mesh (b) is a combinations of a structured mesh (a), where FDM is applied, and a mesh (c), where we use FEM, with a thin overlapping of structured elements.

the assumption of the closeness of the first guess to the correct solution. Furthermore, in our computations we always take the initial tail $V_{1,1} \equiv 0$, which reflects the fact that no a priori knowledge about the medium is given.

6. One of the back bones of the theory of ill-posed problems is that the number of iterations can be chosen as a regularization parameter, see, e.g., page 157 of [33]. Therefore, we have a vector $\left(\overline{s}, \overline{N}, m_1, ..., m_{\overline{N}}\right)$ of regularization parameters, see details about their choice in subsection 7.4. Setting $\overline{N}(h)\, h = \beta = const. > 0$ is in an agreement with, e.g., Lemma 6.2 on page 156 of [33], since this lemma shows a connection between the error in the data and the number of iterations (that lemma is proven for a different algorithm).

7. It seems to be at the first glance that because of (10.22), one can stop the iterative process at $n = 1$. However, our numerical experience shows that this way one cannot obtain good images.

10.4 Some numerical results

We work with the computationally simulated data. That is, the data are generated by computing the forward problem (10.24) with the given function $c(x)$. To solve the forward problem (10.24), we use the so-called hybrid FEM/FDM method. The computational domain in all our tests $G = G_{FEM} \cup G_{FDM}$ is set as $G = [-4.0, 4.0] \times [-5.0, 5.0]$. This domain is split into a finite element domain $G_{FEM} := \Omega = [-3.0, 3.0] \times [-3.0, 3.0]$ and a surrounding domain G_{FDM} with a structured mesh, see Figure 25. The space mesh consists of triangles in Ω and of squares in G_{FDM}, with the mesh size $\tilde{h} = 0.125$ in the overlapping regions. At the top and bottom boundaries of G we use first-order absorbing boundary conditions, which are exact in this particular case. At the lateral boundaries, mirror boundary conditions allow us to assume an infinite space domain in the lateral direction.

The forward problem (10.24) is computed in the rectangle $G \subset \mathbb{R}^2$ (Figure 21). The coefficient $c(x)$ is unknown only in a square $\Omega \subset G$ and

$$c(x) = 1 \text{ in } G \diagdown \Omega. \tag{10.23}$$

Hence, $2d_1 = 1$ in (2.6), (2.7). The trace of the solution of the forward problem is recorded at the boundary $\partial\Omega$. This trace generates the Dirichlet boundary data $\psi(x,s)$ in (10.1) (after the Laplace transform). Next, the coefficient $c(x)$ is "forgotten", and our goal is to reconstruct this coefficient for $x \in \Omega$ from the data $\psi(x,s)$. The boundary of the rectangle G is $\partial G = \partial G_1 \cup \partial G_2 \cup \partial G_3$. Here, ∂G_1 and ∂G_2 are respectively top and bottom sides of the largest rectangle of Figure 25 and ∂G_3 is the union of left and right sides of this rectangle. The forward problem is

$$\begin{aligned}
c(x)\frac{\partial^2 u}{\partial t^2} - \triangle u = 0, &\quad \text{in } G \times (0,T), \\
u(\cdot,0) = 0, \ \frac{\partial u}{\partial t}(\cdot,0) &= 0, \ \text{in } G, \\
\partial_n u\big|_{\partial G_1} &= f(t), \ \text{on } \partial G_1 \times (0,t_1], \\
\partial_n u\big|_{\partial G_1} &= \partial_t u, \ \text{on } \partial G_1 \times (t_1,T), \\
\partial_n u\big|_{\partial G_2} &= \partial_t u, \ \text{on } \partial G_2 \times (0,T), \\
\partial_n u\big|_{\partial G_3} &= 0, \ \text{on } \partial G_3 \times (0,T),
\end{aligned} \tag{10.24}$$

where T is the final time. When calculating the Laplace transform of the boundary data, we integrate for $t \in (0,T)$, thus calculating an approximation of this transform. The plane wave f is initialized at the top boundary ∂G_1 of the computational domain G, propagates during the time period $(0,t_1]$ into G, is absorbed at the bottom boundary ∂G_2 for all times $t \in (0,T)$ and it is also absorbed at the top boundary ∂G_1 for times $t \in (t_1,T)$. Here

$$f(t) = \frac{(\sin(\overline{s}t - \pi/2) + 1)}{10}, \ 0 \le t \le t_1 := \frac{2\pi}{\overline{s}}, T = 17.8t_1.$$

10.4.1 Main discrepancies between the theory and the numerical implementation

It makes sense to summarize in this subsection main discrepancies between the above theory and our numerical implementation. We note that such discrepancies quite often occur in computations of inverse problems.

The first discrepancy is that in order to generate the data for the inverse problem, we have solved the forward problem (10.24) in the finite domain G with the plane wave instead of the Cauchy problem (2.1), (2.2) with the point source. To explain this, we note that our theory needs the problem (2.1), (2.2) only for the asymptotic behavior (2.11), and consequently for (2.16). However, conditions guaranteeing the asymptotic behavior (2.11) (see those conditions in [12]) are very hard to verify computationally. Therefore, in all our

numerical tests we have somewhat verified numerically the asymptotic behavior (2.16). To do this, we have considered functions $g_1(s)$ and $g_2(s)$, for $s \in [6.5, 7.5] \supset [\underline{s}, \overline{s}] = [6.7, 7.45]$, where

$$g_1(s) = s \left\| \nabla \widetilde{v}(x,s) \right\|_{L_2(\Omega)}, g_2(s) = s^2 \left\| \nabla q(x,s) \right\|_{L_2(\Omega)},$$

where functions $\widetilde{v}(x,s)$ and $q(x,s)$ are taken from the solution of the forward problem. We have found that the interval $[\underline{s}, \overline{s}] = [6.7, 7.45]$ was the optimal one for our reconstruction procedure, and we have used it in all our numerical experiments. Graphs of functions $g_1(s)$ and $g_2(s)$ (not presented here) have shown that these functions are very close to constants for $s \in [6.5, 7.5]$, which corresponds well with (2.16). We have also verified numerically in all our tests that the function $w(x,s) > 0$, which justifies the introduction of the function $\widetilde{v}(x,s) = \ln w(x,s)/s^2$. In our opinion, these verifications provide numerical justifications for the above discrepancy.

We describe the 2 $^{\text{nd}}$ main discrepancy in this paragraph. Because of (10.23), we set $2d_1 = 1$. Instead of using the extension procedure described in the beginning of section 5, we simply set $c_{n,k}(x) := 1$ in $G \diagdown \Omega$. In addition, since by (2.6) we need a priori lower bound $c(x) \geq d_1$, we enforce that the coefficient $c(x)$ belongs to the set of admissible coefficient $C_{adm} = \{c(x) \geq 0.5\}$ as follows: If $c_{n,k}(x_0) < 0.5$ for a certain point $x_0 \in \Omega$ and a certain pair (n,k), then we set $c_{n,k}(x_0) := 1$. The only reason why we use the value 1 in this setting is that we are supposed to know that the condition (10.23) is satisfied. Therefore, this setting as well as the fact that we allow the function $c(x)$ to attain values between 0.5 and 1 does not mean that we assume the knowledge of the background value of the function $c(x)$. In principle, this constraint cannot guarantee neither the continuity of the resulting function $c_{n,k}(x)$ nor that $c_{n,k}(x) \geq 1$. Nevertheless, we have observed in our numerical tests that all resulting functions $c_{n,k}$ are continuous and $c_{n,k}(x) \geq 1$ for all x, i.e., "allowed" values between 0.5 and 1, are not actually attained in iterations. Another reasonable setting would be to assign $c_{n,k}(x_0) := 0.5$. We have not done this yet and hope to investigate this topic in the future.

The 3$^{\text{rd}}$ main discrepancy is that our square Ω does not have a smooth boundary, as it is required by the Schauder theorem. Furthermore the Dirichlet boundary value problems for functions $q_{n,k}$ in the square Ω were solved by the FEM, in which the same finite elements were used as ones in the forward problem (10.24). The "inverse crime" was not committed because the forward problem was solved for the hyperbolic equation (10.24), whereas we solve many different elliptic equations in our iterative algorithm. The FEM cannot guarantee that resulting functions $q_{n,k} \in C^{2+\alpha}\left(\overline{\Omega}\right)$, as it is required by Theorem 10.1. Nevertheless, an analogue of Theorem 10.1 can be proved for the discrete case when the FEM analogues of equations for functions $q_{n,k}$ are used, and also the domain Ω with $\partial\Omega \in C^3$ is replaced respectively with either a rectangular prism in $\mathbb{R}^3$ or a rectangle in $\mathbb{R}^2$, as in our numerical examples. To prove this analogue, one needs to use the weak formulations of equations (5.4), (5.6) and the Lax-Milgram theorem instead of the Schauder theorem. Next, because of the equivalency of norms in finite dimensional spaces, the rest of the proof is very similar with the above. However, the latter development is outside of the scope of this publication and might be considered in our future works. Another interesting question here is about the

change of reconstructed images due to the increase of the number of finite elements, because that equivalency of norms "worsens" with the increase of the dimension of the space. This question might also be addressed in future publications.

The 4^{th} main discrepancy is that because of the above mentioned equivalency of norms, as well as because the $L_2(\Omega)$ norm is easier to verify computationally than the $C^{\alpha}\left(\overline{\Omega}\right)$ norm (especially because $\alpha \in (0,1)$), we use $L_2(\Omega)$ norms for our stopping rule. An additional discrepancy is that in order to produce updates for tails, we have solved on each iterative step the forward problem (10.24) instead of solving the elliptic problem for the function w. Next, we have calculated the Laplace transform to obtain the function $w_{n,k}(x, \overline{s})$.

10.4.2 Results of reconstruction

In this subsection we present results of our reconstructions. We have performed numerical experiments to reconstruct the medium, which is homogeneous with $c(x) = 1$ except of either two small squares or a single square, see Figure 25. However, we have not assumed *a priori* knowledge of neither the structure of this medium nor of the background constant $c(x) = 1$ outside of those squares.

In all our numerical experiments we have chosen the step size with respect to the pseudo frequency $h = 0.05$. Hence, $N = 15$ in our case. It is important that in all our tests the regularization parameters where chosen the same. This means that results were not "tilted" towards desired ones. We have chosen two sequences of regularization parameters $\lambda := \lambda_n$ and $\varepsilon = \varepsilon_n$ for $n = 1, ..., \overline{N}$. The formulation of Theorem 10.1 remains almost unchanged for this case. The reason of choosing different values of λ_n and ε_n is that values gradients of functions q_1 and q_2 are very small. Hence, in order not to eliminate totally the influence of the nonlinear term $\left(\nabla q_{n,k-1}\right)^2, n = 1, 2$ in (10.8), the values of λ_1 and λ_2 should not be too large. Next, the values of the nonlinear term start to grow, and we balance them by taking a larger value of λ_n for $n = 3, 4, 5$. For $n > 5$ the values of the nonlinear term become even bigger, and we balance them via increasing the value of λ_n again. This points towards the importance of the introduction of CWFs in the numerical scheme, as compared with the decrease of the step size h. The considerations for choosing different values of ε_n are similar. In all our tests of [] the values of the parameters λ_n and ε_n were:

$$
\begin{aligned}
&\lambda_n = 20, n = 1, 2; \lambda_n = 200, n = 3, 4, 5; \lambda_n = 2000, n \geq 6; \\
&\varepsilon_n = 0, n = 1, 2; \varepsilon_n = 0.001, n = 3, 4, 5; \varepsilon_n = 0.01, n = 6, 7, \\
&\varepsilon_n = 0.1, n \geq 8.
\end{aligned}
$$

We use the following approximation to find $c(x)$ at the point (i, j):

$$
\begin{aligned}
c^{i,j} = &\frac{\tilde{v}_{i+1,j} - 2\tilde{v}_{i,j} + \tilde{v}_{i-1,j}}{dx^2} + \frac{\tilde{v}_{i,j+1} - 2\tilde{v}_{i,j} + \tilde{v}_{i,j-1}}{dy^2} \\
&+ \underline{s}^2 \left(\left(\frac{\tilde{v}_{i+1,j} - \tilde{v}_{i,j}}{dx} \right)^2 + \left(\frac{\tilde{v}_{i,j+1} - \tilde{v}_{i,j}}{dy} \right)^2 \right),
\end{aligned}
$$

where dx and dy are grid step sizes of the discrete finite difference mesh in the directions x and y respectively. We also use the smoothness indicator in values of $c_{n.k}(x)$ via local averaging over the neighboring elements.

The resulting computed function is $c(x) := c_{\overline{N}}(x)$. Recall that the number of iterations is a part of the vectorial regularization parameter in our case. We have used $m_n = 4$ iterations with respect to tails for $n \leq n_0$ and $m_n = 7$ for $n = n_0 + 1, ..., \overline{N}$, where numbers n_0 and $\overline{N}$ are chosen on the basis of an *objective* stopping rule described below. Hence, while the pairs $\left(n_0, \overline{N}\right)$ differ in our tests, the rule of their choice (i.e., the stopping rule) remains the same. As it is always the case in ill-posed problems, the choice of proper regularization parameters and of a proper stopping rule was time consuming. However, we point out that our stopping rule as well as regularization parameters $\lambda_n, \varepsilon_n, m_n, \overline{s}$ once chosen, remained *the same for all* our numerical experiments described in Tests 1-4 below. Hence, results were not "conveniently adjusted" for each specific test in order to obtain the best possible image for that test.

In all our tests we have introduced the multiplicative random noise in the boundary data. Next, we apply the Laplace transform to the boundary data, which helps to both "smooth out" and decrease the noise, due to the integration. Because of that, we have successfully used the following formula for the $s-$derivative of the boundary data $\varphi(x,s)$ in (10.1)

$$\frac{\partial \varphi(x, s_n)}{\partial s} \approx \frac{\varphi(x, s_{n-1}) - \varphi(x, s_n)}{h}, h = 0.05.$$

In all tests of [12] the starting value for the tail was chosen $V_{1,1}(x, \overline{s}) = 0$, which is in an agreement with (10.16) and also reflects the fact that no advanced knowledge about tails is available. While we present results of only two tests here, more numerical results can be found in []. It is also important that in all our tests we have used the same objective stopping rule, which was based on stabilization of relative L_2 norms of discrepancies between two consecutive iterations of both tails and functions $c_{n,k}$, see details in [12].

Test 1. We now test our numerical method on the reconstruction of the structure given on Figure 25c. We introduce $\sigma = 5\%$ of the multiplicative random noise in the boundary data. We take $c = 4$ for both small squares of Figure 25c and $c = 1$ outside of these squares. Hence, the inclusion/background contrast is $4:1$. Figure 26 presents resulting image of the function $c := c_{12,7}$. Figure 27 displays the one-dimensional cross-sections of the images of the function $c_{n,k}$ along the vertical line passing through the middle of the left small square. The imaged function $c(x)$ is superimposed with the correct one. One can see that the value of the function $c(x)$ both inside and outside of the inclusion is imaged correctly, although the location of the inclusion is somewhat shifted to the top.

Test 2. While our method does not require a good *a priori* guess about the solution, the main point of this test is to show that a reconstruction algorithm, which is based on the minimization of a least squares objective functional, might lead to a poor reconstruction, if a good first guess about the solution is unavailable. We use the reconstruction algorithm described in [26-28], where the inverse problem is formulated as an optimal control problem of the minimization of a least squares objective functional. The latter is solved by the

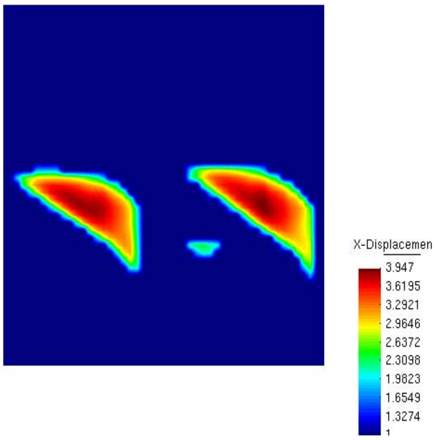

Figure 26: Computed image for Test 1.

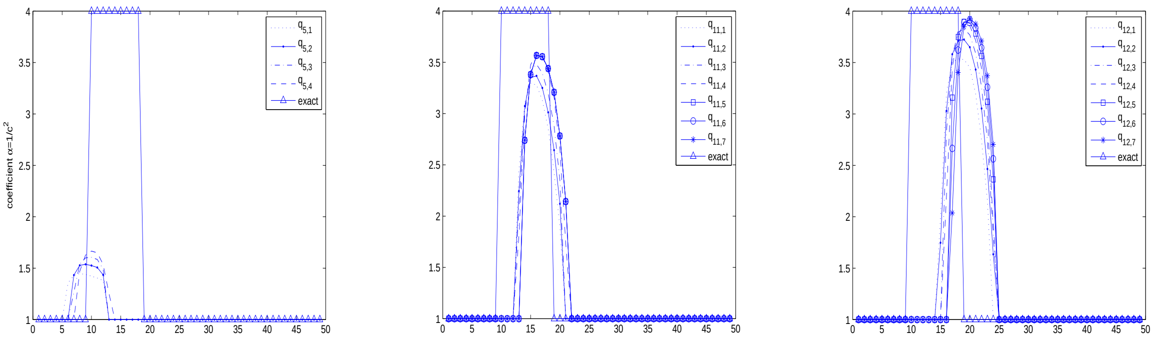

(a) (b) (c)

Figure 27: Computed image for Test 2.

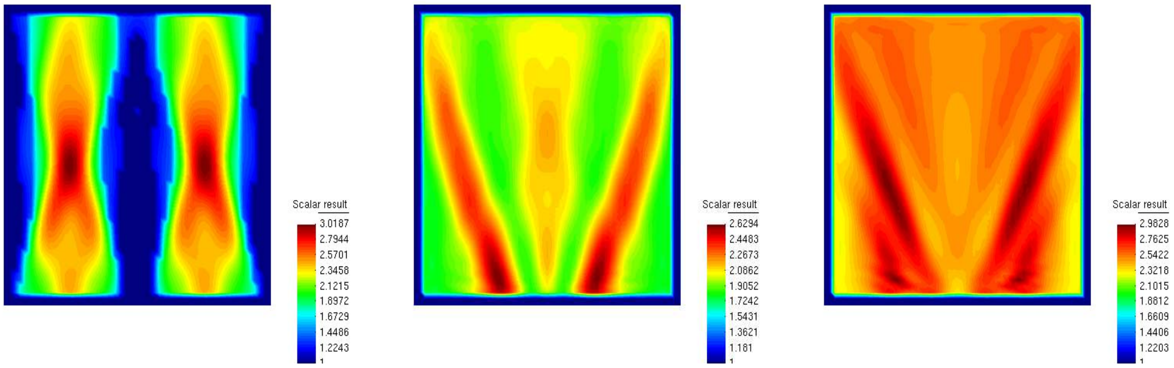

(a) (b) (c)

Figure 28: Computed image for Test 5.

quasi-Newton method, which is known to be a good method for this purpose. We find a stationary point of a Lagrangian, using the forward wave equation (the state equation), the backward wave equation (the adjoint equation), and an equation, which reflects the fact that the gradient with respect to the parameters should vanish. A minimizer of a corresponding least squares objective functional is found via an iterative procedure via solving the forward and backward wave equations for each iterative step and updating the unknown coefficients. We generate the data for the inverse problem using the same computational mesh and the same parameters as ones in Test 1. We start the optimization algorithm with different values of the first guess for the parameter $c_{guess} = const.$ at all points of the computational domain Ω. Figure 28 presents the images of the computed function c_{comp}. for the following initial guesses: on a) $c_{guess} = 1.0$, on b) $c_{guess} = 1.5$, and on c) $c_{guess} = 2.0$. We observe that images deteriorate from a) to c) with the deterioration of the first guess. We conjecture that local minima are achieved in all these three cases, although an investigation of the latter topic is outside of the scope of this publication.

We note that in [26-28] the quasi-Newton method was applied in a combination with the so-called "adaptivity technique". It is known that this technique is capable to improve the quality of some images, which are initially obtained via minimizations of least squares objective functionals. We are not presenting corresponding results here because of space considerations. We refer to the recent work [28] where tests were conducted using the adaptivity technique for a structure similar with one considered in Test 2. It was concluded in [28] that while the adaptivity significantly improves images with the $c_{guess} = 1.0$ and $c_{guess} = 1.5$, the image quality with $c_{guess} = 2$ has deteriorated not only on the coarse mesh but also on the one and two times refined meshes. Hence, the adaptivity technique works well in [28] only in a neighborhood of the initial guess $c_{guess} \in [1, 1.5]$.

10.4.3 An extension of the method of [12].

In the joint effort of the PI with Drs. H. Shan, J.Su, N. Pantong and H.Liu, who were co-authoring in [8], an extension of the above idea of this section for the case of the running source was carried out [8]. Since there is no clear asymptotic behavior of the solution of the equation () when the source runs to infinity, a heuristic treatment of tails was proposed in [8]. Images of [8] are of the same quality as ones of section 6, see Figures 15 and 16. In addition, recently we have figured out how to arrange a “clean”asymptotic behavior and this work is currently in progress. Preliminary results on the latter idea are encouraging.

11 Some Analytical Results of the Project

Although the main target of this project is globally convergent numerical methods for CIPs, it is quite natural that a number of purely analytical results were also obtained, in addition to the above uniqueness Theorem 8.1. These results are reflected in publications [15-20]. In this section we outline most interesting analytical results, also see annual report of 2006 for more details [21].

11.1 Inverse problems for the non-stationary transport equation

Results of this subsection have formed a major part of the Ph.D. thesis of Mr. Sergey E. Pamyatnykh [15], [16], whose Thesis Advisor was the PI. Sergey has defended his thesis in 2006 at The University of North Carolina at Charlotte. No analogs of Theorem 11.1 were known before the publication [15]. Theorem 11.2 [16] is the first global uniqueness result for a non-overdetermined CIP for the transport equation. Previous uniqueness results for CIPs for the transport equation were obtained either for the case of the over-determined data or under some restrictions imposed on coefficients of the transport equation, see [23,48,49]. This is because, unlike results of this subsection, the method of Carleman estimates was not applied previously.

Let $R = const. > 0$,

$$\Omega = \{x \in \mathbb{R}^n : |x| < R\}, \quad S^n = \{\nu \in \mathbb{R}^n : |\nu| = 1\}, Z = \Omega \times S^n,$$

$$H = \Omega \times (-T, T) \times S^n, \quad \Gamma = \partial\Omega \times (-T, T) \times S^n,$$
$$H^+ = \Omega \times (0, T) \times S^n, \quad \Gamma^+ = \partial\Omega \times (0, T) \times S^n,$$
$$H^- = \Omega \times (-T, 0) \times S^n, \quad \Gamma^- = \partial\Omega \times (-T, 0) \times S^n,$$

so that

$$H = H^+ \cup H^- \quad \text{and} \quad \Gamma = \Gamma^+ \cup \Gamma^-.$$

Also, introduce spaces

$$\widetilde{C}^k(\overline{H}), k = 1, 2, \widetilde{C}^k(\overline{H}) = \left\{ u\,(x,t,\nu) : \max_{0\le s\le k} \left\| D^s_{x,t} u\,(x,t,\nu) \right\|_{C(\overline{H})} = \|u\|_{\widetilde{C}^k(\overline{H})} < \infty \right\}.$$

The non-stationary transport equation in the domain H has the form [6]

$$Ku := u_t + (\nu, \nabla u) + a(x,t,\nu)u + -\!\!\!\!\!\!\int_{S^n} g(x,t,\nu,\mu)u(x,t,\mu)d\sigma_\mu = F(x,t,\nu), \qquad (11.1)$$

where $\nu \in S^n$ is a unit vector of the particle velocity, $u(x,t,\nu) \in \widetilde{C}^1(\overline{H})$ is the density of the particle flow, $a(x,t,\nu)$ is the attenuation coefficient, $F(x,t,\nu)$ is the angular density of sources, $g(x,t,\nu,\mu)$ is a scattering indicatrix., and $(\nu, \nabla u)$ denotes the scalar product of vectors ν and ∇u in $\mathbb{R}^n$.

Consider the following boundary condition

$$u(x,t,\nu) = p(x,t,\nu), \qquad (11.2)$$

$$\text{for } (x,t,\nu) \in \Gamma \cap \{(n(x), \nu) < 0\}.$$

Here $(n(x), \nu)$ is the scalar product of the outer unit normal vector $n(x)$ on the surface $\partial\Omega$ and the direction of the velocity ν. Hence, only incoming radiation is given at the boundary in this case. The boundary condition (11.2) together with the initial condition at $t = -T$

$$u(x,-T,\nu) = f(x,\nu), \ \ \forall (x,\nu) \in Z \qquad (11.3)$$

form a classic boundary value problem for the non-stationary transport equation (11.1) in the domain H. This problem means that given the initial condition and the incoming radiation at the boundary, find the density of the particle flow.

Consider now a

A non-standard boundary value problem. Suppose that the initial condition (11.3) is unknown, but the outgoing radiation at the boundary is known instead. In other words, the following function $h(x,t,\nu)$ is known in addition to the function $p(x,t,\nu)$ in (11.2),

$$u(x,t,\nu) = h(x,t,\nu), \qquad (11.4)$$

$$\text{for } (x,t,v) \in \Gamma \cap \{(n(x), \nu) > 0\}.$$

Determine the function $u(x,t,\nu)$ in the domain H.

The problem (11.1), (11.2), (11.4) is ill-posed. Hence, one cannot expect to obtain an existence theorem. However, one can expect to obtain a stability result, i.e., to estimate the function u via functions p and h.

Theorem 11.1 (Lipschitz stability) [15]. *Let in (7.1)* $\|a\|_{C(\overline{H})} \leq r$ *and* $\|g\|_{C(\overline{H}\times S^n)} \leq r$, *where* $r = const. > 0$. *Assume also that the function* $F \in L_2(H)$ *and* $T > R$. *Denote*

$$q(x,t,\nu) = \left\{ \begin{array}{c} p(x,t,\nu) \text{ if } (n(x),\nu) < 0 \\ h(x,t,v) \text{ if } (n(x),\nu) \geq 0 \end{array} \right\}.$$

Let the function $u \in C^1\left(\overline{\Omega} \times [-T,T]\right) \times C(S^n)$ *satisfies conditions (6.14), (6.15), (6.17). Then the following Lipschitz stability estimate is valid*

$$\|u\|_{L_2(H)} \leq C\left[\|q\|_{L_2(\Gamma)} + \|F\|_{L_2(H)}\right],$$

where the positive constant $C = C(r,R,T)$ *depends only on numbers* r, R *and* T.

The PI and Pamyatnykh [16] have considered the following

Inverse Problem. Suppose that the equation (11.1) is satisfied in the domain $H^+ = \Omega \times (0,T) \times S^n$. Suppose that the attenuation coefficient $a(x,\nu)$ is independent on time t and unknown, but the following functions $s(x,\nu)$ and $k(x,t,\nu)$ are known

$$u(x,0,\nu) = s(x,\nu), \tag{11.5}$$

$$u(x,t,\nu)\mid_{\Gamma^+} = k(x,t,\nu). \tag{11.6}$$

Determine the function $a(x,\nu)$.

Thus, the following theorem was proven

Theorem 11.2 [16]. *Suppose that the derivative* $\partial_t g$ *exists in* $\overline{H^+}\times S^n$ *and* $||\partial_t^k g||_{C(\overline{H^+}\times S^n)} \leq r_1$ *for* $k = 0,1$, *where* r_1 *is a positive constant. Let in (7.6)* $|s(x,v)| \geq r_2$, *where* $r_2 = const > 0$. *Assume that there exist two pairs of functions* (a_1,u_1) *and* (a_2,u_2) *satisfying (11.1), (11.2), (11.5), (11.6) and such that*

$$a_1, a_2 \in C\left(\overline{Z}\right) \text{ and } u_i, u_{it}, u_{itt}, \nabla u_i, \nabla u_{it} \in C\left(\overline{H^+}\right), i = 1,2.$$

Suppose also that

$$[(a_i f)(x,\nu)]^2 = [(a_i f)(x,-\nu)]^2, i = 1,2.$$

Let $\|u_{it}\|_{C(\overline{H^+})} \leq r_3$, *where* $r_3 = const > 0$. *Then there exists a number* $T_0 = T_0(R, r_2, r_3) > R$ *such that if* $T > T_0$, *then* $a_1 = a_2$ *in* Z *and* $u_1 = u_2$ *in* H^+. *If the function* $u_2(x,t,\nu) \neq 0$ *in* $\overline{H^+}$, *then it is sufficient to assume that* $T > R$.

11.2 Exact controllability for the non-stationary transport equation

In the work of Klibanov and Yamamoto [17] the exact controllability theorem for the non-stationary transport equation was proved for the first time. Consider the homogeneous transport equation (11.1),

$$Ku := u_t + (\nu, \nabla u) + a(x,t,\nu)u + \int\limits_{S^n} g(x,t,v,\mu)u(x,t,\mu)d\sigma_\mu = 0 \text{ in } H^+, \tag{11.7}$$

where H^+ is defined above with the only difference that now $\Omega \subset \mathbb{R}^n$ is a bounded domain with its boundary $\partial\Omega \in C^\infty$. Assume that functions

$$a \in C^1\left(\overline{H^+}\right), g \in C^1\left(\overline{H^+} \times S^n\right). \tag{11.8}$$

Let

$$\Gamma_- = \{(x,t,\nu) \in \partial\Omega \times (0,T) \times S^n : (n(x),\nu) \leq 0\},$$

Introduce the Hilbert space of real valued functions $L^2_{\cos}(\Gamma_-)$ as the one with the scalar product

$$\langle p,q\rangle = \int_{\Gamma_-} p(x,t,\nu)\, q(x,t,\nu)\, |\cos(n(x),\nu)|\, dS_x dt d\sigma_\nu.$$

Observe that a particular difficulty in working with this scalar product is that the weight function $|\cos(n(x),\nu)|$ has zeros on Γ_-.

We first introduced the weak solution $u \in C([0,T]; L^2(\Omega \times S^n))$ of the equation (11.7) with the initial condition

$$u(x,0,\nu) = 0 \tag{11.9}$$

and the boundary condition

$$u\mid_{\Gamma_-} = p(x,t,\nu) \in L^2_{\cos}(\Gamma_-). \tag{11.10}$$

To do this, we have used modified classic density arguments. Next, we posed the following

The Exact Controllability Problem. Consider an arbitrary function $w(x,\nu) \in L^2(\Omega \times S^n)$. Find such a control function $p_w(x,t,\nu) \in L^2_{\cos}(\Gamma_-)$ that

$$u(x,T,\nu) = w(x,\nu), \tag{11.12}$$

where $u \in C([0,T]; L^2(\Omega \times S^n))$ is the weak solution of the equation (11.7) with the initial condition (11.9) and the boundary condition (11.10), in which $p = p_w$. The time T is the so-called "steering time".

We have modified Theorem 11.1 to prove

Theorem 11.3 [17]. *Let Ω be strictly convex bounded domain with $\partial\Omega \in C^\infty$ and conditions (11.8) hold. Let the steering time $T >$ diameter(Ω). Then for any function $w(x,\nu) \in L^2(\Omega \times S^n)$ there exists a control function $p_w(x,t,\nu) \in L^2_{\cos}(\Gamma_-)$ such that if the function $u \in C([0,T]; L^2(\Omega \times S^n))$ is the weak solution of the equation (11.7) satisfying (11.9) and (11.10) with $p = p_w$ in (11.10), then (11.12) holds.*

11.3 Estimates of initial conditions of parabolic equations and inequalities with the lateral Cauchy data in finite domains

The result of this subsection is published in the work of Klibanov [18]. As it was stated in subsection 1.2, this results was featured as one of the best of 2006 by the Editorial Board of Inverse Problems. Let $\Omega \subset \mathbb{R}^n$ be a bounded domain with the boundary $\partial\Omega \in C^1$. For any

$T = const. > 0$ denote $Q_T = \Omega \times (0,T)\,, S_T = \partial\Omega \times (0,T)\,.$ For any function $s(x), x \in \mathbb{R}^n$ denote $s_i = \partial s/\partial x_i, i = 1, ..., n,$ whenever the differentiation is appropriate. We also denote $\nabla s = (s_1, ..., s_n)\,.$ Let $L = L(x,t,D)$ be an elliptic operator of the second order in Q_T,

$$Lu := L(x,t,D)u = \sum_{i,j=1}^{n} a^{ij}(x,t)u_{ij} + \sum_{i,j=1}^{n} b^j(x,t)u_j + b^0(x,t)u,$$

with its principal part L_0,

$$L_0 u := L_0(x,t,D)u = \sum_{i,j=1}^{n} a^{ij}(x,t)u_{ij},$$

where coefficients

$$a^{ij} = a^{ji}, a^{ij} \in C^1\left(\overline{Q}_T\right) \cap B\left(\overline{Q}_T\right); a_k^{ij}, b^j, b^0 \in B\left(\overline{Q}_T\right),$$

where $B\left(\overline{Q}_T\right)$ is the set of functions bounded in $\overline{Q}_T$. Naturally, we assume the existence of two positive numbers $\sigma_1, \sigma_2, \sigma_1 \le \sigma_2$ such that

$$\sigma_1 |\xi|^2 \le \sum_{i,j=1}^{n} a^{ij}(x,t)\xi_i\xi_j \le \sigma_2 |\xi|^2\,,\ \forall\,(x,t,\xi) \in \overline{Q}_T \times \mathbb{R}^n. \tag{11.13}$$

Let the function $u \in H^{2,1}(Q_T)$ be a solution of the parabolic equation

$$u_t = Lu + f(x,t),\ \text{a.e. in } Q_T, \tag{11.14}$$

with the unknown initial condition $g(x)$,

$$u(x,0) = g(x) \in H^1(\Omega)\,, \tag{11.15}$$

where the function $f \in L_2(Q_T)\,.$ Along with the equation (11.14) we also consider a more general case of the parabolic inequality

$$\int\limits_{Q_T} (u_t - Lu)^2\, dxdt \le M^2, \tag{11.16}$$

where the function $u \in H^{2,1}(Q_T)$ satisfies condition (11.15) and $M = const. > 0$.

Inverse Problem. Assume that the following lateral Cauchy data $h_1(x,t)$ and $h_2(x,t)$ are given

$$u\mid_{S_T} = h_1(x,t),\quad \frac{\partial u}{\partial n}\mid_{S_T} = h_2(x,t), S_T = S \times (0,T)\,, \tag{11.17}$$

where the function $u \in H^{2,1}(Q_T)$ satisfies either conditions (11.14) and (11.15) or conditions (11.15) and (11.16). Estimate the unknown initial condition g and the function u via functions h_1, h_2 and f.

This is an inverse problem of the determination of the initial condition in the parabolic equation using lateral Cauchy data h_1 and h_2. Applications are in such diffusion and heat conduction processes, in which one is required to determine the initial state using boundary time dependent measurements. To describe a more specific application, consider the cooling process of a solid, which is contained in a bounded domain $\Omega \subset \mathbb{R}^3$. Suppose that the initial temperature of this solid is high, unknown, and is the subject of one's interest. Suppose also that interior points of this solid are unavailable for the temperature measurements. Instead one is measuring the time dependence of both the temperature u and the heat flux at the boundary $\partial\Omega$. Assuming that near $\partial\Omega$ the principal part $L_0 = \Delta$, we obtain that the heat flux at the boundary is $\partial u / \partial n \mid_{S_T}$. Hence, in this application the Inverse Problem is the problem of the determination of the spatial distribution of the initial temperature $u(x,0)$, using time dependent boundary measurements.

A particular benefit of considering this applied example is that it helps to understand the naturality of imposing a priori bound on the $L_2(\Omega)-$norm of the gradient $\|\nabla g\|_{L_2(\Omega)}$ in Theorem 11.4. Indeed, this assumption means *a priori* knowledge of the absence of high gradients in the initial temperature, which is quite natural in this application. A similar idea, although in a more general form, is one of building blocks of the theory of ill-posed problems and it follows from the above mentioned fundamental Tikhonov theorem [50].

The idea of the proof of Theorem 11.4 (below) is to combine two types of Carleman estimates: "lateral" and "backwards" ones. Lateral Carleman estimate is the one, which estimates the solution of the parabolic equation (or inequality) via lateral Cauchy data. It estimates that solution in a subdomain G of the time cylinder Q_T. However, since $G \cap \{t = 0\} = \varnothing$, then the lateral Carleman estimate does not provide an estimate for the initial condition $g(x)$. Still, it ensures an estimate of the norm

$$\|u(x, t_0)\|_{L_2(\Omega)} \tag{11.18}$$

via norms of the lateral Cauchy data. In (11.18) $t_0 \in (0,T)$ is a certain constant.

Thus, one should somehow estimate the initial condition $g(x)$ via the norm (11.18). To do so, a backwards Carleman estimate is used. The backwards Carleman estimate is the one, which estimates the solution $u(x,t)$ of the parabolic equation for $t \in (0,t_0) \subset (0,T)$ via the norm (11.18), i.e., it estimates solutions of parabolic equations with the reversed direction of time. However, the previously known such estimate enabled one to estimate the certain norms of the function $u(x,t)$ only in $\Omega \times (\tau, t_0)$ for a $0 < \tau < t_0$. Hence, the case of $u(x,0)$ is a more delicate one. The main new element of the work [18] is a new backwards Carleman estimate, which enabled to estimate $\|u(x,0)\|_{L_2(\Omega)}$, as well as to consider the general case of the operator L with $(x,t)-$dependent coefficients, including the inequality (11.16).

A similar problem was considered earlier by Xu and Yamamoto [51]. However, their technique cannot handle the case of non-self adjoint operator L with $(x,t)-$ dependent coefficient, including the inequality (11.16). This is because they use the so-called "logarithmic stability" method for the backwards estimate, and this method works only with the self-adjoint operator L with x-dependent coefficients, see, e.g., [22] for that method.

The following stability estimate was proven in [18].

Theorem 11.4. *Assume that the above conditions imposed on the coefficients of the elliptic operator are fulfilled. In the case of the problem (11.15)-(11.17) denote $f(x,t) = M$. In both problems (11.14), (11.16), (11.17) and (11.15)-(11.17) denote $F = (h_1, h_2, f)$ and*

$$\|F\| = \left[\|h_1\|^2_{H^1(S_T)} + \|h_2\|^2_{L_2(S_T)} + \|f\|_{L_2(Q_T)}\right]^{1/2}.$$

Suppose that $\|F\| \leq B$, is a positive number. Assume that the function $g \in H^1(\Omega)$. Then there exists a positive constant C such that, for every number $\alpha \in (0,2)$ there exists a number $\beta \in (0,1)$ such that the following stability estimate holds

$$\|g\|^2_{L_2(\Omega)} \leq \frac{C}{\alpha} \|\nabla g\|^2_{L_2(\Omega)} \cdot \ln\left[\frac{B}{\beta \|F\|}\right]^{-1} + C\left(\frac{B}{\beta}\right)^{\alpha} \|F\|^{2-\alpha}. \tag{11.19}$$

The constant C depends only on the operator L and the domain Q_T and the constant β depends on the same parameters as C, as well as on α.

The estimate (11.19) is the so-called *conditional stability estimate,* because it assumes boundedness of a stronger norm $\|\nabla g\|^2_{L_2(\Omega)}$, see above about the applied aspect. Conditional stability estimates are typical ones for ill-posed problems, as it follows from the Tikhonov theorem [50]. While constants like B, α and β do not appear in traditional well-posed problems (at least in the linear case), their appearance is quite natural in ill-posed problems. On the other hand, assuming that $\|F\|$ is sufficiently small, one can drop constants B, α, β, so as the second term in the right hand side of (11.21).

11.4 Stability estimates of initial conditions of parabolic equations and inequalities in infinite domains

The result of this subsection was obtained by the PI and one of his collaborators Dr. A.V. Tikhonravov (Professor of Moscow State University) [19]. Suppose that in the previous subsection the domain $\Omega \subseteq \mathbb{R}^n$ is infinite rather than finite, $\partial\Omega \in C^1$. Consider the same problem as in the previous subsection. Let the function $u \in H^{2,1}(Q_T)$ satisfies the following conditions

$$u_t = Lu + f(x,t), \text{ a.e. in } Q_T, \tag{11.20}$$

$$u \mid_{S_T} = 0, \tag{11.21}$$

$$u(x,0) = g(x) \in H^1(\Omega). \tag{11.22}$$

Conditions imposed on the coefficients of the elliptic operator L are the same as ones in the previous subsection. Along with the equation (7.28) consider a more general parabolic inequality

$$|u_t - L_0 u| \leq M\left[|\nabla u| + |u| + |f|\right], \text{ a.e. in } Q_T, \tag{11.23}$$

where L_0 is the principal part of the elliptic operator L and M is a positive constant. Let $P \in C^2$, $P \subset \overline{\Omega}$ be an arbitrary surface and $P_T = P \times (0,T)$. Consider the following

Inverse Problem. Let $\Phi \subset \Omega$ be a finite subdomain. For either of problems (11.20)-(11.22) or (11.21)-(11.23), estimate the unknown initial condition $g(x)$ in the domain Φ via the lateral Cauchy data $h_3(x,t)$ and $h_4(x,t)$, where

$$u\mid_{P_T}= h_3(x,t), \frac{\partial u}{\partial n}\mid_{P_T}= h_4(x,t). \tag{11.24}$$

The main difficulty of the case of the infinite domain Ω compared with the previous case of the finite domain is that the previously used idea of combining lateral and backwards Carleman estimates does not work in this case. Indeed, lateral Carleman estimates work only in finite subdomain. Hence, the lateral Carleman estimate would enable one only to estimate the norm $\|u(x,t_0)\|_{L_2(\Phi)}$ for a $t_0 = const. \in (0,T)$. Then, however, one cannot use the backwards Carleman estimate (unlike the previous subsection) to estimate the function $g(x)$. The reason of the latter is that any backwards estimate requires the knowledge of the function $u(x,t_0)$ for all $x \in \Omega$. This is why analogues of Theorem 11.5 are unknown.

To overcome this difficulty, a new lateral Carleman estimate for the parabolic operator $\partial_t - L_0$ was derived. The level surface of the corresponding Carleman Weight Function (CWF) is contained in a thin strip $t \in \left\{|t-\delta| < \delta\sqrt{\omega_0}\right\}$, where $\delta > 0$ is sufficiently small and the number $\omega_0 \in (0,1)$ is fixed. The main new feature of this estimate is that, unlike previously known Carleman estimates, this one does not break down when the width $2\delta\sqrt{\omega_0}$ of this strip approaches zero as $\delta = \delta(\|F\|) \to 0^+$ for $\|F\| \to 0$.

Before formulating the stability estimate, we formulate a geometric condition. Let $\Phi \subset \Omega$ be a convex bounded subdomain. We shall say that Φ has the P-property, if the following two conditions are fulfilled: (1) For any point $x \in \Phi$ there exists a point $\widetilde{x}\,(x) \in P$ such that the straight line connecting points x and $\widetilde{x}$ does not lie in the hyperplane, which is tangent to the hypersurface P at the point $\widetilde{x}$ and (2) $dist\,[\Phi, (\partial\Omega \diagdown P)] > 0$, where $dist\,[\Phi, (\partial\Omega \diagdown P)] := ds\,(\Phi)$ is the Hausdorff distance. An example of the P-property is the case when either $P \subseteq \partial\Phi$ or $P \subset \partial\Omega$ and $ds\,(\Phi) > 0$. Another example is when the hypersurface P is a part of a hyperplane, $P \subset \{x_1 = 0\}$, $\Phi \subset \{x_1 > 0\} \cap \Omega$ or $\Phi \subset \{x_1 < 0\} \cap \Omega$ and $ds\,(\Phi) > 0$. The following analogue of Theorem 11.4 was proven

Theorem 11.5 [19]. *Suppose that above conditions imposed on coefficients of the operator $L(x,t,D)$, the domain Ω and the surface P are fulfilled. Let the function $u \in H^{2,1}(Q_T)$ satisfies either conditions (11.20)-(11.22), (11.24) or conditions (11.21)-(11.24). Let $\Phi \subset \Omega$ be a convex bounded subdomain of the domain Ω which possesses the P-property. Let the function $h_3 \in H^1(P_T)$. Consider the vector valued function $F = (h_3, h_4, f)$ and denote*

$$\|F\| = \left[\|h_3\|^2_{H^1(P_T)} + \|h_4\|^2_{L_2(P_T)} + \|f\|^2_{L_2(Q_T)}\right]^{1/2}.$$

Suppose that $\|F\| \leq B$, where B is a positive constant. Choose an arbitrary number $\alpha \in (0,2)$. Then there exist constants $C > 0$ and $\beta \in (0,1)$ such that the following stability estimate holds

$$\|g\|^2_{L_2(\Phi)} \leq \frac{C}{\alpha}\left[\||\nabla g|\|^2_{L_2(\Omega)} + \|g\|^2_{L_2(\Omega\diagdown\Phi)}\right] \cdot \left[\ln\left(\frac{B}{\beta\|F\|}\right)\right]^{-1} + C\left(\frac{B}{\beta}\right)^{\alpha}\|F\|^{2-\alpha}. \tag{11.25}$$

Here the constant $C = C_1 (L, M, \Phi, P)$ depends on the operator L, the constant M in (6.31), the domain Φ and the surface P. The constant β depends on the same parameters as ones listed for C, as well as on the number α.

Hence, if, in particular, it is known *a priori* that the function $g(x)$ has a finite support with $g(x) = 0$ for $x \in \Omega \diagdown \Phi$, then the term $\|g\|^2_{L_2(\Omega \diagdown \Phi)} = 0$ in (11.25).

12 Presentations, Thesis Defense and Publications

12.1 Presentations and Thesis Defense

The above results were presented by the PI on eighteen (18) professional meetings listed below. Trips to some of these meetings were either partially or fully sponsored by this grant. The ARO support was acknowledged in these talks of the PI.

The PI has been the Thesis Advisor of Mr. Sergey E. Pamyatnykh, who has defended his Ph.D. in Mathematics in 2006 at The Department of Mathematics and Statistics of The University of North Carolina at Charlotte. Publications [15] and [16] have formed a major part of his thesis titled *Stability Estimates for Some Ill-Posed and Inverse Problems for the Transport and Hyperbolic Equations.*

1. Colloquium talk in the Department of Mathematics of Iowa State University, Ames, Iowa, March 2006.

2. Colloquium talk in the Department of Mathematics of Colorado State University, Fort Collins, CO, April 2006.

3. Colloquium talk in the Department of Mathematics of University of Carrollton, Carrollton, Georgia, April 2006.

4. The Third International Conference "Inverse Problems: Modelling & Simulation", Fethiye, Turkey, May 2006.

5. The International Conference "Tikhonov and Contemporary Mathematics", Moscow, Russia, June 2006.

6. The International Conference "Inverse Problems in Applied Sciences", Hokkaido University, Sapporo, Japan, July 2006.

7. The Annual International Meeting of Society of Opto-Electronics Engineers (SPIE), San Jose, California, January 2007.

8. The International Workshop on Applied Mathematics and Inverse Problems, Khmelnickyi National University, Khmelnickyi, Ukraine, March 2007. The PI was honored to be named the Chairman of this workshop.

9. The International Workshop on Microlocal Analysis and Harmonic Analysis in Inverse Problems, Marseilles, France, March 2007.

10-12. The International Conference "Applied Inverse Problems" (AIP), University of British Columbia, Vancouver, Canada, 2007. Three (3) presentations on three different minisimposia were made.

13. Dr. A. Timonov has presented results of section 7 on The International Conference "Applied Inverse Problems" (AIP), University of British Columbia, Vancouver, Canada,

June 2007. The support of this project was acknowledged in his talk.

14. Biomedical Imaging Workshop I, at Radon Instutute of Applied and Computational Mathematics of the Austrian Academy of Science, 2007, Linz, Austria.

15. Norwegian Technological University, Trondheim, Norway, 2008.

16. Moscow State University, Moscow, Russia, 2008.

17. UGRA Institute of Information Technologies, Khanty-Mansiisk, Russia, 2008.

18. Fourth International Conference "Inverse Problems: Modeling and Simulations", Fethiye, Turkey, 2008.

12.2 Publications

12.2.1 Publications of the reportage period with the acknowledgment of the support of this grant: published, accepted and submitted

Total 20 papers [1-20] were published/accepted/sibmitted with the acknowledgment of the support of this project. All of them are in refereed journals.

1. M.V. Klibanov and A. Timonov, Numerical studies on the globally convergent convexification algorithm in 2D, *Inverse Problems*, 23, 123-138, 2007.

2. M.V. Klibanov and A. Timonov, A globally convergent convexification algorithm for multidimensional coefficient inverse problems, *Journal of Inverse and Ill-Posed Problems,* 15, 13-17, 2007.

3. J. Xin and M.V. Klibanov, Imaging of land mines by the globally convergent convexification method using a simplified mathematical model, *Inverse Problems in Science and Engineering*, 16, 631-653, 2008.

4. J. Xin and M.V. Klibanov, Comparative studies of the globally convergent convexification algorithm with application to imaging of antipersonnel land mines, *Applicable Analysis*, 86, 1147-1176, 2007.

5. J. Xin and M.V. Klibanov, Numerical solution of an inverse problem of imaging of antipersonnel land mines by the globally convergent convexification algorithm**,** accepted for publication in *SIAM J. Sci. Computing.*

6. J. Xin and M.V. Klibanov, Towards real time imaging of antipersonnel land mines by the convexification algorithm, accepted for publication in *J. Inverse and Ill-Posed Problems.*

7. H. Shan, M.V. Klibanov, H. Li, N. Pantong, and J. Su, Numerical implementation of the convexification algorithm for an optical diffusion tomograph, *Inverse Problems,* 24, 025006 (18 pages), 2008.

8. H. Shan, M.V. Klibanov, H. Li, N. Pantong, and J. Su, A globally accelerated numerical method for optical tomography with continuous wave source, submitted for publication to *J. Inverse and Ill-Posed Problems.*

9. J. Su, H. Shan, H. Liu and M.V. Klibanov, A reconstruction method with data from a multiple-site continuous-wave source for 3-Dimensional optical tomography, *J. of Optical Society of America, A*, 23, 2388-2395, 2006.

10. C. Clason and M.V. Klibanov, The quasi-reversibility method for the thermoacoustic tomography in heterogeneous medium, *SIAM J. Sci. Computing,* 30, 1-23, 2007.

11. M.V. Klibanov, A.V. Kuzhuget, S.I. Kabanikhin and D.V. Nechaev, The quasi-reversibility method for the thermoacoustic tomography and a coefficient inverse problem, *Applicable Analysis*, iFirst, 1-28, 2008.

12. L. Beilina and M.V. Klibanov, A globally convergent numerical method for a coefficient inverse problem, accepted for publication in *SIAM J. Sci. Computing.*

13. M.V. Klibanov, S.I. Kabanikhin and D.V. Nechaev, Numerical solution of the problem of computational time reversal in the quadrant, *Waves in Random and Complex Media,* 16, 473-494, 2006.

14. B. Kaltenbacher and M.V. Klibanov, An inverse problem for a nonlinear parabolic equation with applications in population dynamics and magnetics, *SIAM J. Math. Analysis,* 39, 1863-1889, 2008.

15. M.V. Klibanov and S.E. Pamyatnykh, Lipschitz stability of a non-standard problem for the non-stationary transport equation via a Carleman estimate, *Inverse Problems*, 22, 881-890, 2006.

16. M.V. Klibanov and S.E. Pamyatnykh, Global uniqueness for a coefficient inverse problem for the non-stationary transport equation via a Carleman estimate, *J. Math. Analysis and Applications,* 343, 352-365, 2008.

17. M.V. Klibanov and M. Yamamoto, Exact controllability for the time dependent transport equation, *SIAM J. Control and Optimization,* 46, 2071-2195, 2007.

18. M.V. Klibanov, Estimates of initial conditions of parabolic equations and inequalities via lateral Cauchy data, *Inverse Problems*, 22, 495-514, 2006.

19. M.V. Klibanov and A.V. Tikhonravov, Estimates of initial conditions of parabolic equations and inequalities in infinite domains via lateral Cauchy data, *J. Differential Equations,* 237, 198-224, 2007.

20. M.V. Klibanov, On the recovery of a 2-D function from the modulus of its Fourier transform, *J. Math. Analysis and Applications*, 323, 818-843, 2006.

12.2.2 Other publications

21. M.V. Klibanov, Interim 2005-2006 report on the ARO grant W911NF-05-1-0378.

22. K.A. Ames and B. Straugan, *Non-Standard and Improperly Posed Problems*, Academic, New York, 1997.

23. D.S. Anikonov, A.E. Kovtanyuk and I.V. Prokhorov, *Transport Equation and Tomography*, VSP, Utrecht, The Netherlands, 2002.

24. D.G. Aronson, The role of diffusion in mathematical population biology: Skellam revisited, in: S. Levine (Ed.), *Mathematics in Biology and Medicine*, Lecture Notes in Biomathematics, Vol. 57, Springer, Berlin, pp. 2-6, 1985.

25. F. Bachinger, U. Langer and J Schöberl, Numerical analysis of nonlinear multiharmonic eddy current problems, *Numer. Math.* 100, 593-616, 2005.

26. L. Beilina and C. Clason. An adaptive hybrid fem/fdm method for an inverse

scattering problem in scanning acoustic microscopy, *SIAM J. Sci. Comp.*, 28, 382- 402, 2006.

27. L. Beilina and C. Johnson. A Hybrid FEM/FDM method for an Inverse Scattering Problem, In "*Numerical Mathematics and Advanced Applications*" - ENUMATH 2001. Springer-Verlag, 2001.

28.L. Beilina, M.Hatlo, and H. Krogstad. Adaptive error control in inverse electromagnetic scattering. Technical Report No. 4, NTNU, Norway, 2008. Submitted for publication, available online at http://www.math.ntnu.no/preprint/numerics/.

29. A.L. Bukhgeim and M.V. Klibanov, Uniqueness in the large of a class of multidimensional inverse problems, *Soviet Math. Dokl.*, 17, 244-247, 1981.

30. T. Carleman, Sur un probleme d'unicite pur les systemes d'equations aux partielles a deux variables independantes, *Ark. Mat. Astr. Fys.*, 26B, No 17, 1-9, 1939.

31. B.B. Das, F. Liu and R.R. Alfano, Time-resolved fluorescence photon migration studies in biomedical and model random media, *Rep. Prog. Physics*, 60, 227-292, 1997.

32. H. Egger, H. W. Engl and M.V. Klibanov, Global uniqueness and Holder stability for recovering a nonlinear source term in a parabolic equation, *Inverse Problems*, 21, 271-290, 2005.

33. H. W. Engl, M. Hanke, and A. Neubauer. *Regularization of Inverse Problems*, Kluwer Academic Publishers, Boston, 2000.

34. Yu. A. Gryazin, M.V. Klibanov and T.R. Lucas, Numerical solution of a subsurface imaging problem, *SIAM J. Appl. Math.,* 62, 664-683, 2001.

35. J. Gyselinck, P. Dular, C. Geuzaine, W. Legros, Harmonic-balance finite-element modeling of electromagnetic devices: A Novel Approach, *IEEE Trans. Magnet.* 38, 521-524, 2002.

36. V. Isakov, Uniqueness of recovery of some quasilinear partial differential equations, *Comm. Part. Diff. Equations*, 26, 1947-1973, 2001.

37. B. Kaltenbacher, M. Kaltenbacher, and S. Reitzinger, Identification of nonlinear $B-H$ curves based on magnetic field computations and using multigrid preconditioners for ill-posed problems, *Europ. J. Appl. Math.* 14, 15–38, 2003.

38. M.V. Klibanov, Inverse problems in the 'large' and Carleman bounds, *Differential Equations,* 20, 755-760, 1984.

39. M.V. Klibanov, Inverse problems and Carleman estimates, *Inverse Problems,* 8, 575-596, 1992.

40. M.V. Klibanov and O.V. Ioussoupova, 1995 Uniform strict convexity of a cost functional for three-dimensional inverse scattering problem *SIAM J Math. Analysis,* 26, 147-179, 1995.

41. M.V. Klibanov and A. Timonov, *Carleman Estimates For Coefficient Inverse Problems and Numerical Applications,* VSP, Utrecht, The Netherlands, 2004.

42. M.V. Klibanov and A. Timonov, A sequential minimization algorithm based on the convexification approach, *Inverse Problems,* 19, 331-354, 2003.

43. M.V. Klibanov and A. Timonov, A globally convergent convexification algorithm for the inverse problem of frequency sounding in one dimension, *Numerical Methods and*

Programming, 4, 52-81, 2003, see http://num-meth.srcc.msu.ru

44. M.V. Klibanov and A. Timonov, A unified framework for constructing of globally convergent numerical algorithms for multidimensional coefficient inverse problems, *Applicable Analysis,* 83, 933-955, 2004.

45. M.V. Klibanov, A class of inverse problems for nonlinear parabolic equations, *Siberian Math. J.*, 27, 697-707, 1987.

46. M.V. Klibanov, Global uniqueness for a multidimensional inverse problem for a nonlinear parabolic equation, *Inverse Problems*, 20, 1003-1032, 2004.

47. V.G. Romanov, *Inverse Problems of Mathematical Physics*, VNU Press, The Netherlands, 1986.

48. P. Stefanov, Inverse problems in transport theory, in *Inside out: inverse problems and applications, Math. Sci. Res. Inst. Publ.*, 47, 111-131, 2003, Cambridge University Press, Cambridge, U.K.

49. A. Tamasan, An inverse boundary value problem in two-dimensional transport, *Inverse Problems,* 18, 209-219, 2002.

50. A.N. Tikhonov and V. Ya. Arsenin, *Solutions of Ill-Posed Problems* Winston & Sons. Washington, D.C., 1977.

51. D. Xu and M. Yamamoto, Stability estimates in state-estimation for a heat process, *Proceedings of the Second ISAAC Congress*, 1 (2000), 193–198, Kluwer Academic Press, Dordrecht.